MONTANA STATE UNIVERSITY

Junction analysis and temperature effects in semi-conductor heterojunctions
by Naresh Tandan

A thesis submitted to the Graduate Faculty in partial fulfillment of the requirements for the degree of DOCTOR OF PHILOSOPHY in Electrical Engineering
Montana State University
© Copyright by Naresh Tandan (1974)

Abstract:
A new classification for semiconductor heterojunctions has been formulated by considering the different mutual positions of conduction-band and valence-band edges.

To the nine different classes of semiconductor heterojunction thus obtained, effects of different work functions, different effective masses of carriers and types of semiconductors are incorporated in the classification. General expressions for the built-in voltages in thermal equilibrium have been obtained considering only nondegenerate semiconductors. Built-in voltage at the heterojunction is analyzed. The approximate distribution of carriers near the boundary plane of an abrupt n-p heterojunction in equilibrium is plotted. In the case of a p-n heterojunction, considering diffusion of impurities from one semiconductor to the other, a practical model is proposed and analyzed. The effect of temperature on built-in voltage leads to the conclusion that built-in voltage in a heterojunction can change its sign, in some cases twice, with the choice of an appropriate doping level. The total change of energy discontinuities (&ΔEc + ΔEv) with increasing temperature has been studied, and it is found that this change depends on an empirical constant and the 0°K Debye temperature of the two semiconductors. The total change of energy discontinuity can increase or decrease with the temperature. Intrinsic semiconductor-heterojunction devices are studied? band gaps of value less than 0.7 eV. are suggested if such devices are to be used at room temperature. Built-in voltage in the case of intrinsic semiconductor heterojunction devices varies slightly with the temperature. With -proper choice of effective masses, the built-in voltage remains essentially constant with the temperature. The advantages of intrinsic semiconductor devices are discussed. A three-dimensional energy-distance-momentum diagram is described; it suggests a change in the wave vector of a carrier, in transit from one semiconductor to other. Thus, the probability of transition of a carrier across the heterojunction is reduced.

JUNCTION ANALYSIS AND TEMPERATURE EFFECTS IN SEMICONDUCTOR HETEROJUNCTIONS

by

NARESH TANDAN

A thesis submitted to the Graduate Faculty in partial fulfillment of the requirements for the degree

of

DOCTOR OF PHILOSOPHY

in

Electrical Engineering

Approved:

Head, Major Department

Chairman, Examining Committee

Graduate Dean

MONTANA STATE UNIVERSITY
Bozeman, Montana

March, 1974

ACKNOWLEDGMENTS

I wish to express my deep appreciation to my advisor, Professor N. A. Shyne, for his thoughtful guidance and encouragement in this research. Thanks are also due to Professor J. P. Hanton for his useful suggestions and discussions in this research.

My thanks to the department head, Professor P. E. Uhlrich, for his encouragement and financial support throughout my stay at Montana State University.

My thanks to my parents without whose moral support and encouragement throughout all my graduate work I could not have completed this work. Finally, thanks to my wife, Anita, for typing the entire first draft.

TABLE OF CONTENTS

	Page
VITA	ii
ACKNOWLEDGMENTS	iii
TABLE OF CONTENTS	iv
LIST OF TABLES	vii
LIST OF FIGURES	viii
LIST OF SYMBOLS	xiii
ABSTRACT	xvi
Chapter	
1. INTRODUCTION	1
HISTORICAL REVIEW	1
Anderson's Theory	1
Summary of Other Theories	7
PROSPECTS OF DEVELOPMENT AND TECHNOLOGICAL APPLICATION	9
CONTENTS OF THE THESIS AND ASSUMPTIONS	11
2. CLASSIFICATION OF SEMICONDUCTOR HETEROJUNCTIONS	16
INTRODUCTION	16
CLASSIFICATION	17
IMPORTANCE OF CLASSIFICATION	27

Page

3. ANALYSIS OF ELECTRIC FIELD 45

GENERAL THEORY 45

BUILT-IN VOLTAGES 52

DISTRIBUTION OF CARRIERS 60

PRACTICAL MODEL OF n-p SEMICONDUCTOR HETEROJUNCTION 64
Model and Assumption 66
Calculation of Electric Field and Capacitance 67

4. TEMPERATURE EFFECTS IN SEMICONDUCTOR HETEROJUNCTIONS 75

TEMPERATURE DEPENDENCE OF CARRIER CONCENTRATION 76

EVALUATION OF FERMI LEVEL AT DIFFERENT TEMPERATURE RANGES 79

TEMPERATURE DEPENDENCE OF BUILT-IN VOLTAGE 83

TEMPERATURE DEPENDENCE OF DISCONTINUITIES 100

5. INTRINSIC SEMICONDUCTOR HETEROJUNCTION 105

INTRINSIC CONDUCTIVITY 106

THEORY OF INTRINSIC SEMICONDUCTOR DEVICES 108

DEVICES USING AN INTRINSIC AND AN EXTRINSIC SEMICONDUCTOR 112

ADVANTAGES OF INTRINSIC SEMICONDUCTOR DEVICES 113

Page

6. CONCLUSIONS AND SUGGESTIONS 114

APPENDIX

A. 3-D ENERGY BAND DIAGRAM 118

B. CHANGE OF TOTAL ENERGY DISCONTINUITIES ($\Delta E_c + \Delta E_v$) 123

BIBLIOGRAPHY 128

LIST OF TABLES

Appendix Table		Page
1.	Change in Discontinuities With Changing Temperature for Ge-GaAs Heterojunction . . .	125
2.	Change in Discontinuities With Changing Temperature for GaP-Si Heterojunction . . .	126
3.	Change in Discontinuities With Changing Temperature for Si-Ge Heterojunction	127

LIST OF FIGURES

Figure		Page
1.	Energy-band diagram for two isolated semiconductors in which space charge neutrality is assumed to exist in every region	3
2.	Energy-band diagram of a n-p hetero-junction in thermal equilibrium	5
3.	Energy-band diagram for two isolated semiconductors in which space charge neutrality is assumed to exist in every region with $\chi_{2h}>\chi_{1h}>\chi_{1e}>\chi_{2e}$	19
4.	Energy-band diagram for two isolated semiconductors in which space charge neutrality is assumed to exist in every region with $\chi_{1h}=\chi_{2h}$; $\chi_{2h}>\chi_{1e}>\chi_{2e}$ . . .	19
5.	Energy-band diagram for two isolated semiconductors in which space charge neutrality is assumed to exist in every region with $\chi_{1h}>\chi_{2h}>\chi_{1e}>\chi_{2e}$	20
6.	Energy-band diagram for two isolated semiconductors in which space charge neutrality is assumed to exist in every region with $\chi_{1h}>\chi_{1e}$; $\chi_{1e}=\chi_{2h}$; $\chi_{2h}>\chi_{2e}$.	20
7.	Energy-band diagram for two isolated semiconductors in which space charge neutrality is assumed to exist in every region with $\chi_{1e}>\chi_{2h}$	21
8.	Energy-band diagram for two isolated semiconductors in which space charge neutrality is assumed to exist in every region with $\chi_{2h}>\chi_{1h}>\chi_{2e}$; χ_{2e}	21

Figure		Page
9.	Energy-band diagram for two isolated semiconductors in which space charge neutrality is assumed to exist in every region with $\chi_{2h}>\chi_{1h}>\chi_{2e}>\chi_{1e}$	23
10.	Energy-band diagram for two isolated semiconductors in which space charge neutrality is assumed to exist in every region with $\chi_{2h}>\chi_{1h}=\chi_{2e}>\chi_{1e}$	23
11.	Energy-band diagram for two isolated semiconductors in which space charge neutrality is assumed to exist in every region with $\chi_{2e}>\chi_{1h}$	24
12.	Semiconductor heterojunction classification chart	26
13.	Energy-band diagram of two semiconductors in thermal equilibrium that defines working space $\chi_{2h}>\chi_{1h}>\chi_{1e}>\chi_{2e}$	28
14.	Energy-band diagram of two semiconductors in thermal equilibrium that defines the working space $\chi_{1h}=\chi_{2h}$; $\chi_{2h}>\chi_{1e}>\chi_{2e}$	31
15.	Energy-band diagram of two semiconductors in thermal equilibrium that defines the working space $\chi_{1h}>\chi_{2h}>\chi_{1e}>\chi_{2e}$	33
16.	Energy-band diagram of two semiconductors in thermal equilibrium that defines the working space $\chi_{1h}>\chi_{2h}$; $\chi_{2h}=\chi_{1e}$; $\chi_{1e}>\chi_{2e}$	35
17.	Energy-band diagram of two semiconductors in thermal equilibrium that defines the working space $\chi_{1h}>\chi_{1e}>\chi_{2h}>\chi_{1e}$	35

Figure		Page
18.	Energy-band diagram of two semiconductors in thermal equilibrium that defines the working space $\chi_{2h}>\chi_{1h}>\chi_{2e}$; $\chi_{2e}=\chi_{1e}$	38
19.	Energy-band diagram of two semiconductors in thermal equilibrium that defines the working space $\chi_{2h}>\chi_{1h}>\chi_{2e}>\chi_{1e}$	40
20.	Energy-band diagram of two semiconductors in thermal equilibrium that defines the working space $\chi_{2h}>\chi_{1h}$; $\chi_{1h}=\chi_{2e}$; $\chi_{2e}>\chi_{1e}$	42
21.	Energy-band diagram of two semiconductors in thermal equilibrium that defines the working space $\chi_{2h}>\chi_{1h}$	42
22.	Energy-band diagram of isolated n-p semiconductors of the same element in which space charge neutrality is assumed to exist in every region	49
23.	Energy-band diagram of n-p homojunction in thermal equilibrium	50
24.	Energy-band diagram of two isolated semiconductors in which space charge neutrality is assumed to exist in every region with $\phi_{m_1}<\phi_{m_2}$	54
25.	Approximate distribution of carriers near the boundary plane of a germanium p-n junction at room temperature	61
26.	The approximate distribution of carriers near the boundary plane of an abrupt n-p Ge-GaAs heterojunction in equilibrium at 300°K	65

Figure		Page
27.	Energy-band diagram of two isolated semiconductors. The n-type impurity has diffused into p-type broad-gap semiconductor, thus forming an n-n heterojunction and an n-p homojunction . . .	68
28.	Practical model of semiconductor heterojunction (n-p) in thermal equilibrium . . .	68
29.	n-p heterojunction in practice consists of an isotype heterojunction (n-n) and homojunction (n-p). Isotype heterojunction is shown to have shifted "t" units into an n-type semiconductor	69
30.	Variation of Fermi level with temperature for (a) n-type and (b) p-type semiconductors, of various impurity densities, those marked "2" to intermediate densities, and those marked "3" to relatively high impurity densities	84
31.	Two isolated semiconductors as discussed in Case 1, space charge neutrality is assumed to exist in every region. (a) at room temperature, (b) at an elevated temperature where narrow-gap semiconductor becomes intrinsic, making built-in-voltage to increase and (c) at a temperature where broad-gap semiconductor also become intrinsic, shows a charge in polarity of built-in-voltage if compared with Figure (a)	87
32.	An approximate plot of built-in voltage at the heterojunction with respect to temperature in Case 1	89
33.	Energy-band diagram of isolated Ge-Si in which space charge neutrality is assumed to exist in every region at 300°K	90

Figure		Page
34.	Energy-band diagram of isolated Ge-Si in which space charge neutrality is assumed to exist in every region at 450°K.	94
35.	Energy-band diagram of isolated Ge-Si in which space charge neutrality is assumed to exist in every region at 600°K	96
36.	Built-in voltage at the Ge-Si heterojunction as considered in the example of Case 1 . . .	97
37.	Two isolated semiconductors as discussed in Case 2, space charge neutrality is assumed to exist in every region with $\Delta E_y > \Delta E_c$. (a) At room temperature, (b) at an elevated temperature where narrow-gap semiconductor becomes intrinsic making built-in voltage to change sign, and (c) at a temperature where broad-gap semiconductor also becomes intrinsic, changing the sign of built-in voltage once over again	99
38.	Built-in voltage at the n-n heterojunction with respect to temperature in Case 2 . . .	101
39.	Change in total discontinuities with changing temperature are plotted for GaP-Si, Ge-GaAs and Ge-Si heterojunctions .	103
40.	Carrier concentration has been plotted for an abrupt intrinsic semiconductor heterojunction, $n_1=p_1 \neq n_2=p_2$	109
41.	Energy-band diagram of InAs ± GaSb, in which space charge neutrality is assumed to exist in every region at 300°K	111

Appendix

B.	E - X - K plot of two isolated direct gap semiconductors	122

LIST OF SYMBOLS

Subscript "1" represents narrow-gap semiconductor

Subscript "2" represents broad-gap semiconductor

C	Capacitance in Farad.
E_c	Energy of conduction band gap in eV.
ΔE_c	Energy discontinuity in energy band diagram of a heterojunction (associated with electron affinity difference) in eV.
E_F	Fermi level, n and p semiconductor in eV.
E_{Fi}, E_{FI}	Intrinsic Fermi level in semiconductor in eV.
E_g	Energy band gap in eV.
E_v	Energy of valence-band edge in eV.
ΔE_v	Energy discontinuity in the valence-band energy diagram of a heterojunction in eV.
h	Planck's constant in Joule-sec.
$\hbar$	$\frac{h}{2\pi}$
J_n	Electron current density in A cm^{-2}.
J_p	Hole current density in A cm^{-2}.
K	Momentum wave vector.
k	Boltzmann's constant in eV° k^{-1}.
m_e^*	Electron effective mass Kg.
m_{de}^*	Density-of-state effective mass for electron in Kg.

m^*_{dh}	Density-of-state effective mass for holes in Kg.
m^*_{lh}	Light hole mass in Kg.
m^*_{hh}	Heavy hole mass in Kg.
m^*_l	Effective mass along the longitudinal ellipsoidal energy surface in Kg.
m^*_t	Effective mass along the transverse ellipsoidal energy surface in Kg.
m^*_h	Effective mass of hole.
N_a, N_A	Acceptor density in cm^{-3}.
N_C	Effective density of energy states at the conduction band edge in cm^{-3}.
N_d, N_D	Donor density in cm^{-3}.
N_V	Effective density of energy states at the valence-band edge in cm^{-3}.
n_o, n	Free electron density in the conduction band in cm^{-3}.
n_d	Unionized donors in cm^{-3}.
n_i	Intrinsic carrier concentration in a semiconductor cm^{-3}.
p_o, p	Hole density in cm^{-3}.
P_a	Unionized acceptors in cm^{-3}.
q	Charge of an electron, 1.6×10^{-19} conlomb.
T	Absolute temperature in °K.
V_{BHT}	Built-in voltage in heterojunction in volts.

V_{BHM}	Built-in voltage in homojunction in volts.
x	Distance in cm.
γ	Emitter injection efficiency.
ε	Dielectric constant of the semiconductor in F cm^{-1}.
μ_n	Mobility of electrons in cm^2 v^{-1} sec^{-1}.
μ_p	Mobility of holes in cm^2 v^{-1} sec^{-1}.
ϕ_m	Work function of a semiconductor in eV.
χ_e	Electron affinity of a semiconductor in eV.
χ_h	$(\chi_e + E_g)$ in eV.
$\psi(x)$	Electrostatic potential difference as a function of distance in volts.
σ	Conductivity in mhos.
θ	Debye temperature.

ABSTRACT

A new classification for semiconductor heterojunctions has been formulated by considering the different mutual positions of conduction-band and valence-band edges. To the nine different classes of semiconductor heterojunction thus obtained, effects of different work functions, different effective masses of carriers and types of semiconductors are incorporated in the classification. General expressions for the built-in voltages in thermal equilibrium have been obtained considering only nondegenerate semiconductors. Built-in voltage at the heterojunction is analyzed. The approximate distribution of carriers near the boundary plane of an abrupt n-p heterojunction in equilibrium is plotted. In the case of a p-n heterojunction, considering diffusion of impurities from one semiconductor to the other, a practical model is proposed and analyzed. The effect of temperature on built-in voltage leads to the conclusion that built-in voltage in a heterojunction can change its sign, in some cases twice, with the choice of an appropriate doping level. The total change of energy discontinuities ($\Delta E_C + \Delta E_V$) with increasing temperature has been studied, and it is found that this change depends on an empirical constant and the 0°K Debye temperature of the two semiconductors. The total change of energy discontinuity can increase or decrease with the temperature. Intrinsic semiconductor-heterojunction devices are studied; band gaps of value less than 0.7 eV. are suggested if such devices are to be used at room temperature. Built-in voltage in the case of intrinsic semiconductor heterojunction devices varies slightly with the temperature. With proper choice of effective masses, the built-in voltage remains essentially constant with the temperature. The advantages of intrinsic semiconductor devices are discussed. A three-dimensional energy-distance-momentum diagram is described; it suggests a change in the wave vector of a carrier, in transit from one semiconductor to other. Thus, the probability of transition of a carrier across the heterojunction is reduced.

Chapter 1

INTRODUCTION

Historical Review

A semiconductor heterojunction is a junction between two dissimilar semiconductors where the crystal structure is continuous across the interface. Semiconductor heterojunction research is an important area of device study which has evolved from the research of the last decade. The barriers introduced into the energy-band diagram by the energy-gap difference of two semiconductors allows a new degree of freedom to the device designer. For example, in GaAs injection lasers [1], the addition of $Al_xGa_{1-x}As$ confinement barriers has resulted in a major reduction in 300°K threshold current densities. Electrooptical effects in heterojunctions that are promising include infrared to visible upconversion systems [2], the window effect [3], solar cells [4] and photo transistors [5]. High yield photo cathodes [6], cold cathodes [7] and electron multipliers [8] of the negative-electron affinity type represent yet other families of devices where heterojunctions are involved.

The heterojunction structure was first considered by Preston [9]. Gubanov [10] produced an analysis of

heterojunctions with n-n, p-p and p-n combinations. Shockley [11] proposed a circuit device incorporating a change in the magnitude of the forbidden gap in the transition region of p-n junction. Kroemer [12] proposed the use of a heterojunction as a wide-gap emitter to increase the injection efficiency of transistors. The Anderson theory [3] is discussed in the following section and a brief summary of other theories is discussed on page 7.

Anderson's Theory. The energy-band model of an ideal abrupt heterojunction without interface states was proposed by Anderson based on the previous work of Shockley. This model is important as it can adequately explain most of the transport processes, and only a slight modification [13] of the model is needed to account for non-ideal cases such as interface states. Consider the energy-band profile of the two isolated semiconductors as shown in Figure 1. The two semiconductors are assumed to have different band gaps (E_{g_1},E_{g_2}), different dielectric constants (ε_1,ε_2), different work function (ϕ_{m_1},ϕ_{m_2}), and different electron affinities (χ_{1e},χ_{2e}). The work function is defined as the energy required to remove an electron from the Fermi level (E_F) to a position just outside of

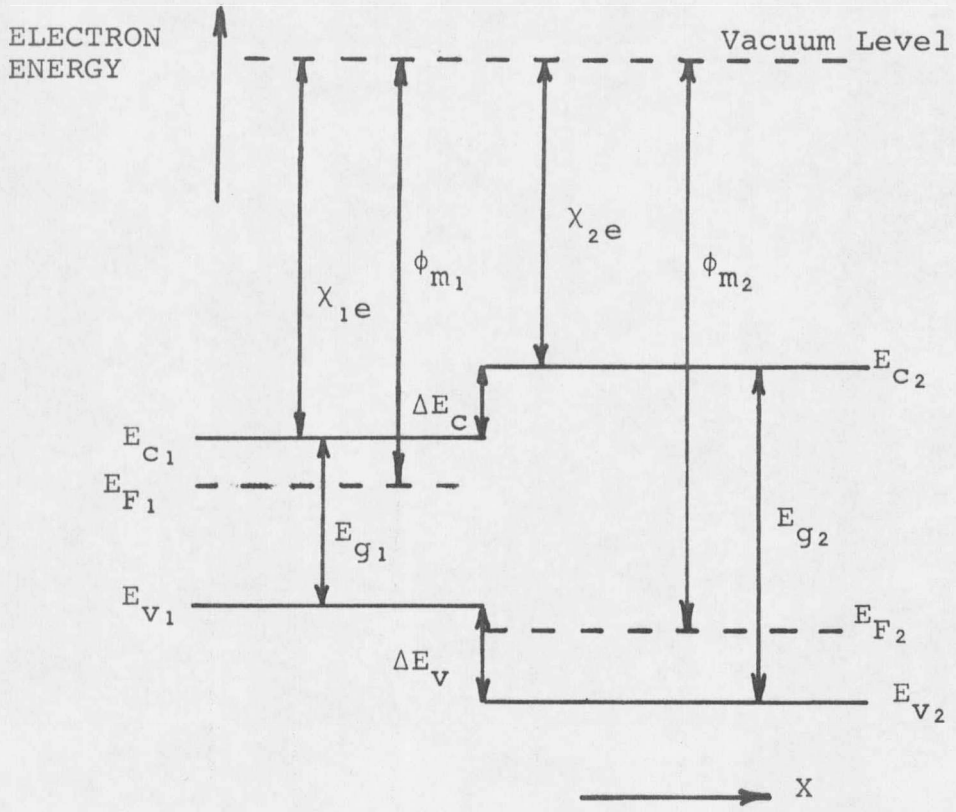


Figure 1. Energy-band diagram for two isolated semiconductors in which space charge neutrality is assumed to exist in every region.

the material. The bottom of the conduction-band is represented by E_c and the top of the valence-band is represented by E_v. The subscripts 1 and 2 refer to the narrow-gap and wide-gap semiconductors, respectively. Electron affinity is defined as the energy required to remove an electron from the bottom of conduction-band to a position just outside of the material. It is assumed that space charge neutrality exists in every region and thus band edges ($E_{c_1}, E_{c_2}, E_{v_1}, E_{v_2}$) are shown to be horizontal. The difference in energy of the conduction-band edges in the two materials is represented by ΔE_c and that in the valence-band edges is ΔE_v.

A junction formed between an n-type narrow-gap semiconductor and a p-type wide-gap semiconductor is considered. The energy-band profile of such a junction at equilibrium is shown in Figure 2.

The electrostatic potential difference between any two points can be represented by the vertical displacement of the band edges between these two points in a semiconductor. An electrostatic field can be represented by the slope of the edges on a band diagram. The total built-in voltage (V_{BHT}) is equal to the sum of the partial built-in

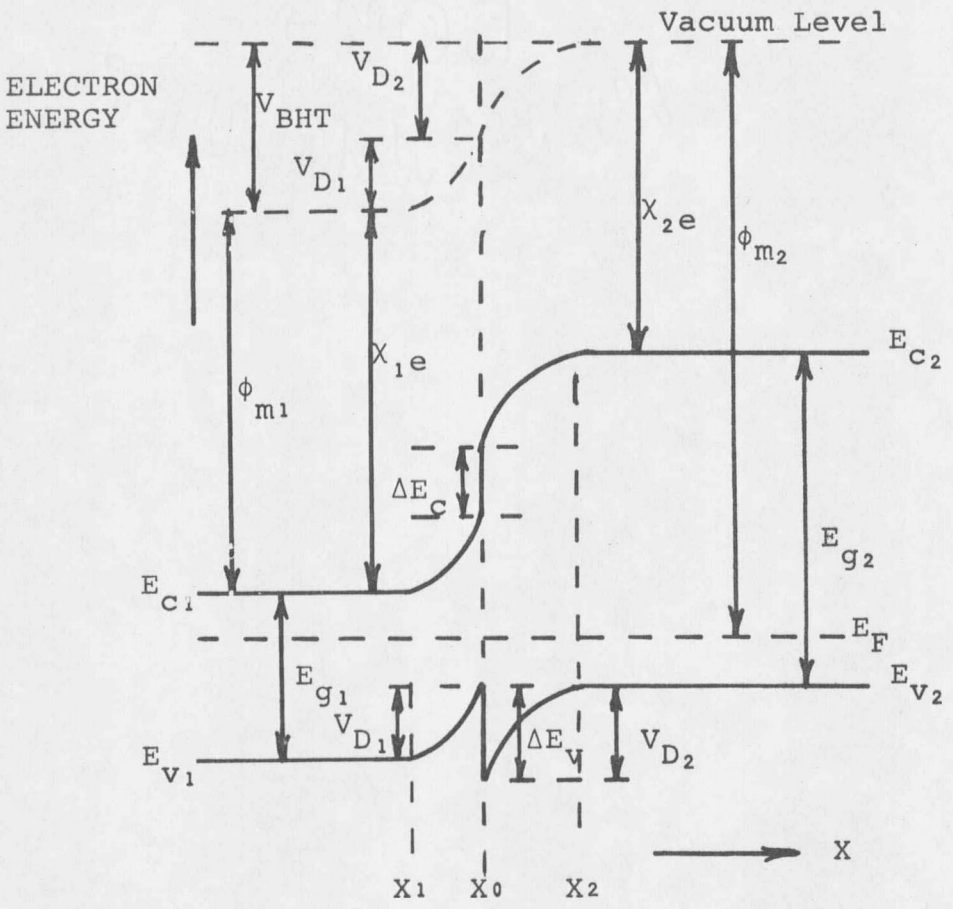


Figure 2. Energy-band diagram of n-p heterojunction in thermal equilibrium.

voltages ($V_{D_1} + V_{D_2}$), where V_{D_1} and V_{D_2} are the electrostatic potentials supported at equilibrium by semiconductors 1 and 2, respectively. Since the Fermi level must coincide on both sides in equilibrium and the vacuum level is everywhere parallel to the band edges and is continuous, the discontinuity in the conduction band edges (ΔE_c) and valence-band edges (ΔE_v) is invariant with doping in those cases where E_g and χ are not functions of doping (i.e., nondegenerate semiconductors). A degenerate semiconductor is one in which Fermi level lies in the conduction or in the valence-band. It is assumed that the electron density is zero for $X>X_1$, and the hole density is zero for $X<X_2$. Then at any point in the transition region, the space charge density is merely equal to the donor or acceptor density.

$$p_1 = q\, N_{D_1} \qquad X_1 \leq X \leq X_0$$

$$p_2 = q\, N_{A_2} \qquad X_0 \leq X \leq X_2$$

where N_{D_1} is the donor concentration in semiconductor 1 and N_{A_2} is the acceptor concentration in semiconductor 2. The solution of Poisson's equation in the one dimensional case with appropriate doping levels gives the solution for an abrupt junction as follows [3]:

Transition region width $W = (X_2 - X_0) + (X_0 - X_1)$

$$= \left[\frac{2\,\varepsilon_1 \varepsilon_2 (V_{BHT} - V)(N_{A_2} + N_{D_1})}{q(\varepsilon_1 N_{D_1} + \varepsilon_2 N_{A_2}) N_{D_1} N_{A_2}} \right]^{1/2}$$

The transition capacitance is given by a generalization of the result for homojunctions.

$$C = \left[\frac{q\, N_{D_1} N_{A_2}\, \varepsilon_1 \varepsilon_2}{2(\varepsilon_1 N_{D_1} + \varepsilon_2 N_{A_2})} \; \frac{1}{(V_{BHT} - V)} \right]^{1/2}$$

Figure 2 shows that the potential barrier for electrons is considerably greater than that for holes, and so hole current will predominate. The application of Shockley's homojunction diffusion theory, along with a diode emission model is sufficient to predict the saturation current and current-voltage characteristics of the heterojunction.

Summary of other theories. Most of the other theories have modified the ideal model of semiconductor heterojunctions as proposed by Anderson. Perlman and Feucht [13,14] used a classical kinetic-emission model to predict the current-voltage characteristic of an abrupt p-n heterojunction. This took into account the effect of changes in electron affinity, electron effective masses, dielectric constant and band gap at the junction. The p-n

heterojunction was found to have two operating modes; one similar to a homojunction, where minority-carriers build up at the depletion region edge limiting current, and another similar to a metal-semiconductor junction, where the current is limited by a potential barrier in the n-type semiconductor. On increasing the forward bias, the homojunction mode of operation changes to the metal-semiconductor mode.

Oldham and Milnes [15] studied the effect of interface states. For a lattice mismatch of the order of 2 to 4%, the dislocations were assumed to lie in a sheet and to be similar to grain boundaries. They concluded that the interface resembles a low-density,free surface with edge dislocations producing deep states in the gap. Due to the presence of interface states, the ideal model of Anderson gets distorted.

Van Ruyen, Papenhuijzen and Verhoeven [16] considered two semiconductors, each with a free surface. They considered a heterojunction with a significant number of interface states. Interface states were thought to play a decisive role since they can store sufficient charge to make the surfaces behave like a thin metal layer. Contact

between the two different surfaces leads to the formation of a dipole layer.

Prospects of Development and Technological Application

Let us consider the way in which p-n homojunctions were developed [17]. The first incomplete theory of their behaviour was given by Davydoy in 1938 and a full design theory incorporating the ideas of injection was published by Shockley in 1949. Early experimental germanium p-n junctions were described in 1950 and, as they were in the form of grown junctions, they were of high quality but suffered from a high cost of manufacture. The alloy-junction provided a cheap and usable junction but did not give high performance or good reliability. The diffusion process introduced about 1956 led to higher quality devices with better performance, but it was really the discovery in 1959 of the planar process and subsequent work on epitaxial growth which made possible the production of high quality transistors and diodes and paved the way for the integrated circuits. Excellent development and research work has been carried out on other materials but no really significant production of p-n junction devices has

been realized in materials other than silicon, with the possible exceptions of germanium alloy devices and gallium arsenide (phosphide) diodes. Silicon devices have been developed over a period of about 25 years and have now reached a state where integrated circuits of high complexity and high reliability can be manufactured in quantity.

The problems with heterojunctions are more difficult to solve both from theoretical and practical points of view. The basic theoretical ideas were published by Anderson approximately 10 years ago and since that time a considerable amount of work has been carried out. The outlook for production of heterojunctions for normal electronic devices seems uncertain. To compete with normal silicon devices which have been manufactured rather than produced by research workers in a laboratory, the heterojunction devices would need to be more reliable, or to have improved characteristics, or to be cheaper. It seems unlikely at present for heterojunctions to compete with homojunction devices for normal use. However, looking at special applications, there is a hope for technological applications. The main area for development seems to be

in the region of applying optical properties, particularly for detectors, electroluminescent lamps and lasers. Single heterojunctions lasers [18] are manufactured at present, though still in the process of development.

The device potential of the heterojunction is greatly reduced when significant numbers of interface states are present at the junction. Therefore, the development of semiconductor pairs with a very small mismatch of lattice constant is in progress, so as to minimize the number of interface states. One such developed pair is GaAs - $Al_xGa_{1-x}As$: it finds application in heterojunction lasers.

Contents of the Thesis and Assumptions

Heterojunctions are classified as graded and abrupt, depending on whether the junction is graded or abrupt. Another classification involves the predominant impurity type on either side of the junction. n-n or p-p junctions are called isotype heterojunctions and n-p or p-n junctions are called anisotype heterojunctions. A new classification is presented, considering different mutual positions of conduction and valence-band edges. Nine different classes of a semiconductor heterojunction are obtained. Each such

class has some unique properties, which are discussed, considering the effect of different work functions. Different effectives masses of carriers and different types of semiconductors (direct or indirect gap) are incorporated in the classification. These parameters provide information regarding the structure of conduction and valence-bands, and the mobility and lifetime of carriers in the two semiconductors. A large number of unique semiconductor heterojunctions are thus possible; some of them exist at present, others may develop in the future.

A general theory that describes the formation of the electric field at the junction is presented. A general expression for built-in voltage is formulated in three different forms considering nondegenerate semiconductors. The built-in voltage is split into two components. It turns out that one component is similar to that of a homojunction and can be controlled by the doping level while the other component arises as a result of energy discontinuities and different effective masses, and is fixed once the two semiconductors are chosen. Approximate distribution of the carriers near the boundary plane of an arbitrary abrupt np heterojunction in equilibrium is

plotted. A practical model of a p-n heterojunction is proposed and analyzed. In reality, due to diffusion of impurities from one semiconductor to the other, a p-n semiconductor heterojunction consists of an isotype heterojunction and a p-n homojunction.

A theory describing the temperature dependence of carrier concentration and the evaluation of Fermi level at different temperature ranges is discussed. Two different cases are considered with $\Delta E_v > \Delta E_c$, and it shows that the built-in voltage in case of a heterojunction may change sign under certain conditions of doping level and that it may change twice with another preferred doping profile in the two semiconductors. The total change of energy discontinuities ($\Delta E_c + \Delta E_v$) with increasing temperature has been studied, and it is shown that this change depends on an empirical constant and on the Debye temperature of the two semiconductors. The total change of energy discontinuities has been computed for GaP - Si, Ge - GaAs and Ge - Si heterojunctions pairs. In the case of GaP-Si and Ge-GaAs heterojunctions, the total energy discontinuity decreases with temperature, while in the case of the Ge-Si heterojunction, the total change of energy discontinuities with temperature between 0°K to 800°K.

Intrinsic semiconductor heterojunctions are possible and are studied on the basis of intrinsic conductivity. Intrinsic conductivity of a semiconductor is found to be an important consideration. For moderate conductivity, the energy-band gap of a semiconductor should be small if the device is to be used at room temperature. A band gap of a value less than 0.7 eV. is suggested. The built-in voltage changes only slightly with the temperature in the case of an intrinsic semiconductor heterojunction. It is concluded that, if the choice of effective masses is as follows:

$$\frac{m^*_{1h}}{m^*_{2h}} \cdot \frac{m^*_{2e}}{m^*_{1e}} = 1,$$

then the built-in voltage remains essentially constant with the temperature. It is suggested that a narrow-gap intrinsic semiconductor and a broad-gap extrinsic semiconductor can also be used.

Appendix A considers a three-dimensional energy-distance-momentum diagram. Since, in general, the conduction-bands and valence-bands of two semiconductors are not alike, it is concluded that the wave vector of a

carrier should change while the carrier is crossing the heterojunction.

Chapter 2

CLASSIFICATION OF SEMICONDUCTOR HETEROJUNCTIONS

Introduction

Semiconductor heterojunctions can be classified in several ways [19]. If the material changes abruptly on an atomic scale from one material to another, the junction is referred to as "abrupt". If there is an appreciable intermixing of the components, the heterojunction is referred to as "graded".

Another classification involves the predominant type of impurity on either side of the junction. In the case of similar doping on either side of a junction, the junction is called an isotype heterojunction (n-n or p-p). An anisotype heterojunction is one with different types of doping on either side of the junction. These include n-p or p-n heterojunctions.

The properties of a semiconductor heterojunction depend on the various parameters of the two semiconductors. The two fundamental parameters are electron affinities and energy gaps. A possible system of classification can be chosen using the above parameters which acquire unique positions in the energy-versus-distance diagram. On each

of such diagrams, other parameters of interest can be incorporated, such as work function, type of semiconductors (direct or indirect) and the effective masses of carriers. External influences (such as light or applied voltage), which can modify the properties of junction, are not considered in this classification.

Classification

Consider an energy-band diagram of two isolated semiconductors with energy gaps of E_{g_1} and E_{g_2} shown in Figure 1. The two electron affinities are χ_{1e} and χ_{2e}, according to the usual practice of specifying the first semiconductor as narrow-gap and the second semiconductor as broad-gap. Only nondegenerate semiconductors are under consideration. The energy discontinuities in the conduction and valence-bands are represented by ΔE_c and ΔE_v. ΔE_c is defined as positive when $\chi_{1e} > \chi_{2e}$, negative when $\chi_{1e} < \chi_{2e}$, and zero when $\chi_{1e} = \chi_{2e}$. Similarly, ΔE_v is defined as positive when $\chi_{2h} > \chi_{1h}$, negative if $\chi_{2h} < \chi_{1h}$ and zero when $\chi_{2h} = \chi_{1h}$. The above idea is introduced in order to satisfy the relation $E_{g_2} - E_{g_1} = \Delta E_c + \Delta E_v$, irrespective of the mutual position of the bands. Different values of electron affinities, band gaps and work function

give new shapes to the energy-band diagram, resulting in new properties being shown. Therefore, considering all possible different mutual positions of the bands by attributing different values of electron and hole affinity, the following different cases are obtained.

Figure 3 represents the case of $\chi_{2h} > \chi_{1h} > \chi_{1e} > \chi_{2e}$ and shows that ΔE_c and ΔE_v both are positive. The magnitude of ΔE_c and ΔE_v are not considered important for the classification proposed. This is the most common case where heterojunctions have been studied, as for example, Ge-GaAs, AlSb-GaSb, and Ge-Si.

Figure 4 represents the case where ΔE_v is zero and ΔE_c is positive; i.e., $\chi_{1h} = \chi_{2h}, \chi_{2h} > \chi_{1e} > \chi_{2e}$. The GaAs - $Al_xGa_{1-x}As$ heterojunction is an example of this class.

Figure 5 represents the case where ΔE_v is negative, ΔE_c is positive and possibly can be greater than E_{g_1}, but less than E_{g_2}; i.e., $\chi_{1h} > \chi_{2h} > \chi_{1e} > \chi_{2e}$. The CdSe-Se and InP-GaAs heterojunctions are examples of this class.

Figure 6 represents two isolated semiconductors with $\chi_{1h} > \chi_{2h}$. $\chi_{2h} = \chi_{1e}, \chi_{1e} > \chi_{2e}$, i.e., $\Delta E_c = E_{g_2}$ and $-\Delta E_v = E_{g_1}$. No such pair exists at present.

Figure 7 represents the case where the mutual position of bands are such as to give $-\Delta E_v > E_{g_1}$ and

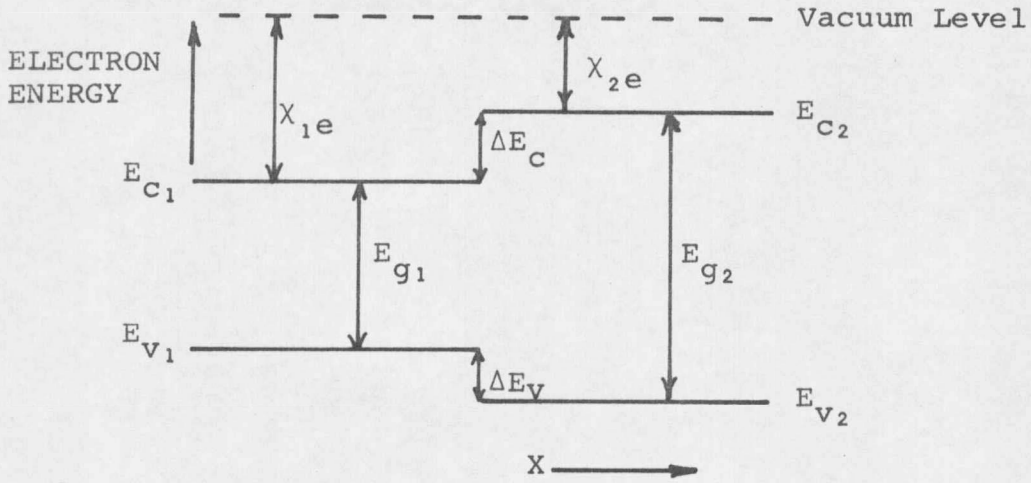


Figure 3. Energy-band diagram for two isolated semiconductors in which space charge neutrality is assumed to exist in every region with $\chi_{2h} > \chi_{1h} > \chi_{1e} > \chi_{2e}$

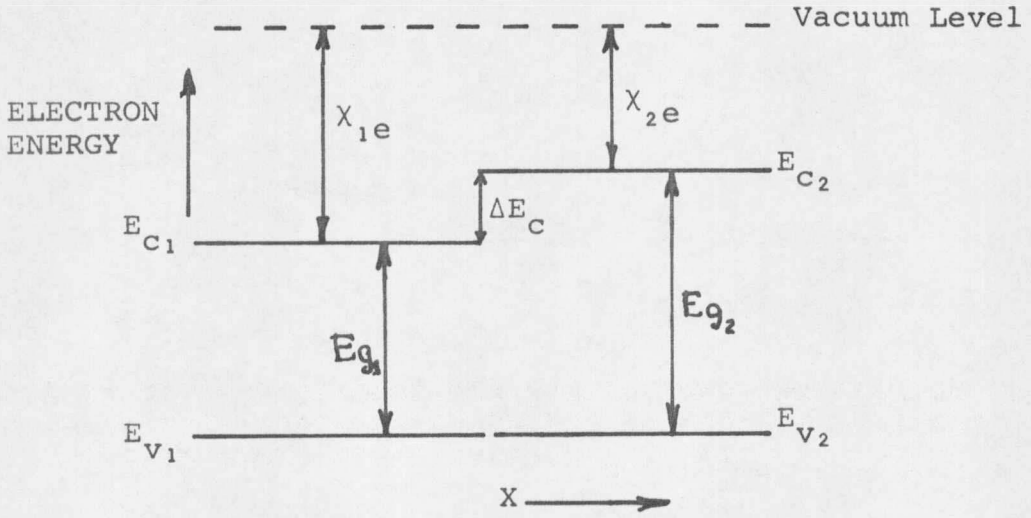


Figure 4. Energy-band diagram for two isolated semiconductors in which space charge neutrality is assumed to exist in every region with $\chi_{1h} = \chi_{2h}$; $\chi_{2h} > \chi_{1e} > \chi_{2e}$.

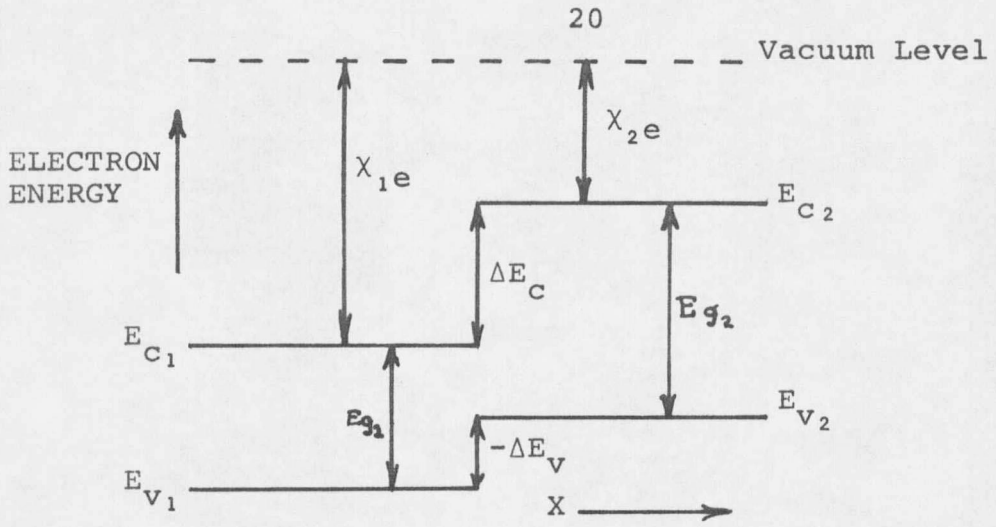


Figure 5. Energy-band diagram for two isolated semiconductors in which space charge neutrality is assumed to exist in every region with $\chi_{1h} > \chi_{2h} > \chi_{1e} > \chi_{2e}$.

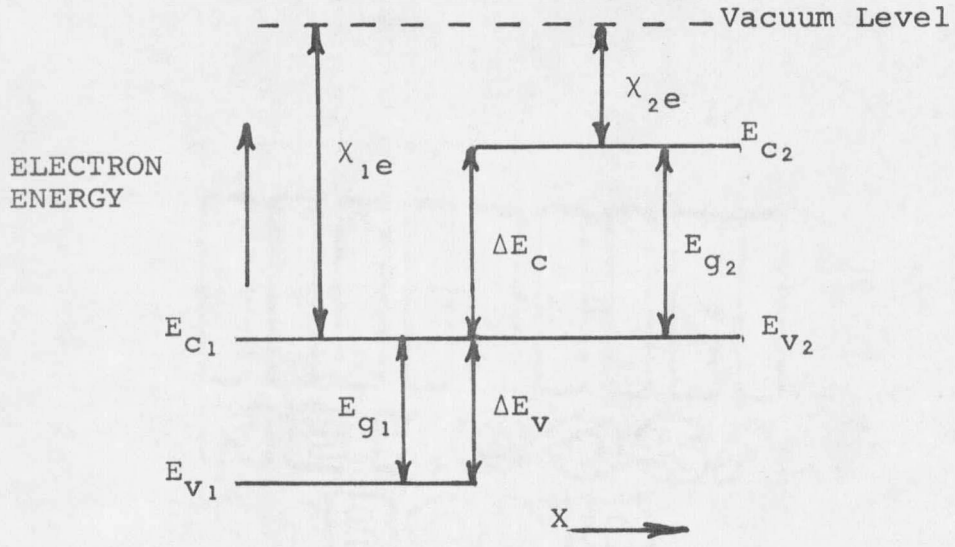


Figure 6. Energy-band diagram for two isolated semiconductors in which space charge neutrality is assumed to exist in every region with $\chi_{1h} > \chi_{1e}$; $\chi_{1e} = \chi_{2h}$; $\chi_{2h} > \chi_{2e}$.

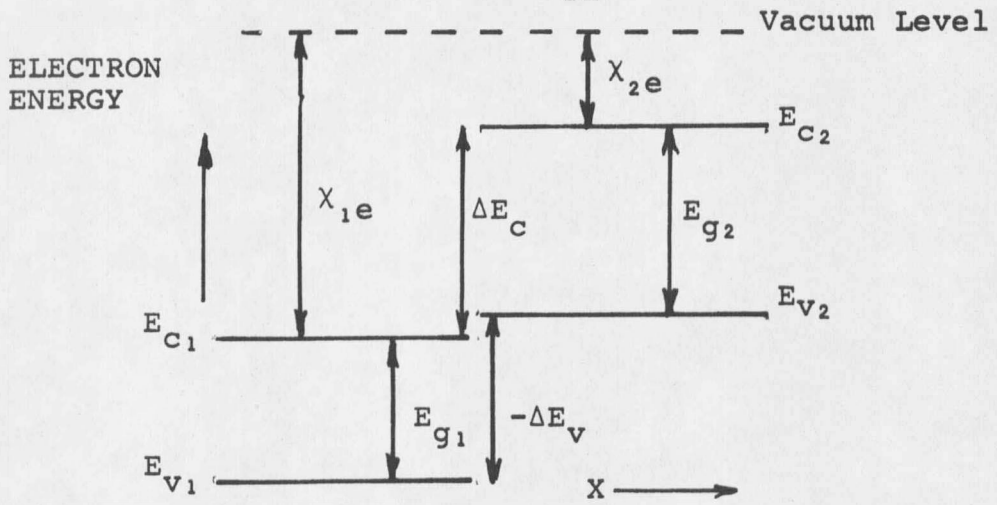


Figure 7. Energy-band diagram with two isolated semiconductors in which space charge neutrality is assumed to exist in every region with $\chi_{1e} > \chi_{2h}$.

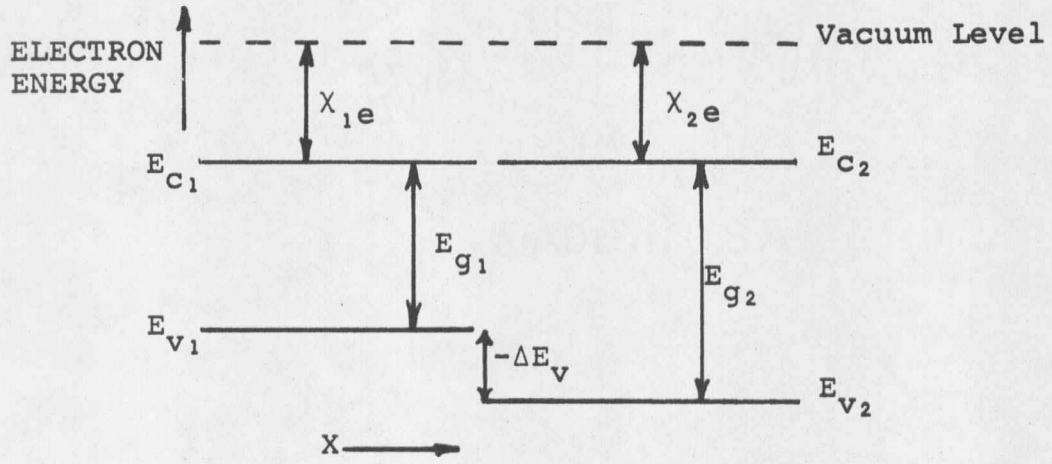


Figure 8. Energy-band diagram with two isolated semiconductors in which space charge neutrality is assumed to exist in every region with $\chi_{2h} > \chi_{1h} > \chi_{2e}$; $\chi_{2e} = \chi_{1e}$.

$\Delta E_c > E_{g_2}$. The GaAs-CsO_2 heterojunction pair is an example of this kind. Similar to Figure 4, where there was no discontinuity in the valence-band, Figure 8 represents the case where there is no discontinuity in the conduction band, $\chi_{2h} > \chi_{1h} > \chi_{2e}$; $\chi_{2e} = \chi_{1e}$ thus making $\Delta E_c = 0$ and ΔE_v is positive. The GaSb-GaAs heterojunction is an example of this class.

Figure 9 represents the case of $\chi_{2h} > \chi_{1h} > \chi_{2e} > \chi_{1e}$, resulting in a negative discontinuity in conduction-band with positive discontinuity in the valence-band as $\Delta E_v < E_{g_1}$. ZnTe-Cds heterojunction is an example of this kind.

Figure 10 represents another unique case where $\chi_{2h} > \chi_{1h}$; $\chi_{1h} = \chi_{2e}$; $\chi_{2e} > \chi_{1e}$ thus making $-\Delta E_c = E_{g_1}$, $\Delta E_v = E_{g_2}$. No such pair exists at present.

Figure 11 represents pairs of semiconductors with $\chi_{2e} > \chi_{1h}$, making $-\Delta E_c > E_{g_1}$ and $\Delta E_v > E_{g_2}$. No such pair exists at present.

Thus, nine different cases in the energy-versus-distance diagram are obtained. Let us call each one a working space. In each working space, other important constraints can be imposed, such as work function, effective masses of carriers and type of semiconductors. Hence,

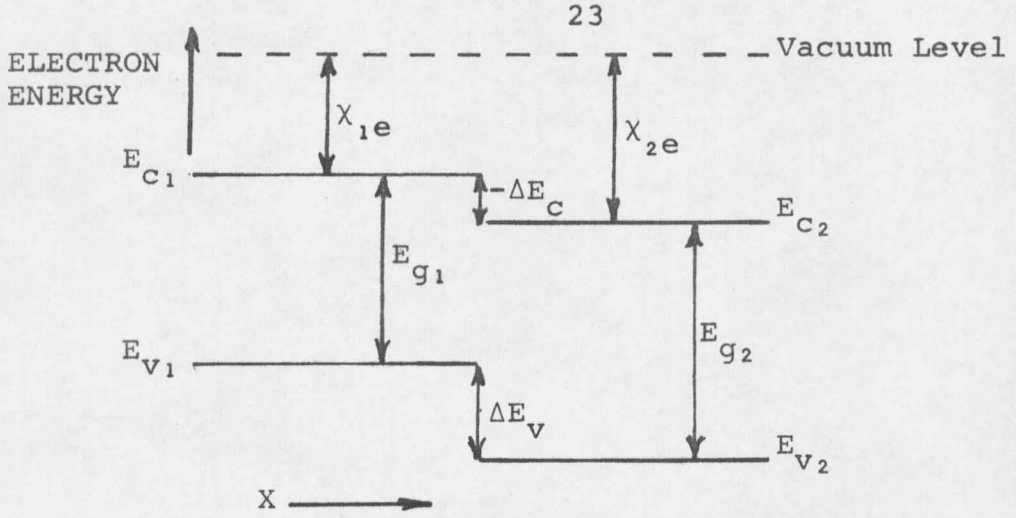


Figure 9. Energy-band diagram for two isolated semiconductors in which space charge neutrality is assumed to exist in every region with $\chi_{2h} > \chi_{1h} > \chi_{2e} > \chi_{1e}$.

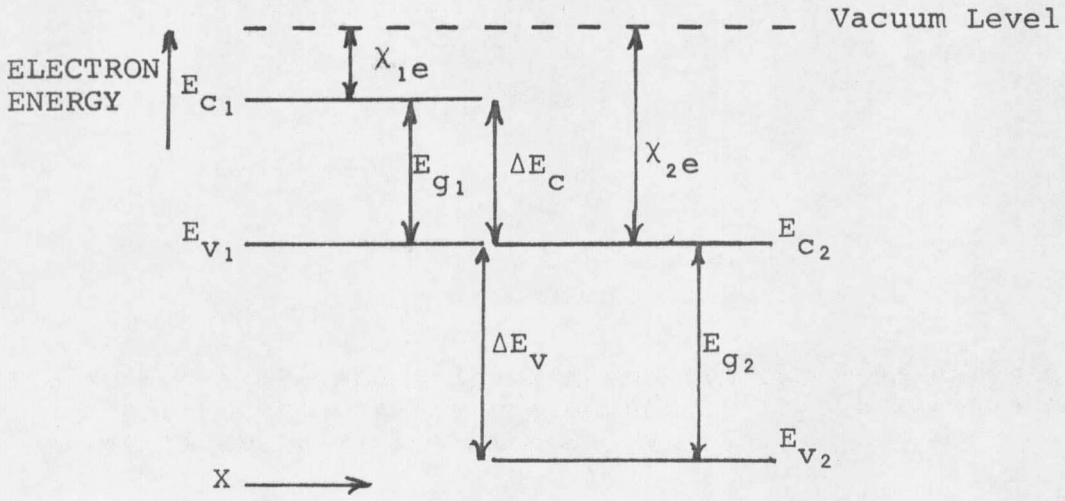


Figure 10. Energy-band diagram for two isolated semiconductors in which space charge neutrality is assumed to exist in every region with $\chi_{2h} > \chi_{1h} = \chi_{2e} > \chi_{1e}$.

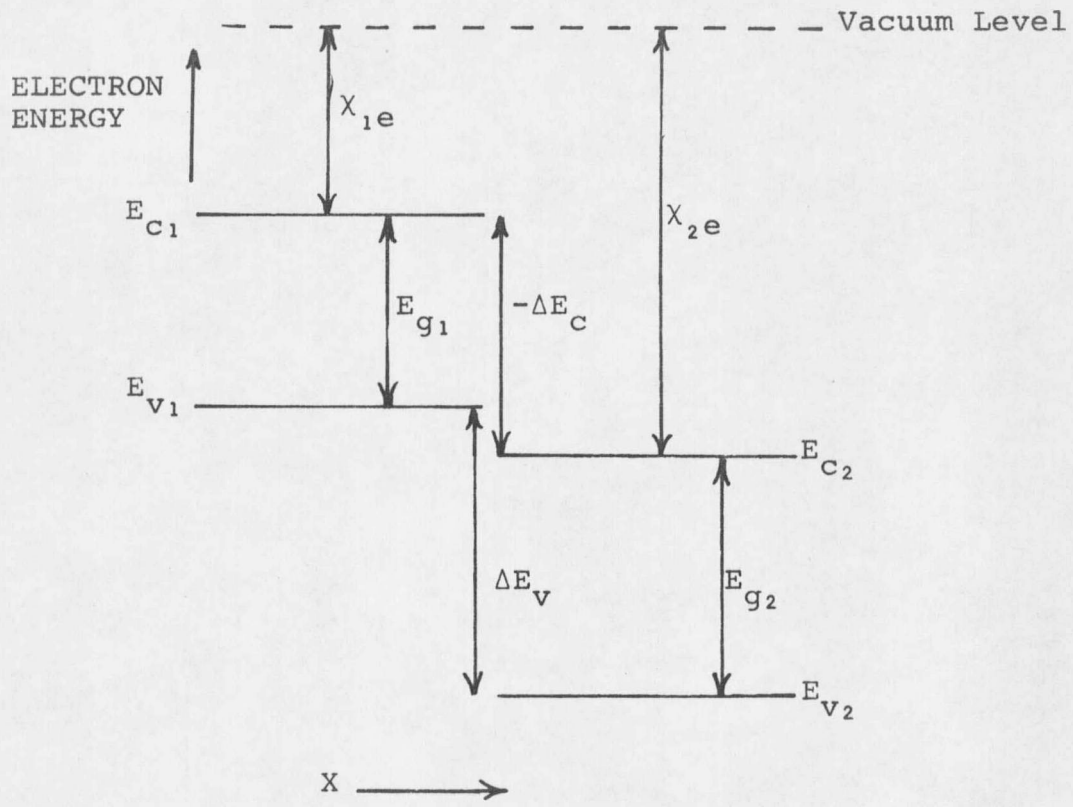


Figure 11. Energy-band diagram for two isolated semiconductors in which space charge neutrality is assumed to to exist in every region with $\chi_{2e} > \chi_{1h}$.

the following four possible constraints, each in three different forms, are possible and can be summarized as:

(1) $\phi_{m_1} > \phi_{m_2}$ or $\phi_{m_1} = \phi_{m_2}$ or $\phi_{m_1} < \phi_{m_2}$

(2) $m^*_{1e} > m^*_{2e}$ or $m^*_{1e} = m^*_{2e}$ or $m^*_{1e} < m^*_{2e}$

(3) $m^*_{1h} > m^*_{2h}$ or $m^*_{1h} = m^*_{2h}$ or $m^*_{1h} < m^*_{2h}$

(4) Direct gap semiconductor - Direct gap semiconductor, junction.

or

Direct gap semiconductor - Indirect gap semiconductor, junction.

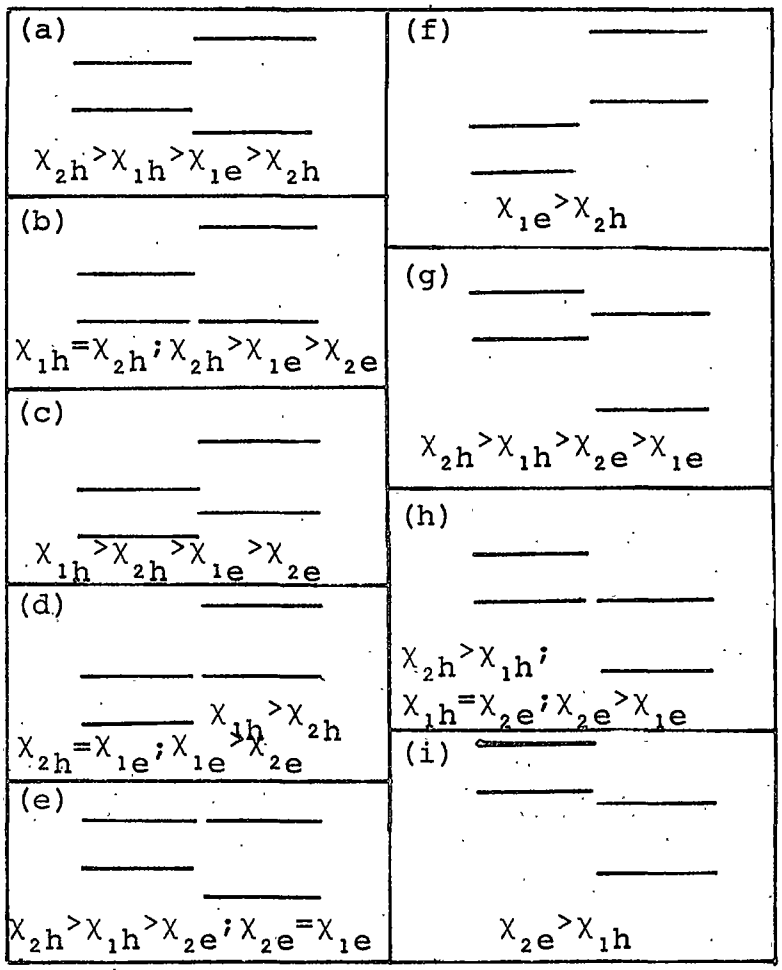
or

Indirect gap semiconductor - Indirect gap semiconductor, junction.

Hence, considering exhaustively all possible combinations of the above parameters and nine working spaces, a total number of different semiconductor heterojunctions can be $9 \times (3)^4 = 729$. Most of the junctions classified do not exist at present; however, they may exist in future with the development of new semiconductor materials with new parameters. The classification presented here is very general and unique; it includes the intrinsic semiconductor heterojunction also, and takes care of junctions yet to be discovered. On the following page a summary of the

Semiconductor Heterojunction Classification Chart

I. Working Spaces



II Fermi Level	III Electron Mass	IV Hole Mass	V Type of Semiconductor
$\phi_{m_1}>\phi_{m_2}$	$m^*_{1e}>m^*_{2e}$	$m^*_{1h}>m^*_{2h}$	Direct gap - Direct gap
$\phi_{m_1}=\phi_{m_2}$	$m^*_{1e}=m^*_{2e}$	$m^*_{1h}=m^*_{2h}$	Direct gap - Indirect gap
$\phi_{m_1}<\phi_{m_2}$	$m^*_{1e}<m^*_{2e}$	$m^*_{1h}<m_{2h}$	Indirect gap - Indirect gap

Figure 12. Semiconductor heterojunction classification chart.

semiconductor heterojunction classification chart is provided.

Importance of Classification

This section considers some of the general properties of each working space as influenced by the position of the Fermi level in the two semiconductors.

(a) Consider the most common working space described by $\chi_{2h} > \chi_{1h} > \chi_{1e} > \chi_{2e}$, as shown in Figure 3. It represents positive discontinuities in the conduction and valence-bands when isolated. On junction formation, however, the resultant barriers of electron and holes depend on the position of the Fermi level in each semiconductor. Three different cases are discussed.

If $\phi_{m_1} = \phi_{m_2}$, then on junction formation, isolated discontinuities appear as electron and hole barriers. No built-in voltage will be formed as shown in Figure 12(a).

If $\phi_{m_1} < \phi_{m_2}$, then on junction formation, the hole barrier from semiconductor 1 is independent of ΔE_c and will depend on the built-in potential supported by semiconductor 2. The electron barrier, however, will increase to $(V_{BHT} + \Delta E_v)$ as shown in Figure 13(b). In such a junction the hole current will dominate in a forward bias.

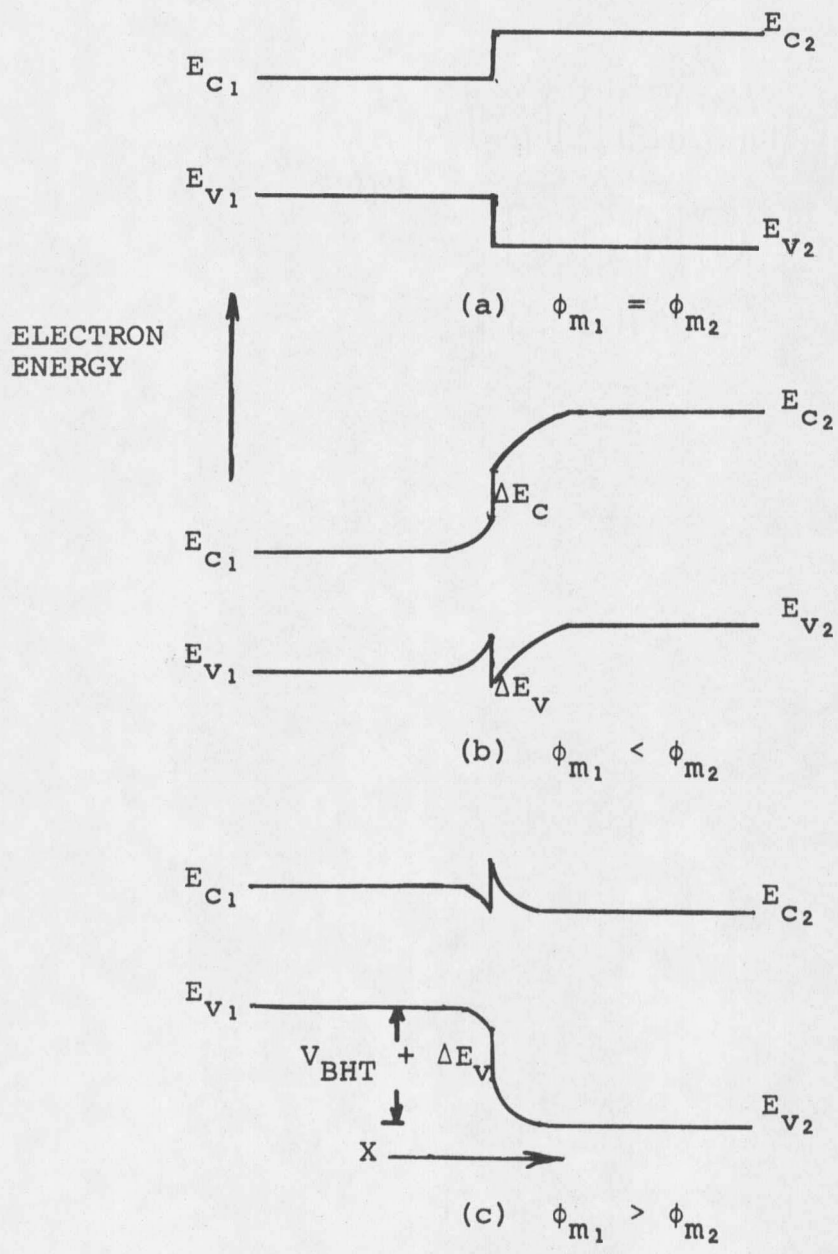


Figure 13. Energy-band diagram of two semiconductors in a thermal equilibrium that defines working space $\chi_{2h} > \chi_{1h} > \chi_{1e} > \chi_{2e}$.

This fact is also supported by Anderson [3] in connection with Ge-GaAs heterojunction. Hence, in such a structure, hole current will dominate electron current, where interface states do not play a significant role. If, however, interface states are present, the current may be governed by recombination and tunneling mechanisms via interface states [20]. Kroemer [12] has suggested that this kind of structure is useful for producing a wide-gap emitter transistor. Such a transistor will have a very high injection efficiency. A p-n-p wide-gap-emitter transistor will be obtained from such a structure. The injection efficiency of a p-n-p transistor is given by:

$$\gamma = \frac{J_p}{J_n + J_p} .$$

It can be noted from Figure 13(b) that electron current will be negligible due to the large electron barrier compared to the hole barrier. Therefore, high injection efficiency can be achieved.

If $\phi_{m_1} > \phi_{m_2}$, then on junction formation, the electron barrier from semiconductor 2 to semiconductor 1 is independent of ΔE_c and will depend on the built-in potential supported by semiconductor 2. The hole barrier, however, will

increase to $V_{BHT} + \Delta E_v$ as shown in Figure 13(c). When such a junction is forward biased, the electron current will dominate over hole current. An n-p-n wide-gap-emitter transistor can be obtained form such a structure, that will provide a high injection efficiency of electrons. Anderson [3] has obtained a photocell action from such a structure.

(b) Consider the next working space described by $\chi_{1h}=\chi_{2h}$, $\chi_{2h}>\chi_{1e}>\chi_{2e}$ (Figure 4). This configuration represents a positive discontinuity in the conduction-band and no discontinuity in the valence-band when isolated. On junction formation, however, the resultant barriers for electron and holes are obtained depending on the position of the Fermi level in each semiconductor. Three different cases are discussed.

If $\phi_{m_1}=\phi_{m_2}$, then on junction formation an isolated discontinuity appears in the conduction-band as an electron barrier. No built-in voltage will be formed as shown in Figure 14(a).

If $\phi_{m_1}<\phi_{m_2}$, then the hole barrier is V_{BHT}, with the valence-band being similar to that of the valence-band of a homojunction. The electron barrier, however, will increase to $(\Delta E_c + V_{BHT})$ as shown in Figure 14(b). This structure has been used for the confinement of electrons

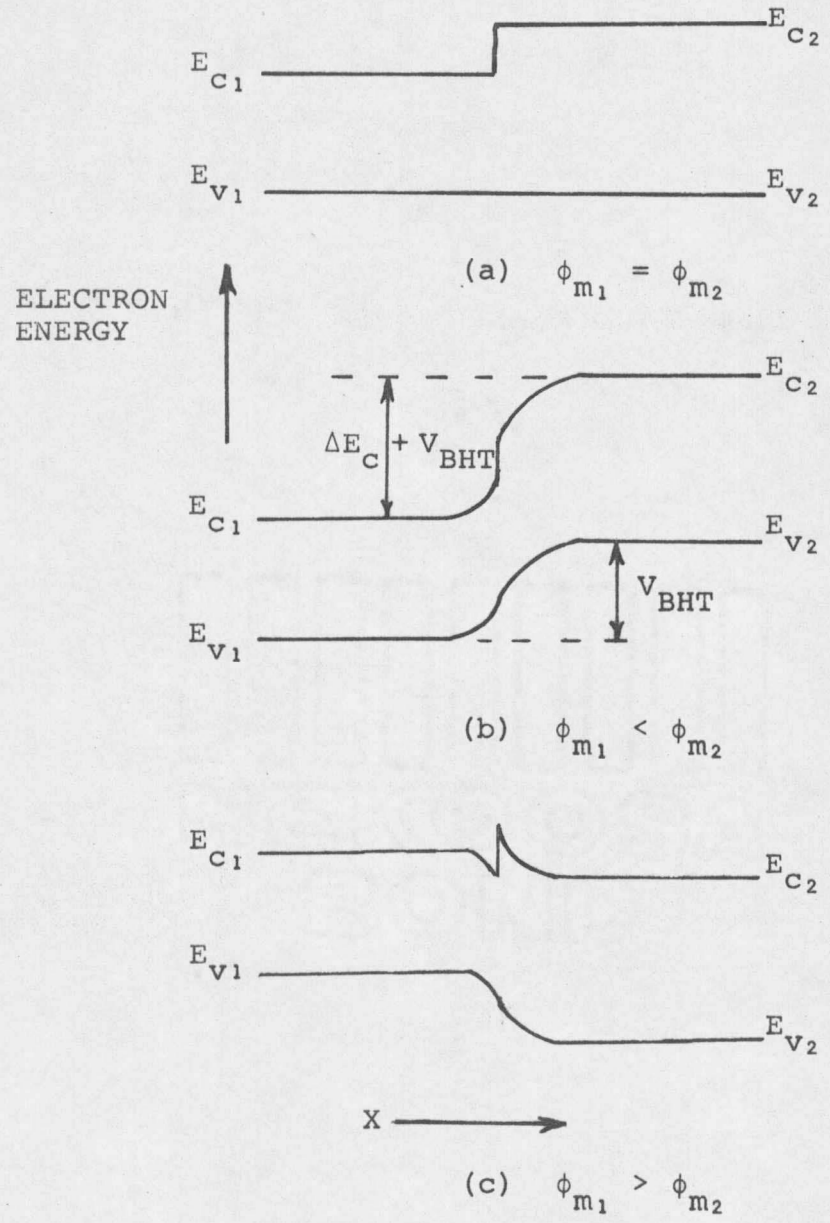


Figure 14. Energy-band diagram of two semiconductors in thermal equilibrium that defines the working space $\chi_{1h}=\chi_{2h}$; $\chi_{2h}>\chi_{1e}>\chi_{2e}$.

in a GaAs-$Al_xGa_{1-x}As$ heterostructure laser [1]. A p-n-p wide-gap-emitter transistor can be obtained from such a structure that will provide a high injection efficiency of holes.

If $\phi_{m_1} > \phi_{m_2}$, then on junction formation, the electron barrier from semiconductor 2 to semiconductor 1 is independent of ΔE_c and will depend on the built-in potential supported by semiconductor 2. The hole barrier is equal to V_{BHT} as shown in Figure 14(c).

Such a structure does not suggest any improvement in injection efficiency over a homojunction transistor, due to the absence of a positive discontinuity in valence-band.

(c) Consider the next working space described by $\chi_1 h > \chi_2 h > \chi_1 e > \chi_2 e$ as shown in Figure 5. It represents a positive discontinuity in the conduction-band and a negative discontinuity in the valence-band, when the two semiconductors are isolated. On junction formation, the resultant barrier of electrons and holes is obtained, depending on the position of the Fermi level in each semiconductor. Three different cases are shown in Figure 15 arising from $\phi_{m_1} = \phi_{m_2}$; $\phi_{m_1} < \phi_{m_2}$ and $\phi_{m_1} > \phi_{m_2}$

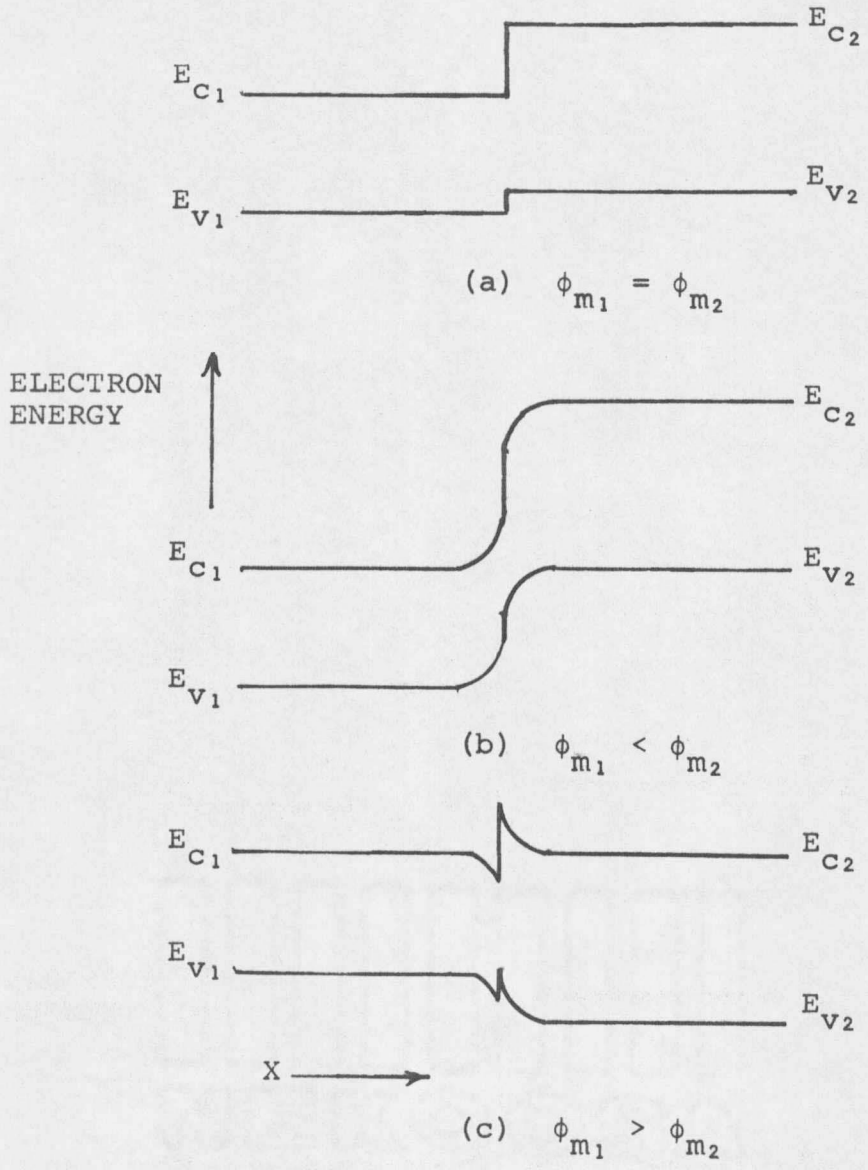


Figure 15. Energy-band diagram of two semiconductors in thermal equilbrium that defines the working space $\chi_{1h} > \chi_{2h} > \chi_{1e} > \chi_{2e}$.

It can be seen that for $\phi_{m_1} < \phi_{m_2}$, the electron barrier increases to $(\Delta E_c + V_{BHT})$ and the hole barrier also increases to $(\Delta E_v + V_{BHT})$. For $\phi_{m_1} > \phi_{m_2}$, both electron and hole barrier are independent of ΔE_c and ΔE_v.

The CdSe-Se heterojunction as studied by Moore et al. [21] and Lang et al. [22] belongs to this working space. P-Se/n-CdSe shows excellent rectification properties and a 70-volt reverse breakdown voltage.

(d) Consider the next working space described by $\chi_{1h} > \chi_{2h}$; $\chi_{2h} = \chi_{1e}$; $\chi_{1e} > \chi_{2e}$ as shown in Figure 6. It represents positive discontinuity ΔE_c equal to E_{g_2} and a negative discontinuity ΔE_v equal to E_{g_1}. On junction formation, the resultant barrier for electrons and holes is obtained depending on the position of the Fermi level.

It can be seen that $\phi_{m_1} < \phi_{m_2}$ is possible only if the narrow-gap semiconductor is a highly degenerate n-type and the broad-gap semiconductor is a highly degenerate p-type. The $\phi_{m_1} = \phi_{m_2}$ case is also possible with degenerate semiconductors only. For $\phi_{m_1} > \phi_{m_2}$, however, a heterojunction is possible with nondegenerate semiconductors as shown in Figure 16.

It can be seen that a high electric field is present in the transition region. Such a diode should,

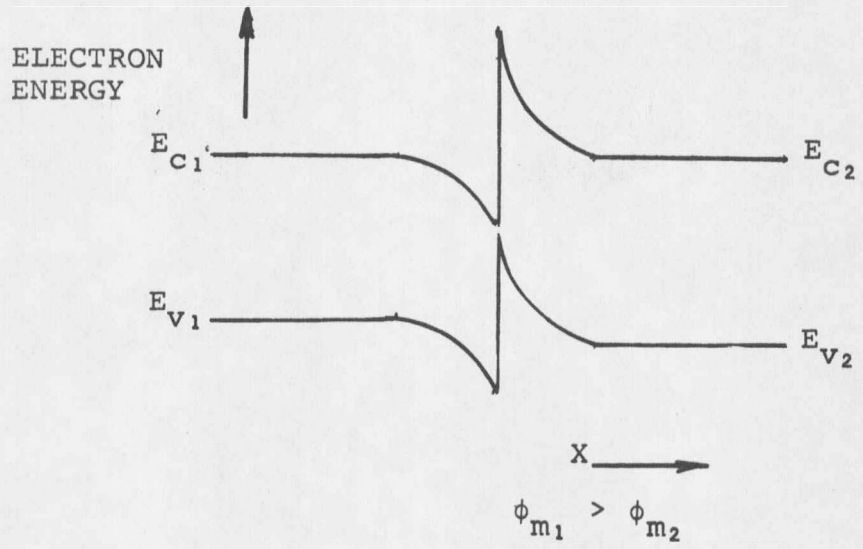


Figure 16. Energy-band diagram of two semiconductors in thermal equilibrium that defines the working space $\chi_{1h} > \chi_{2h}$; $\chi_{2h} = \chi_{1e}$; $\chi_{1e} > \chi_{2e}$.

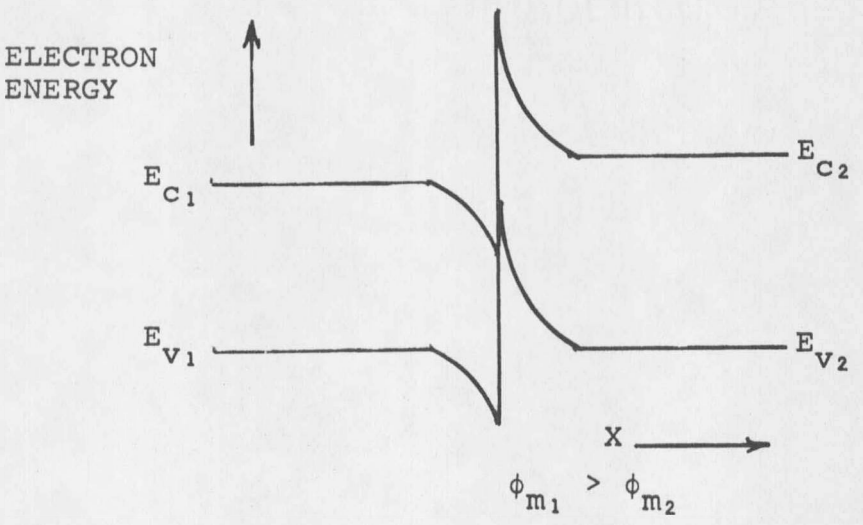


Figure 17. Energy-band diagram of two semiconductors in thermal equilibrium that defines the working space $\chi_{1h} > \chi_{1e} > \chi_{2h} > \chi_{1e}$.

therefore, have a low avalanche breakdown voltage. This electric field may also be used to produce a low work function of the narrow gap semiconductor [23] by applying a thin coating of broad-gap semiconductor on to the narrow-gap semiconductor. This produces high-yield photoemissive cathodes [23].

(e) Consider the next working space described by $\chi_{1h} > \chi_{1e} > \chi_{2h} > \chi_{1e}$, as shown in Figure 7. It represents a positive discontinuity ΔE_c greater than E_{g_2}, and a negative discontinuity ΔE_v greater than E_{g_1}.

As discussed in case (d), $\phi_{m_1} < \phi_{m_2}$ and $\phi_{m_1} = \phi_{m_2}$ may be possible in this case only with highly degenerate semiconductors. These cases will not be discussed here since the discontinuity itself will depend on the doping level [3].

For $\phi_{m_1} > \phi_{m_2}$, a high electric field can be obtained as shown in Figure 17. Such a diode should have a low avalanche breakdown voltage. The GaAs-Cs_2O heterojunction as proposed by Sonnenberg [23] is an example of this class. A thin coating of Cs_2O on GaAs can produce negative electron affinity [23] for GaAs. Such a structure may, therefore, be used to produce high-yield photoemissive cathodes.

(f) Consider the next working space described by $\chi_{2h} > \chi_{1h} > \chi_{2e}$; $\chi_{2e} = \chi_{1e}$ as shown in Figure 8. This configuration represents no discontinuity in the conduction-band but a positive discontinuity in the valence-band when isolated. On junction formation, however, the resultant barrier of electrons and holes is obtained, depending on the position of the Fermi level in each semiconductor. Three different cases are discussed.

If $\phi_{m_1} = \phi_{m_2}$, then on junction formation, an isolated discontinuity in the valence-band appears as a hole barrier. No built-in voltage will be formed as shown in Figure 18(a).

If $\phi_{m_1} < \phi_{m_2}$, then the hole barrier from semiconductor 2 to 1, depends on the built-in potential supported by semiconductor 2. The electron barrier from semiconductor 1 to 2 is V_{BHT}, as shown in Figure 18(b)

Such a structure does not suggest any improvement in injection efficiency over a homojunction transistor, because a positive discontinuity in the conduction-band is absent.

If $\phi_{m_1} < \phi_{m_2}$, then on junction formation, the electron barrier from semiconductor 2 to semiconductor 1 is

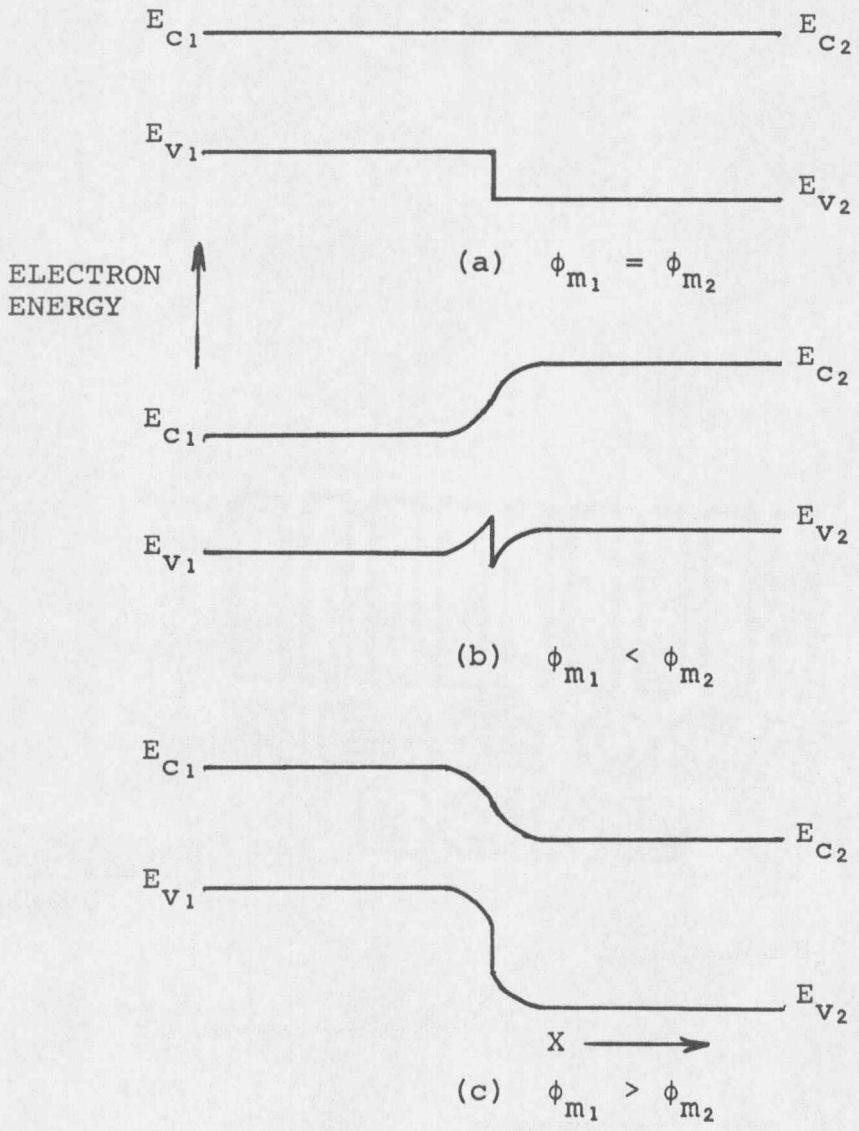


Figure 18. Energy-band diagram of two semiconductors in thermal equilibrium that defines working space $\chi_{2h} > \chi_{1h} > \chi_{2e}$; $\chi_{2e} = \chi_{1e}$.

V_{BHT}. The hole barrier will, however, become $(V_{BHT} + \Delta E_v)$, as shown in Figure 18(c). A n-p-n wide-gap emitter transistor can be obtained from such a structure that will provide a high injection efficiency of electrons.

GaSb-GaAs is an example belonging to this class. It is not of much interest, primarily because of the mismatch in lattice constants.

(g) Consider the next working space described by $\chi_{2h} > \chi_{1h} > \chi_{2e} > \chi_{1e}$, as shown in Figure 9. It represents a negative discontinuity in the conduction-band and a positive discontinuity in the valence-band, when two semiconductors are isolated. Three different cases are shown in Figure 19 arising due to $\phi_{m_1} = \phi_{m_2}$, $\phi_{m_1} < \phi_{m_2}$ and $\phi_{m_1} > \phi_{m_2}$.

It can be seen that for $\phi_{m_1} < \phi_{m_2}$ the electron and hole barriers are independent of ΔE_c and ΔE_v as shown in Figure 19(b). For $\phi_{m_1} > \phi_{m_2}$, the electron and hole barriers are $(\Delta E_c + V_{BHT})$ and $(\Delta E_v + V_{BHT})$, respectively, as shown in Figure 19(c).

A similarity of this work space with that described in Figure 5 and discussed in (c) should be noted. In this case broad-gap semiconductor is of lower electron affinity and in (c) case, the narrow-gap semiconductor is of a lower electron affinity.

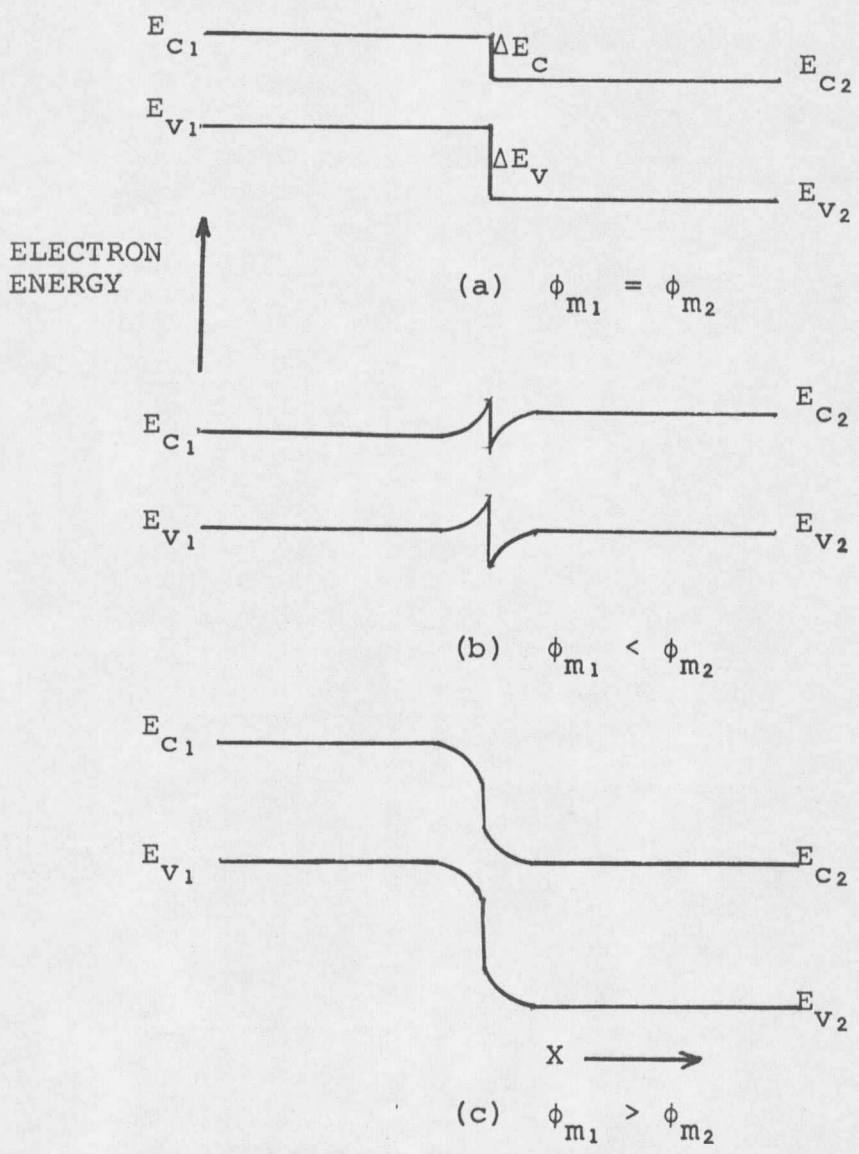


Figure 19. Energy-band diagram of two semiconductors in thermal equilibrium that defines the working space $\chi_{2h} > \chi_{1h} > \chi_{2e} > \chi_{1e}$.

A ZnTe-CdS heterojunction is an example of this class. This class has been studied by S. N. Dobrynin [24] theoretically. He has concluded that in this working space if the lower electron-affinity material is p-type and the higher electron-affinity material is n-type, the best tunneling condition are possible. Thus, a heterojunction tunnel diode is possible in this working space or in the one described in case (c), which shows improved performance over the homojunction tunnel diode.

(h) Consider the next working space described by $\chi_{2h} > \chi_{1h}$; $\chi_{1h} = \chi_{2e}$; $\chi_{2e} > \chi_{1e}$, as shown in Figure 10. It represents a negative discontinuity in the conduction-band equal to E_{g_1} and a positive discontinuity in the valence-band equal to E_{g_2}. The similarity of this working class with that discussed in (d) should be noted.

It can be seen that $\phi_{m_1} > \phi_{m_2}$ and $\phi_{m_1} < \phi_{m_2}$ is possible with degenerate semiconductors only and, hence, is not considered. For $\phi_{m_1} < \phi_{m_2}$, however, a heterojunction is possible with a nondegenerate semiconductor and as shown in Figure 20.

It can be noted that a high electric field is present in the transition region. Such a diode should, therefore, have a low avalanche breakdown voltage. This

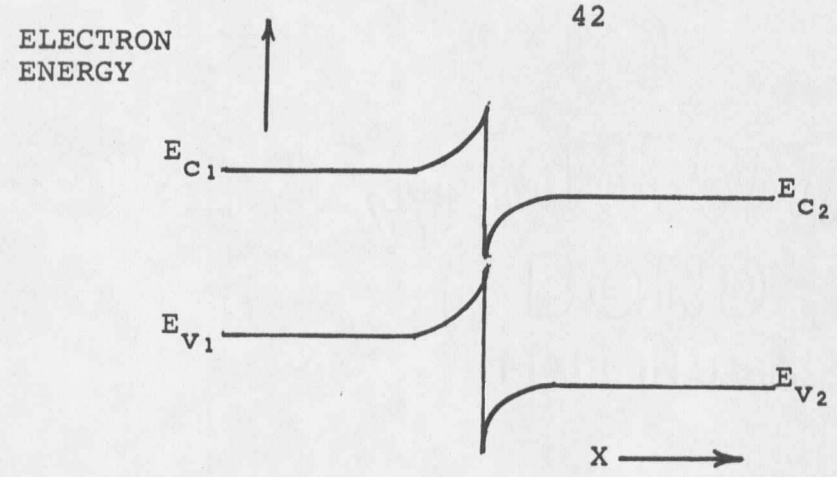


Figure 20. Energy-band diagram of two semiconductors in thermal equilibrium that defines the working space $\chi_{2h} > \chi_{1h}$; $\chi_{1h} = \chi_{2e}$; $\chi_{2e} > \chi_{1e}$.

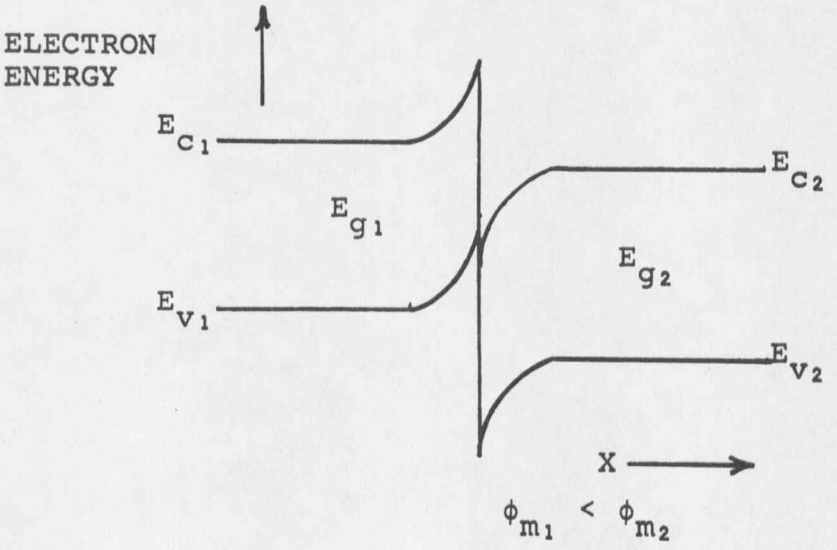


Figure 21. Energy-band diagram of two semiconductors in thermal equilibrium that defines the working space $\chi_{2h} > \chi_{1h}$.

electric field may also be used to produce low work function of the broad-gap semiconductor [23] by a thin coating of the narrow-gap semiconductor, thus producing a high-yield photoemissive cathode.

(i) Consider the next working space described by $\chi_{2e} > \chi_{1h}$. It represents a negative discontinuity of electron energy in the conduction-band, greater than E_{g_1} and a positive discontinuity of electron energy in the valence-band, greater than E_{g_2}, when isolated.

When a junction is formed, the resultant electron and hole barrier is produced which depends on the position of the Fermi levels in the two semiconductors. As discussed in (h), $\phi_{m_1} > \phi_{m_2}$ and $\phi_{m_1} = \phi_{m_2}$ are not considered here.

For $\phi_{m_1} < \phi_{m_2}$, however, a nondegenerate heterojunction is possible and as is shown in Figure 21.

It can be noted that a high electric field is present in the transition region. Such a diode should, therefore, have a low avalanche breakdown voltage. It can also be used in producing high-yield photoemissive cathodes.

Given a pair of semiconductors with known electron affinities and energy gaps, a unique working space can be assigned. Some general properties of the given heterojunction pair are thus known.

By knowing which semiconductor has the greater effective masses of electrons or holes, we get some idea about the structure of the conduction and the valence-band, respectively (see, for example, Appendix A). Effective masses also give some idea about the mobilities in the two semiconductors. A direct-gap semiconductor has a short lifetime of excited carriers compared to indirect-gap semiconductors. By knowing the type of semiconductor involved, one has more knowledge of the structure in E - K space (see Appendix A).

Chapter 3

ANALYSIS OF ELECTRIC FIELD

This chapter describes a theory of electric field formation in metal-metal junctions, homojunctions and heterojunctions. Expressions for built-in voltage are derived. Distributions of carrier concentrations are plotted, and a practical model of the n-p semiconductor heterojunction is proposed and analyzed.

General Theory

Junctions between metals, metals and semiconductors or different semiconductors with different doping levels, result in a built-in electric field at the contact. Two different metals, in general, have different conductivities at a given temperature because different concentrations of electrons are available at that temperature:

$$n_{cu} = 8 \times 10^{22}/cm^3, \; n_{Ag} = 6 \times 10^{22}/cm^3.$$

If a contact is made between two different conductors, an exchange of electrons will take place by diffusion corresponding to the concentration gradient, which causes the substance whose concentration of electrons is initially lower to become more negative than the other. Thus, a

potential is set up at the boundary. This potential does not allow additional net diffusion to take place. A semiconductor homojunction and semiconductor heterojunction are considered in the following discussion.

Semiconductor homojunction. Suppose that an abrupt p-n junction is somehow formed instantaneously by joining a uniform p-type sample to a uniform n-type sample to form a single crystal. At the instant of formation there exists a uniform concentration n_1 of mobile free electrons, and p_1 mobile free holes, on the n-side extending to the junction. On the p-side a uniform concentration of p_2 mobile holes and n_2 free electrons also extend to the junction. These concentrations are related to the net donor and acceptor densities at a temperature, while, of course, on either side the electron and hole densities satisfy the relation:

$$n_1 p_1 = n_2 p_2 = n_i^2.$$

Since the concentration n_1 of electrons on the n-side is much larger than the electron concentration n_2 on the p-side, at the instant of formation there exists an enormous

gradient in the concentration of electrons at the junction between the two regions. The same situation exists with respect to hole concentration at the junction. The large initial concentration gradients set up diffusion currents; electrons from the n-region flow down the respective concentration gradients into the region of opposite conductivity type leaving the region near the junction depleted of majority carriers. This initial diffusion flow cannot continue indefinitely because as the regions near the junction become depleted of majority carriers, the charges of the fixed donor and acceptor ions near the junction are no longer balanced by the charges of the mobile free carriers which were formerly there, and so an electric field is built up. The direction of this electric field is such as to oppose the flow of electrons out of the n-region and the flow of holes out of the p-region, and thus the magnitude of the field builds up to the point where its effect exactly counteracts the tendency for majority carriers to diffuse down the concentration "hill" into the region of the opposite conductivity type. A condition of thermal equilibrium is established in which the region near the junction is depleted of majority carriers and in which

space charge layers containing high electric fields are formed near the junction.

Alternatively, the situation can be described in terms of an energy-band model. Consider the energy-band diagram of isolated n-p semiconductors as shown in Figure 22. The position of the Fermi level in the n-type semiconductor is represented by E_{F_1} and in the p-type semiconductor is represented by E_{F_2}.

It is known that within a solid or system of solids in thermal equilibrium the Fermi level E_F has everywhere the same value. Hence, when a junction is formed, we expect an exchange of carriers. The electrons will move to the p-type semiconductor or, equivalently, the holes will move to the n-type semiconductors. The energy-band diagram of an n-p homojunction in thermal equilibrium is described in Figure 23. The electrostatic potential difference $\psi(x)$ between any two points can be represented by the vertical displacement of the band edges. The distance over which ψ changes is called the transition region. The electrostatic field can be represented by the slope of the band edges on the diagram. The built-in voltage, V_{BHM}, is represented on the diagram.

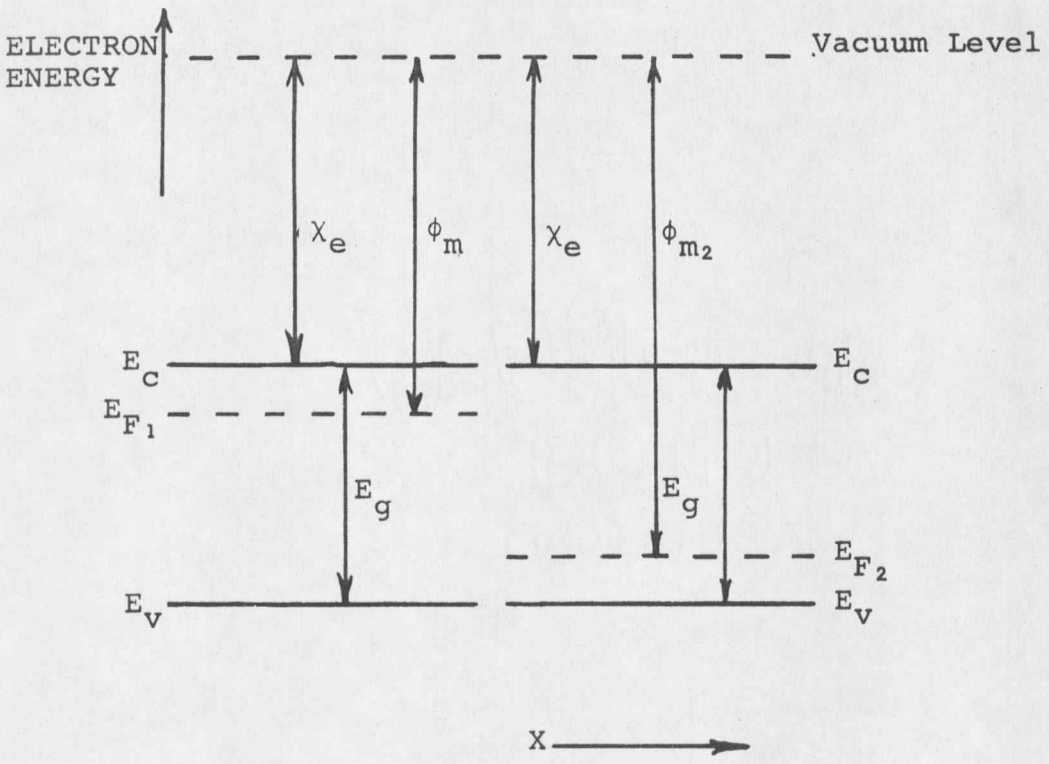


Figure 22. Energy-band diagram of isolated n-p semiconductors of the same element in which space charge neutrality is assumed to exist in every region.

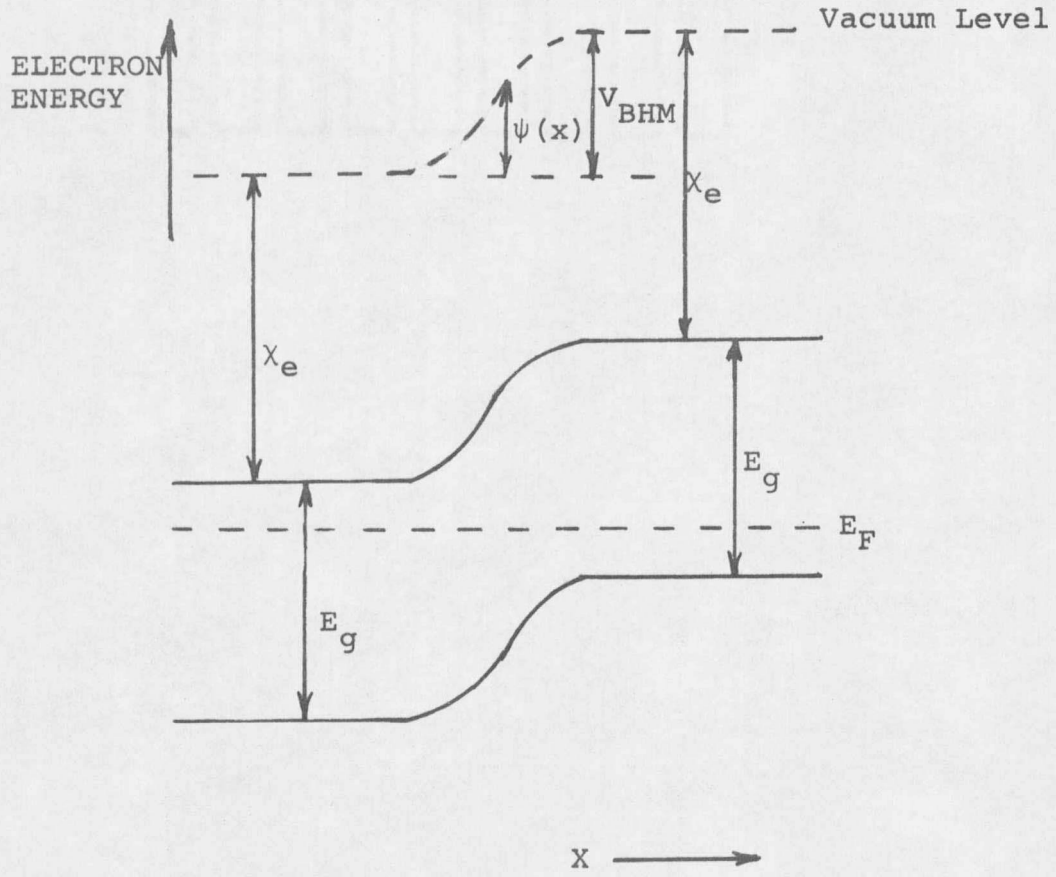


Figure 23. Energy-band diagram of n-p homojunction in thermal equilibrium.

Semiconductor heterojunction. In the case of heterojunctions, the situation is complicated by energy discontinuities ($\Delta E_c, \Delta E_v$). In two isolated semiconductors, as shown in Figure 1, the positive discontinuities ($\Delta E_c, \Delta E_v$) represent barriers for holes and electrons to flow from the narrow-gap semiconductors to the broad-gap semiconductors. At the instant of formation there exists a uniform concentration of n_1 mobile free electrons and p_1 mobile free holes on the n-side extending to the junction, and on the p-side, a uniform concentration of p_2 mobile holes and n_2 free electrons, also extending to the junction. In the case of extrinsic semiconductors these concentrations are related to the net donor and acceptor densities at a given temperature, while, of course, on either side electron and hole densities satisfy the relations:

$$n_1 p_1 = n_{i_1}^2, \quad n_2 p_2 = n_{i_2}^2.$$

In general, the concentration n_1 of electrons on the n-side is much larger than the electron concentration n_2 on the p-side. At the instant of formation there exists an enormous gradient in the concentration of electrons at

the junction between the two regions. The same situation exists with respect to hole concentration at the junction. Built-in voltage, in the case of a heterojunction, is a function of energy discontinuities ($\Delta E_c, \Delta E_v$), effective masses ($m^*_{1e}, m^*_{2e}, m^*_{1h}, m^*_{2h}$) and concentration gradients as shown in the following section. Therefore, in the case of a heterojunction in addition to concentration gradient, the effect of unequal discontinuities and effective masses should be considered.

At the time of junction formation, a flow of appropriate carriers takes place across the junction and the Fermi levels of the two semiconductors line up in thermal equilibrium. The flow of carriers in turn gives rise to a built-in voltage which does not allow any further flow. In the next section, the built-in voltage in heterojunctions will be derived for a general case.

Built-in Voltage

Consider a semiconductor heterojunction composed of semiconductors with only 1/2% or less mismatch in the lattice constant so that the effects of interface states can be ignored [25]. Nondegenerate semiconductors are

under consideration so that Boltzmann statistics is valid. Assume that thermal equilibrium exists so that the Fermi levels are lined up. Donors and acceptors are assumed to be ionized so that the built-in voltage expression is independent of acceptor and donor ionization energies. Consider an n-p isolated semiconductor with $\phi_{m_2} > \phi_{m_1}$, as shown in Figure 24.

When the junction is formed to line up Fermi levels, higher energy electrons flow to lower energy levels (and/or higher energy holes should go to lower energy levels), making the lower energy side negative with respect to the higher energy side. The built-in voltage in a semiconductor heterojunction is given by: $V_{BHT} = \frac{E_{F_1} - E_{F_2}}{q}$

where $E_{F_1} = E_{c_1} - kT \ln \left(\frac{N_{c_1}}{N_{D_1}}\right)$

$$E_{F_2} = E_{v_2} + kT \ln \left(\frac{N_{v_2}}{N_{A_2}}\right)$$

where: N_c is the density of states in conduction-band and is given by

$$N_c = 2\left(\frac{2\pi m_c^* kT}{\hbar^2}\right)^{3/2},$$

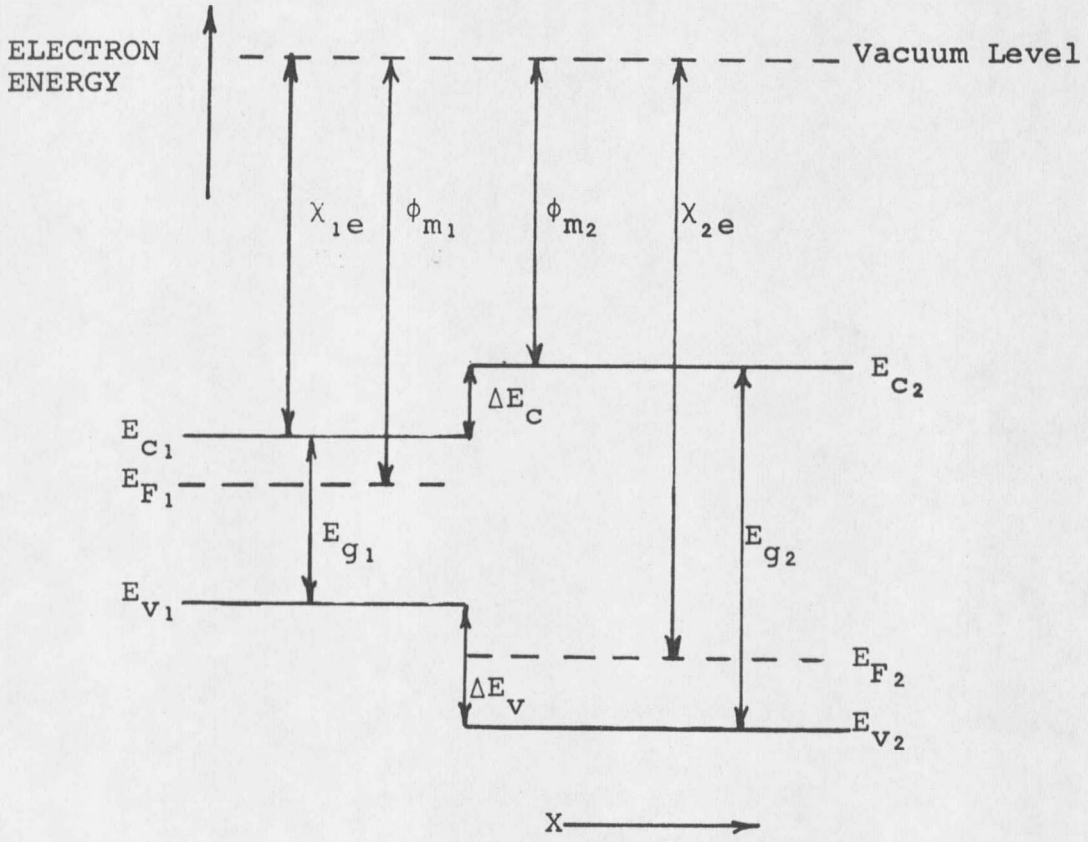


Figure 24. Energy-band diagram for two isolated semiconductors in which space charge neutrality is assumed to exist in every region with $\phi_{m_1} < \phi_{m_2}$.

and N_V is the density of states in valence-band, given by

$$N_V = 2\left(\frac{2\pi m_h^* kT}{\bar{h}^2}\right)^{3/2}.$$

Therefore, $$V_{BHT} = \frac{E_{c_1} - E_{v_2}}{q} - \frac{kT}{q} \ln \left(\frac{N_{c_1}}{N_{D_1}} \cdot \frac{N_{v_2}}{N_{A_2}}\right)$$

From Figure 1 we obtain

$$V_{BHT} = \frac{E_{g_1} + \Delta E_v}{q} - \frac{kT}{q} \ln \left(\frac{N_{c_1}}{N_{D_1}} \cdot \frac{N_{v_2}}{N_{A_2}}\right).$$

But $E_{g_1} = kT \ln \left(\frac{N_{c_1} N_{v_1}}{n_1 p_1}\right)$, and the donors and acceptors are assumed to be all ionized, i.e., $N_{D_1} = n_1$; $N_{A_2} = p_2$ and hence:

$$V_{BHT} = \frac{\Delta E_v}{q} - \frac{kT}{q} \ln \left(\frac{N_{c_1}}{n_1} \cdot \frac{N_{v_2}}{p_2} \cdot \frac{n_1 p_1}{N_{c_1} \cdot N_{v_1}}\right)$$

$$\text{or} \quad V_{BHT} = \frac{\Delta E_v}{q} - \frac{kT}{q} \ln \left(\frac{N_{v_2}}{N_{v_1}} \cdot \frac{p_1}{p_2}\right). \qquad (1)$$

But, $E_{g_2} - E_{g_1} = \Delta E_v + \Delta E_c = kT \ln \left(\frac{N_{c_2}}{N_{c_1}} \cdot \frac{N_{v_2}}{N_{v_1}} \cdot \frac{n_1 p_1}{n_2 p_2}\right)$.

We can put the above expression in the form of,

$$V_{BHT} = \frac{-\Delta E_c}{q} + \frac{kT}{q} \ln \left(\frac{N_{c_2}}{N_{c_1}} \cdot \frac{n_1}{n_2}\right). \qquad (2)$$

Equations 1 and 2 can be combined in the form of:

$$V_{BHT} = \frac{\Delta E_v - \Delta E_c}{2q} + \frac{kT}{2q} \ln \left(\frac{p_2\ n_1}{p_1\ n_2} \cdot \frac{N_{v_1} \cdot N_{c_2}}{N_{c_1} \cdot N_{v_2}}\right). \qquad (3)$$

Equations 1, 2 and 3 are equivalent so that depending on the kind of heterojunction involved, one can select the appropriate equation. The above relations hold for all kinds of heterojunctions classified with $\phi_{m_2} > \phi_{m_1}$. For $\phi_{m_2} < \phi_{m_1}$, V_{BHT} changes sign in all equations. Since the discontinuities ($\Delta E_c, \Delta E_v$) depend on band gaps and electron affinities, the above equation can be helpful to the designer in choosing appropriate semiconductors for required built-in voltage.

The built-in voltage for an intrinsic semiconductor heterojunction can be obtained by simply substituting $p_1 = n_1$ and $p_2 = n_2$ in equation 3.

$$V_{BHT}\Big|_{\text{intrinsic}} = \frac{\Delta E_v - \Delta E_c}{2q} + \frac{kT}{2q} \ln \left(\frac{N_{v_1}}{N_{c_1}} \cdot \frac{N_{c_2}}{N_{v_2}}\right)$$

$$= \frac{\Delta E_v - \Delta E_c}{2q} + \frac{3}{4}\frac{kT}{q} \ln \left(\frac{m^*_{1h}\ m^*_{2e}}{m^*_{1e}\ m^*_{2h}}\right) \qquad (4)$$

The distributions of built-in voltages supported on each side of the junction are not equal. The transition region lies more on the side of lower conductivity. Generally,

built-in voltages supported by a wide-gap semiconductor is greater in heterojunctions.

The built-in voltage expression, described by equation 3 can be rewritten in the form of:

$$V_{BHT} = \frac{\Delta E_v - \Delta E_c}{2q} + \frac{kT}{2q} \ln \left(\frac{N_{v_1} N_{c_2}}{N_{c_1} \cdot N_{v_2}}\right) + \frac{kT}{2q} \ln \left(\frac{p_2 n_1}{p_1 n_2}\right).$$

or $$V_{BHT} = [V_{BHT_1}] + [V_{BHT_2}].$$

where $$V_{BHT_1} = \frac{\Delta E_v - \Delta E_c}{2q} + \frac{kT}{2q} \ln \left(\frac{N_{v_1}}{N_{c_1}} \cdot \frac{N_{c_2}}{N_{v_2}}\right) \quad (5)$$

and $$V_{BHT_2} = \frac{kT}{2q} \ln \left(\frac{p_2 n_1}{p_1 n_2}\right). \quad (6)$$

V_{BHT_1} is the component of built-in voltage obtained from unequal discontinuities and effective masses; i.e., the built-in voltage due to intrinsic semiconductors. This component of built-in voltage is fixed when two semiconductors are chosen. By changing temperature or pressure, slight variations in this component may be achieved. This component of voltage can also be changed by heavy doping which can change basic properties of semiconductors.

The other component of built-in voltage V_{BHT_2} arises because of different carrier concentrations on the two sides of the junction. This component resembles the total

built-in voltage in a homojunction and it vanishes for an intrinsic junction.

It should be noted that the sign of V_{BHT_1} is fixed for a heterojunction depending upon the basic properties of the semiconductors, while the sign of V_{BHT_2} is controllable by doping levels in two semiconductors. To have the net built-in voltage be zero, V_{BHT_1} and V_{BHT_2} are required to be equal in magnitude but opposite in sign.

The component of built-in voltage, V_{BHT_1} if it exists, must result from some difference in charge across the junction. Let us find an equivalent charge ratio $(\frac{Q_1}{Q_2})$ due to unequal discontinuities ($\Delta E_c \neq \Delta E_c$) and effective masses. For simplicity let us equate $\frac{kT}{2q} \ln (\frac{Q_1}{Q_2})$ to V_{BHT_1}, described by equation (5), i.e., we can represent V_{BHT_1} in a form which is similar to V_{BHT_2}:

$$\frac{kT}{2q} \ln (\frac{Q_1}{Q_2}) = V_{BHT_1}$$

$$\frac{kT}{2q} \ln [\frac{Q_1}{Q_2}] = \frac{\Delta E_v - \Delta E_c}{2q} + \frac{kT}{2q} \ln \left\{ \frac{N_{v_1} \cdot N_{c_2}}{N_{c_1} \cdot N_{v_2}} \right\}$$

This equation can be solved for $\frac{Q_1}{Q_2}$ and the solution can be expressed as follows:

$$\frac{Q_1}{Q_2} = e^{\frac{\Delta E_v - \Delta E_c}{kT}} \cdot \left[\frac{N_{v_1} \cdot N_{c_2}}{N_{c_1} \quad N_{v_2}}\right] \tag{7}$$

Now the built-in voltage at the heterojunction can be expressed as

$$\begin{aligned} V_{BHT} &= V_{BHT_1} + V_{BHT_2} \\ &= \frac{kT}{2q} \ln \left(\frac{Q_1}{Q_2}\right) + \frac{kT}{2q} \ln \left[\frac{p_2 \; n_1}{n_2 \; p_1}\right] \\ &= \frac{kT}{2q} \ln \left[\frac{p_2 \; n_1}{n_2 \; p_1} \frac{Q_1}{Q_2}\right] \end{aligned} \tag{8}$$

where Q_1 and Q_2 are related by the equation (7). For a homojunction we have,

$$\Delta E_v = \Delta E_c = 0 \; ,$$
$$N_{v_1} = N_{v_2} = N_v \; ,$$
$$N_{c_1} = N_{c_2} = N_c \; .$$

Hence, equation (7) gives $\frac{Q_1}{Q_2} = 1$.

Therefore, built-in voltage in the case of homojunction is given by equation (8), as

$$V_{BHM} = \frac{kT}{2q} \ln \left[\frac{p_2 \; n_1}{n_1 \; p_2}\right],$$

which is known to be true.

Distribution of Carriers

The distribution of carriers at a semiconductor heterojunction differs considerably from that of a homojunction. For a homojunction, of course, the np product is equal to n_i^2 everywhere in the semiconductor at thermal equilibrium. Concentration gradients of both holes and electrons must exist at the junction. The concentration gradients near the metallurgical junction are normally very large because the equilibrium minority-carrier concentrations are usually at least three orders of magnitude below the corresponding majority-carrier concentration. The approximate distribution of carriers near the boundary plane of a typical germanium pn junction in equilibrium at room temperature is shown in Figure 25.

For a semiconductor heterojunction, the relation $n_1 p_1 = n_{i_1}^2 \neq n_2 p_2 = n_{i_2}^2$ suggests that under ideal conditions, there exists an abrupt change in the carrier concentration across heterojunction. Consider the following relations that must be true on either side of the junction in thermal equilibrium.

$$n_1 p_1 = n_{i_1}^2 = N_{c_1} N_{v_1} e^{-\frac{E_{g_1}}{kT}}$$

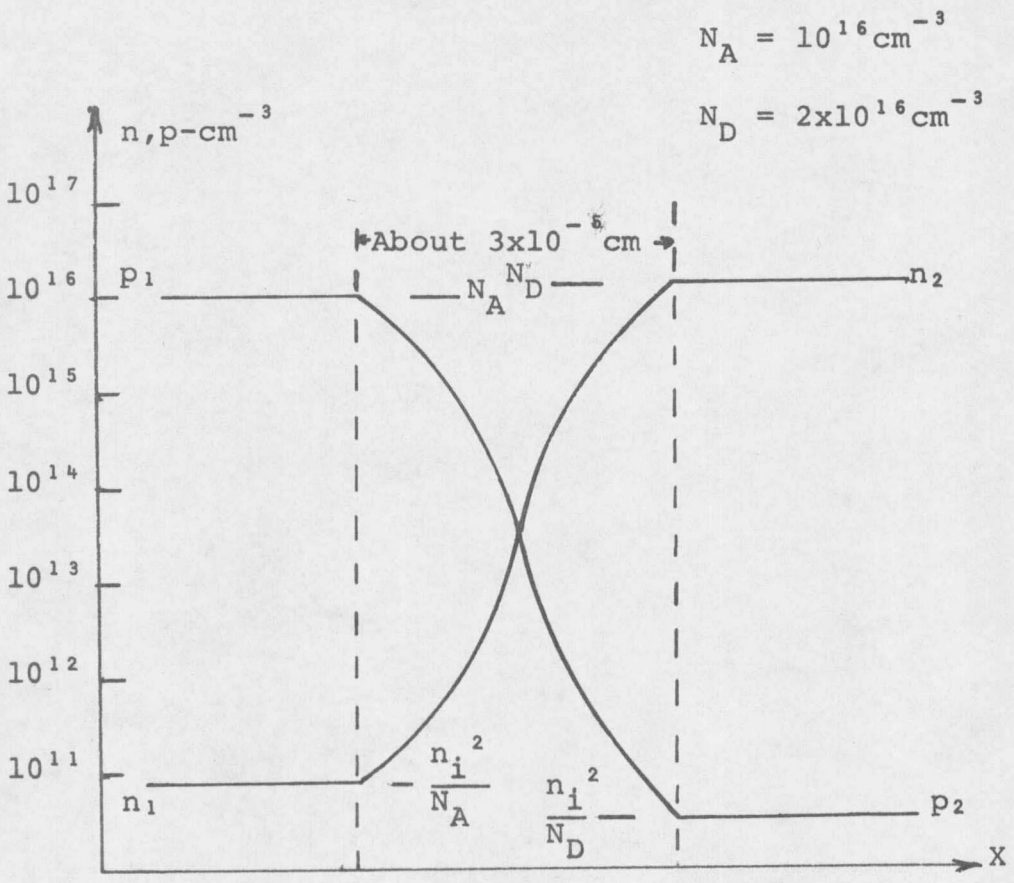


Figure 25. Approximate distribution of carriers near the boundary plane of a germanium p-n junction at room temperature [26].

$$n_2 p_2 = n_{i_2}^2 = N_{c_2} N_{v_2} e^{\frac{-E_{g_2}}{kT}} \quad \text{and} \quad n_{i_1} > n_{i_2}$$

Therefore,

$$\frac{n_1}{n_2} = \frac{p_2}{p_1} \cdot \left(\frac{m^*_{n_1}}{m^*_{n_2}} \cdot \frac{m^*_{p_1}}{m^*_{p_2}}\right) e^{+\left(\frac{\Delta E_c + \Delta E_v}{kT}\right)}$$

or $$\frac{n_1}{n_2} = K^* \frac{p_2}{p_1},$$

where $$K^* = \left(\frac{m^*_{n_1}}{m^*_{n_2}} \frac{m^*_{p_1}}{m^*_{p_2}}\right) e^{+\left(\frac{\Delta E_c + \Delta E_v}{kT}\right)} \qquad (9)$$

is a constant which is much greater than one for $n_{i_1} > n_{i_2}$.

Consider the following example:

Consider GaSb-InAs, a heterojunction, which has the following constants [27]:

$$m^*_{n_1} = .02 \qquad m^*_{n_1} = 0.41$$

$$m^*_{n_2} = .04 \qquad m^*_{h_2} = 0.5$$

$$\Delta E_c = 0.84 \text{ eV.}$$

$$\Delta E_v = -0.52 \text{ eV.}$$

$$K^* = \left(\frac{0.02 \times .41}{0.04 \times .5}\right) e^{+\left(\frac{\Delta E_c + \Delta E_v}{kT}\right)}$$

For $T = 300°K$

$$K^* = (0.41) e^{+12.7}$$

$$K^* = 1 \times 10^5 >> 1.$$

(a) The value of the constant K^* in the case of homojunction is given as follows:

$$m^*_{n_1} = m^*_{n_2} = m^*_e$$

$$m^*_{p_1} = m^*_{p_2} = m^*_h$$

and $\Delta E_c + \Delta E_v = 0$

Hence, $K^* = 1$ for any homojunction.

(b) The value of the constant K^* in the case of a heterojunction with $\Delta E_c = 0$ and $m^*_{n_1} = m^*_{n_2}$ is given by

$$K^* = \left(\frac{m^*_{p_1}}{m^*_{p_2}}\right) e^{-\frac{\Delta E_v}{kT}}$$

(c) The value of the constant K^* in the case of a heterojunction with $\Delta E_v = 0$ and $m^*_{p_1} = m^*_{p_2}$ is given by

$$K^* = \left(\frac{m^*_{n_1}}{m^*_{n_2}}\right) e^{-\Delta E_c/kT}.$$

Detailed knowledge of the distribution of the carrier at the heterojunction is not available; however, an estimate of approximate distributions of the carriers is possible for an abrupt heterojunction. On the narrow-gap semiconductor's side, $n_1 p_1 = n_{i_1}^2$ must be satisfied at each

point while on the broad-gap semiconductor side, $n_2p_2=n_{i_2}^2$ at each point. Near the junction, the analogy with the homojunction is used to bring n_1 as close to n_2 and to bring p_1 as close to p_2 as possible still satisfying $n_1p_1 = n_{i_1}^2$ and $n_2p_2 = n_{i_2}^2$. It is to be noted that the concentrations of electrons and holes in each semiconductor is independent of the energy discontinuities ΔE_c and ΔE_v.

Consider the following example:

Let us plot the carrier concentration of Ge-GaAs heterojunction:

$n_1p_1 = 5.76 \times 10^{26}$ for Ge at 300°K [28]

$n_2p_2 = 1.21 \times 10^{14}$ for GaAs at 300°K [28]

Let $n_1 = 5.76 \times 10^{20}$ gives $p_1 = 10^6$

Let $p_2 = 10^{12}$ gives $n_2 = 1.21 \times 10^2$

Figure 26 describes the plot of the carrier concentration. It shows an abrupt change in concentration of the electrons and holes.

Practical Model of n-p Semiconductor Heterojunction

Experiments [29,30] carried out on semiconductor heterojunctions indicate that the interface between two different crystals do not coincide with the plane of the

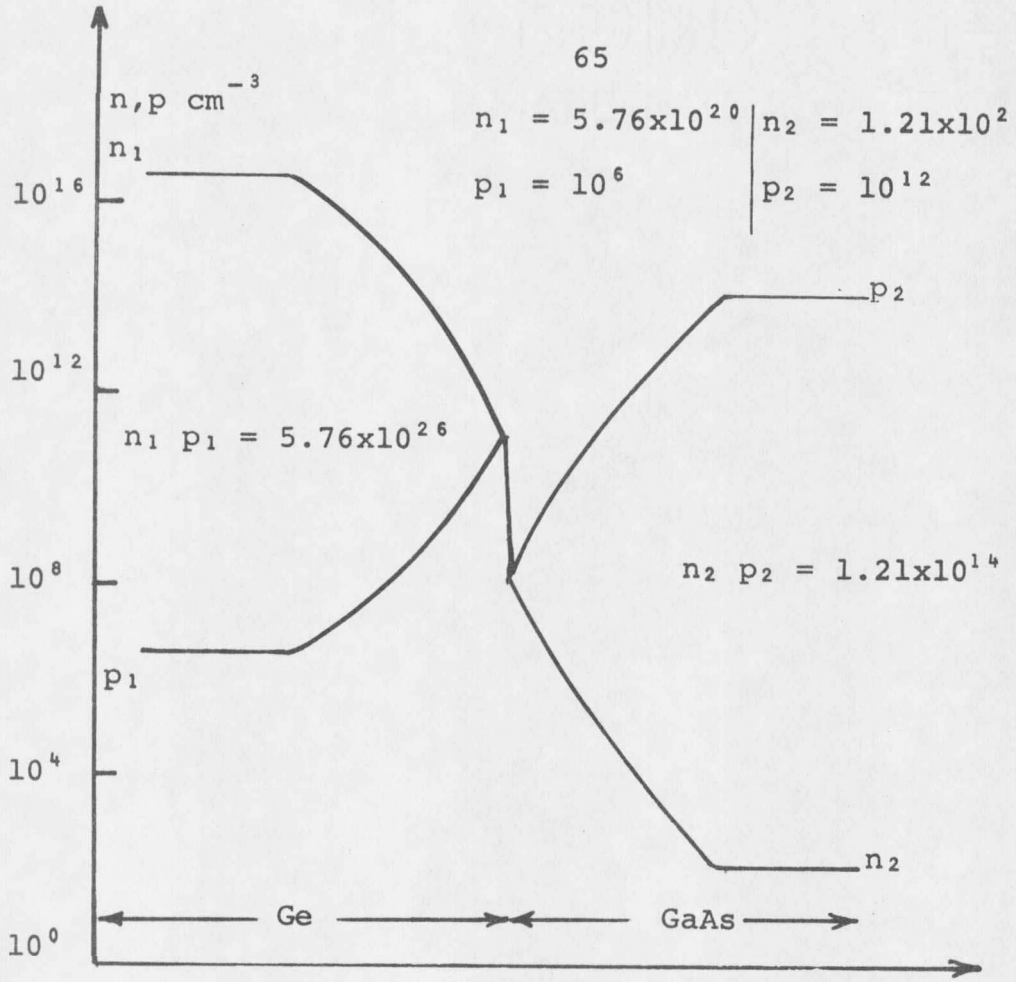


Figure 26. The approximate distribution of carriers near the boundary plane of an abrupt n-p Ge-GaAs hetero-junction in equilibrium at 300°K.

p-n heterojunction. In the process of formation of a p-n heterojunction, the two planes can differ to such an extent that the resulting p-n junction is a homojunction which can be located on either side of the heterojunction. The practical model assumes that the plane of the heterojunction and the corresponding to the p-n junction do not coincide and that the heterojunction lies inside the space-charge region of the p-n junction. This, in reality, is the case found most frequently.

Model and Assumption. It will be assumed that the boundary between two different semiconductors and the p-n junction is abrupt and that the distributions of the acceptor and donor impurities are homogeneous. It is also assumed that the acceptors and donors are completely ionized. The p-n junction in question is nondegenerate and the effect of electrons and the holes in the space-charge region will not be considered. Moreover, the surface charge in the plane of the heterojunction will be ignored and, of course, as usual the one dimensional case will be considered.

According to the model, a heterojunction is a combination of an isotype heterojunction and homojunction.

This homojunction can be in the narrow-gap semiconductor or in the wide-gap semiconductor, depending upon the diffusion coefficients and the nature of the semiconductor. Figure 27 represents the energy-band model of a heterojunction, where the n-type impurity of the narrow-gap semiconductor has penetrated into the broad-gap p-type semiconductor.

The built-in voltage at the heterojunction is given by:

$$V_{BHT} = \frac{E_{F_1} - E_{F_2}}{q}$$

Built-in voltage at the homojunction is:

$$V_{BHM} = \frac{E_{F_2} - E_{F_3}}{q}$$

The built-in voltages V_{BHT} and V_{BHM} in this case have different polarities. Figure 28 represents the energy-band model in thermal equilibrium. The Fermi level lines up throughout the system. Calculation of the electric field, transition region and capacitance will be presented in the next section. It can be noted that such problems do not arise in intrinsic semiconductor devices.

Calculation of electric field and capacitance. Figure 29 shows the model under study. The interface between

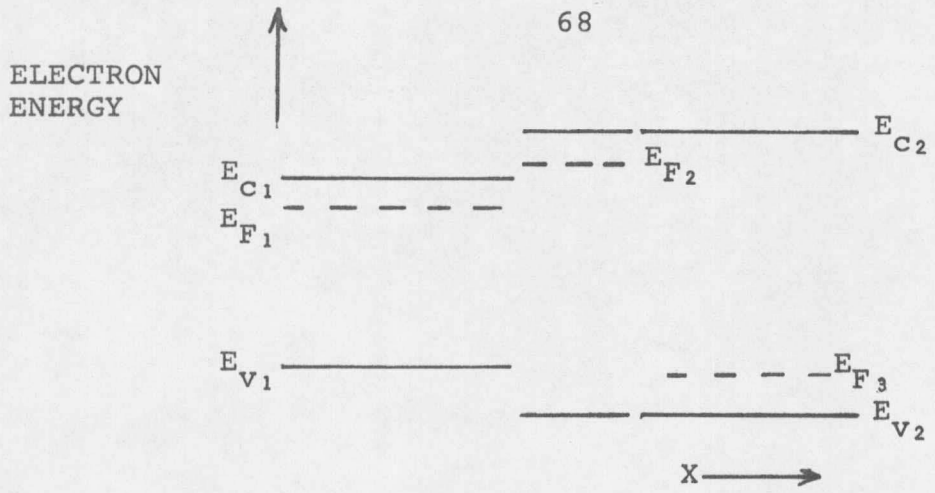


Figure 27. Energy-band diagram of two isolated semiconductors. The n-type impurity has diffused into a p-type broad-gap semiconductor, thus forming an n-n heterojunction and an n-p homojunction.

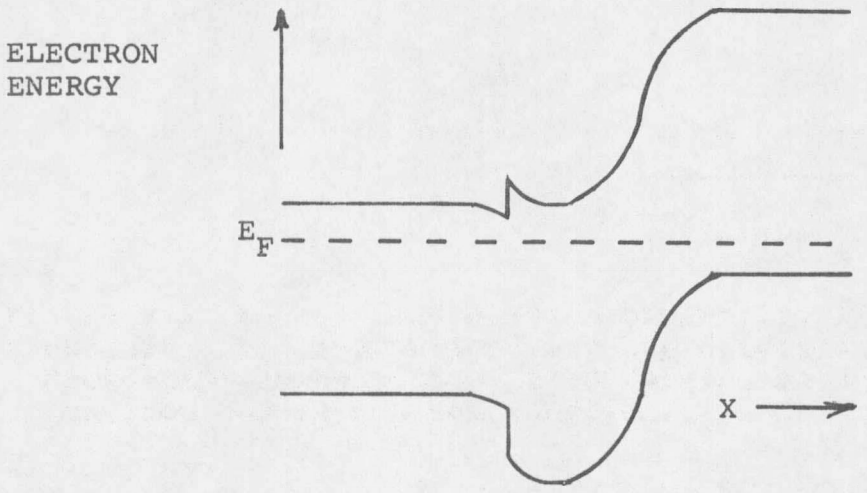


Figure 28. Practical model of semiconductor heterojunction (n-p) in thermal equilibrium.

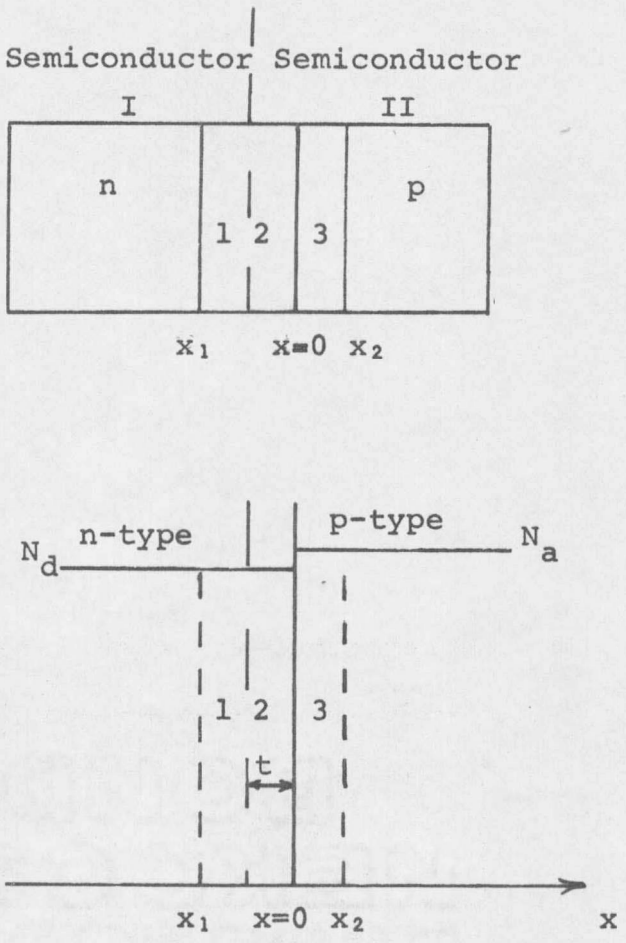


Figure 29. n-p heterojunction in practice consists of an isotype heterojunction (n-n) and homojunction (n-p). Isotype heterojunction is shown to have shifted "t" units into an n-type semiconductor.

the two different crystals do not coincide with the plane of p-n junction. Assume the p-n junction is located at x=0 and the heterojunction is shifted a distance "t" toward the n-type semiconductor. The electric field in this model can be approximated by solving Poisson's equation in three regions. Region 1 corresponds to the donor impurities in semiconductor I; region 2 correspond to the donor impurities in semiconductor II; and region 3 denotes the region containing acceptor impurities in the semiconductor III.

The required boundary conditions are [30]:

$$E_1\Big|_{x=-x_1} = 0 \; ; \; E_1\,\varepsilon_1\Big|_{x=-t} = E_2\,\varepsilon_2\Big|_{x=-t}$$

$$E_2\Big|_{x=0} = E_3\Big|_{x=0} \; ; \; E_3\Big|_{x=x_2} = 0$$

$$V_1\Big|_{x=-x_1} = 0 \; ; \; V_1\Big|_{x=-t} = V_2\Big|_{x=-t}$$

$$V_2\Big|_{x=0} = V_3\Big|_{x=0} \; ; \; V_3\Big|_{x=x_2} = -V_a + V_{BHM}$$

The following expressions have been obtained, using Poisson's equation.

Region 1

$$\nabla \cdot \vec{D} = \rho = q\,N_D$$

considering only a one-dimensional case,

$$\frac{dE_1}{dx} = \frac{q}{\varepsilon_1} N_d$$

$$\int dE_1 = \int_{-x_1}^{x} \frac{q}{\varepsilon_1} N_d + C_1$$

$$E_1 = \frac{q}{\varepsilon_1} N_d \ (x+x_1) + C_1$$

now $E_1\big|_{x = -x_1} = 0$ is a boundary condition

Therefore, $C_1 = 0$

and $E_1 = \frac{q}{\varepsilon_1} N_d \ (x+x_1)$. (10)

Since $\vec{E} = -\nabla V$

$$E_1 = - \frac{dV_1}{dx} = \frac{q}{\varepsilon_1} N_d \ (x+x_1)$$

Therefore, $V_1(x) = - \frac{q}{2\varepsilon_1} N_d \ (x+x_1)^2 + C_2$

Since $V_1\big|_{x = -x_1} = 0$ is a boundary condition, $C_1 = 0$

Region 2

$$\frac{dE_2}{dx} = \frac{qN_d}{\varepsilon_2}$$

Therefore, $E_2 = \frac{qN_d}{\varepsilon_2} (x+x_1) + C_3$

Boundary condition $E_1\varepsilon_1\big|_{x = -t} = E_2\varepsilon_2\big|_{x = -t}$,

yields $E_2 = \frac{qN_d}{\varepsilon_2} (x+x_1)$; (11)

therefore, $V_2(x) = \frac{-q}{2\varepsilon_2} N_d \ (x+x_1)^2 + C_4$

Boundary condition $V_1(-t) = V_2(-t)$, yields

$$V_2(x) = \frac{-q}{2\varepsilon_2} N_d \ (x+x_1)^2 - \frac{qN_d}{2} (x_1-t)^2 \left[\frac{1}{\varepsilon_1} - \frac{1}{\varepsilon_2}\right]$$

Solving the expression, the following relation is obtained:

$$V_2(x) = -\frac{qN_d}{\varepsilon_2}\left[x^2 + 2x_1\,(x+t) - t^2 + (x_1-t)^2\,\frac{\varepsilon_2}{\varepsilon_1}\right] \quad (12)$$

Region 3

$$\nabla.\vec{D} = \rho = q\,N_a$$

$$\frac{dE_3}{dx} = \frac{qN_a}{\varepsilon_2}$$

$$E_3(x) = \frac{qN_a}{\varepsilon_2}\,(x_2-x) + C_5$$

The boundary condition is $E_3\big|_{x\,=\,x_2} = 0$; therefore $C_5 = 0$;

Hence $$E_3(x) = \frac{qN_a}{\varepsilon_2}\,(x_2-x) \quad (13)$$

$$\frac{dV_3}{dx} = -\frac{qN_a}{\varepsilon_2}\,(x_2-x)$$

$$V_3(x) = +\frac{qN_a}{2\varepsilon_2}\,(x_2-x)^2 + C_6$$

and $$V_3(x)\Big|_{x=x_2} = -V_a + V_{BHM},$$

where V_a is the applied voltage and V_{BHM} is the contact potential [30].

Therefore, $$V_3(x) = \frac{qN_a}{2\varepsilon_2}\,(x_2-x)^2 - (V_{BHM}-V_a) \quad (14)$$

The following expressions are obtained for the width of the space-charge region in the n-type and p-type of the model studied.

The boundary condition $E_2\big|_{x=0} = E_3\big|_{x=0}$

$$\text{gives } x_2 = \frac{N_d}{N_a} x_1 . \tag{15}$$

Also using boundary condition $V_2\big|_{x=0} = V_3\big|_{x=0}$

and solving a quadratic equation, x_1 can be obtained as follows:

$$x_1^2 \left(\frac{\varepsilon_2}{\varepsilon_1} + \frac{N_d}{N_a}\right) + 2x_1 t\left(1 - \frac{\varepsilon_2}{\varepsilon_1}\right) - t^2\left(1 - \frac{\varepsilon_2}{\varepsilon_1}\right) - \left(\frac{V_{BHM} - V_a}{N_D}\right) = 0$$

$$x_1 = \frac{(\varepsilon_2 - \varepsilon_1)\, t\, N_a}{(N_a\varepsilon_2 + N_d\varepsilon_1)} +$$

$$\left[\frac{(V_{BHM} - V_a)\, N_a 2\varepsilon_1\varepsilon_2}{N_d q(\varepsilon_2 N_a + \varepsilon_1 N_d)} - \frac{t^2(\varepsilon_2 - \varepsilon_1)\varepsilon_1 N_a (N_a + N_d)}{(\varepsilon_2 N_a + \varepsilon_1 N_d)^2}\right]^{1/2} \tag{16}$$

Using equation 15, the following relation is obtained:

$$x_2 = \frac{N_d\, t\, (\varepsilon_2 - \varepsilon_1)}{(N_a\varepsilon_2 + N_d\varepsilon_1)} +$$

$$\left[\frac{(V_{BHM} - V_a) 2\varepsilon_1\varepsilon_2 N_d}{qN_a(N_a\varepsilon_2 + N_d\varepsilon_1)} - \frac{t^2\varepsilon_1(\varepsilon_2 - \varepsilon_1) N_d^2 [N_a + N_d]}{N_a(N_a\varepsilon_2 + N_d\varepsilon_1)^2}\right]^{1/2} \tag{17}$$

For t=0, in equations 16 and 17, we obtain an expression of the transition region width $W=x_1+x_2$ as described in chapter one and originally obtained by Anderson. Also for t=0 and $\varepsilon_1=\varepsilon_2=\varepsilon$, the transition region width is transformed to the standard expression appropriate for a homojunction. The expressions presented here are valid for $x_1>t$.

Capacitance: The charge per unit junction area [31] is given as follows:

$$|Q| = q\,N_d\,x_1 = q\,N_a\,x_2$$

$$C = \left|\frac{dQ}{dV_a}\right| = \left[\frac{q\,N_a\,N_d\,\varepsilon_1\,\varepsilon_2^{\,2}}{2(V_{BHM}-V_a)(N_a\varepsilon_2+N_d\varepsilon_1)\varepsilon_2-4t^2(\varepsilon_2-\varepsilon_1)qN_d(N_a+N_D)}\right]^{1/2} \qquad (18)$$

For t=0, capacitance reduces to the expression presented in chapter one, obtained by Anderson. For $\varepsilon_1=\varepsilon_2=\varepsilon$ it reduces to the standard capacitance formula for a homojunction.

Chapter 4

TEMPERATURE EFFECTS IN SEMICONDUCTOR HETEROJUNCTIONS

This chapter describes a study made to predict how the properties of a junction vary, while the properties of two different semiconductors vary differently at various temperatures. In the following section, the temperature dependence of the carrier concentration is discussed briefly and an expression describing a change in concentration due to a small change of temperature is obtained. Evaluation of the Fermi level at different temperature ranges is discussed. The variation of Fermi level is also discussed. The temperature dependence of the built-in voltage is discussed next by considering two different cases. Finally, the temperature dependence of energy discontinuities (ΔE_c,ΔE_v) is studied. The total change of the energy discontinuities ($\Delta E_c + \Delta E_v$) in three different cases has been computed and plotted for 0°K to 1000°K.

Temperature Dependence of Carrier Concentration

The product of hole and electron concentrations at thermal equilibrium is independent of impurity concentration.

$$n_o p_o = N_c N_v \, e^{-E_g/kT} \tag{19}$$

where N_c is the density of states in the conduction-band and N_v is the density of states in the valence-band as defined in chapter three.

Therefore, equation (19) becomes

$$n_o p_o = 32 \left(\frac{\pi k m}{h^2}\right) \left(\frac{m_e^* m_h^*}{m^2}\right) T^3 \, e^{-E_g/kT} \tag{20}$$

where: k is Boltzmann's constant

$\hbar = \frac{h}{2\pi}$, where h is Planck's constant

m_e^* is the effective mass of an electron

m_h^* is the effective mass of a hole

m is the true mass of an electron outside the solid.

Equation (20) can be approximated by the following equation

$$n_o p_o = AT^3 \, e^{-E_g(T)/kT} \tag{21}$$

where A can be assumed as a constant since the effective masses do not vary significantly with temperature, i.e.,

Temperature Dependence of Carrier Concentration

The product of hole and electron concentrations at thermal equilibrium is independent of impurity concentration.

$$n_o p_o = N_c N_v \, e^{-E_g/kT} \tag{19}$$

where N_c is the density of states in the conduction-band and N_v is the density of states in valence-band as defined in chapter three.

Therefore, equation (19) becomes

$$n_o p_o = 32 \left(\frac{\pi k m}{h^2}\right) \left(\frac{m_e^* m_h^*}{m^2}\right) T^3 \, e^{-E_g/kT} \tag{20}$$

where: k is Boltzmann's constant

$\hbar = \frac{h}{2\pi}$, where h is Planck's constant

m_e^* is the effective mass of an electron

m_h^* is the effective mass of a hole

m is the true mass of an electron outside the solid.

Equation (20) can be approximated by the following equation

$$n_o p_o = AT^3 \, e^{-E_g(T)/kT} \tag{21}$$

where A can be assumed as a constant since the effective masses do not vary significantly with temperature, i.e.,

the energy bands move with temperature without changing shape [40]. Equation (21) shows that narrow band-gap semiconductors are more sensitive to temperature than wide-gap semiconductors.

In order to account for band-gap variations with temperature, the following relation [32,33] can be used [see Appendix B].

$$E_g(T) = E_g(0) - \frac{\alpha T^2}{(\beta+T)} \qquad (22)$$

where α is an empirical constant and β is the 0°K Debye* temperature. Equation (20) now becomes

$$n_o p_o = AT^3 \exp - [E_g(0) - \frac{\alpha T^2}{(\beta+T)}]/kT.$$

Since $n_o p_o = n_i^2$, it can also be written as

$$n_i = A^{1/2} T^{3/2} \exp [\frac{-E_g(0)}{2kT}] \cdot \exp [\frac{\alpha T}{2K(\beta+T)}].$$

In general, $T^{3/2}$ term is not important and since α is very small [see Appendix B], the above expression can be approximated as

---

*Debye temperature $\theta = \frac{\hbar wm}{k}$, where wm is the maximum frequency of vibration of coupled atoms in a crystal, chosen in such a way that total number of normal modes of frequency less than wm shall be just 3N, since this is the actual number of normal modes which exist for a crystal of N atoms.

$$n_i(T_1) = B \exp\left[\frac{-E_g(0)}{2kT_1}\right]$$

where B is a slowly varying function of temperature and is given by

$$B = A^{1/2}\, T^{3/2} \exp\left[\frac{\alpha T}{2k(\beta+T)}\right].$$

Now consider a small change of temperature and we can find the corresponding change in concentration.

$$n_i(T_1+\Delta T) = B \exp\left[\frac{-E_g(0)}{2k(T_1+\Delta T)}\right]$$

or $$n_i(T+\Delta T) = B \exp\left[\frac{-E_g(0)}{2kT_1\left(1+\frac{\Delta T}{T_1}\right)}\right]$$

For $\frac{\Delta T}{T_1} << 1$

$$n_i(T+\Delta T) \cong B \exp\left(\frac{-E_g(0)}{2kT_1}\right)\left[1 - \frac{\Delta T}{T_1}\right]$$

$$\cong B \exp\left(\frac{-E_g(0)}{2kT_1}\right) \exp\left[\frac{E_g(0)\Delta T}{2kT_1\, T_1}\right]$$

$$n_i(T_1+\Delta T) = n_i(T_1) \exp\left[\frac{E_g(0)\Delta T}{2kT_1^{\,2}}\right]$$

Therefore, the change in concentration due to a rise in temperature ΔT is in direct proportion to the exponent of the increment ΔT.

Evaluation of Fermi Level
at Different Temperature Ranges

In a semiconductor at equilibrium there must be either a thermal hole or a positively charged donor ion for every free electron. The entire crystal must be thus electrically neutral. This electrical neutrality condition can be expressed by equating the algebraic sum of all negative and positive charges to zero.

$$p_o - n_o + N_d - N_a + P_a - n_d = 0 \qquad (23)$$

$(N_d - n_d)$ represent ionized donors

$(N_a - P_a)$ represent ionized acceptors

N_d = ionized donors

N_a = ionized acceptors

P_a = unionized acceptors

n_d = unionized donors

For all but the lowest temperature and the highest value of impurity concentration, the Boltzmann approximation will be valid for both conduction and valence-bands and for both donor and acceptor levels, whereby the concentration of unionized donors and acceptors, p_a and n_d, may be neglected in equation (19). That is assuming all donors and acceptors are ionized. Equation (23) gives the following relation:

$$p_o - n_o + N_d - N_a = 0 \qquad (24)$$

where $n_o = N_c \exp - \left(\frac{E_c - E_F}{kT}\right)$

and $p_o = N_v \exp -\left(\frac{E_F - E_v}{kT}\right)$; thus equation (24) becomes

$$N_v \exp\left[-\frac{(E_F - E_v)}{kT}\right] - N_c \exp\left[-\frac{(E_c - E_F)}{kT}\right] + N_d - N_a = 0 \qquad (25)$$

For simplicity let,

$$\alpha = \exp\,[E_F/kT]$$

$$\beta_c = \exp\,[-E_c/kT]$$

$$\beta_v = \exp\,[E_v/kT]\ . \qquad (26)$$

Now equation (25) takes the form of

$$\alpha^2 - \frac{(N_d - N_a)}{N_c \beta_c}\ \alpha - \frac{N_v \beta_v}{N_c \beta_c} = 0.$$

Solving this quadratic equation for α and taking the logarithm of the result, the following relation can be obtained:

$$\ln\alpha = \frac{E_F}{kT} = \ln\left[\frac{N_d - N_a}{2N_c\beta_c} + \sqrt{\frac{N_d - N_a}{2N_c\beta_c}^{\,2} + \frac{N_v\beta_v}{N_c\beta_c}}\right] \qquad (27)$$

where the positive sign of the radical in equation (27) must be chosen, since when $N_d = N_a = 0$, $e^{E_F/kT}$ must be a positive

quantity. It can be put in another convenient form using the formula:

$$\ln\left(a + \sqrt{a^2+x^2}\right) = \ln x + \mathrm{Sinh}^{-1}\frac{x}{a}$$

Using this relation, and substituting the values given by equation (26) for β_v and β_c, E_F can be expressed as

$$E_F = 1/2(E_v+E_c) + kT \ln\left(\frac{m_p^*}{m_h^*}\right)^{3/4} + kT\,\mathrm{Sinh}^{-1}\frac{N_d-N_a}{2\sqrt{N_cN_v}\,e^{\frac{-\Delta E}{2kT}}} \qquad (28)$$

The first two terms on the right side of this equation represent the Fermi level E_{Fi} for an intrinsic semiconductor, and since

$$n_i = \sqrt{N_cN_v}\;\; e^{-\Delta E/2kT},$$

we may write equation (28) as

$$E_F = E_{Fi} + kT\,\mathrm{Sinh}^{-1}\left(\frac{N_d-N_a}{2n_i}\right) \qquad (29)$$

This expression gives the Fermi level for a doped semiconductor in the range over which the Boltzmann approximation is satisfied. This expression is valid if donors and acceptors can be regarded as completely ionized, i.e., intermediate range of temperature. In the low temperature range when donors and acceptors are not ionized completely

and at high temperatures where there is a thermal generation of carriers will both be considered next. If the net impurity concentration $|N_d - N_a|$ is much larger than n_i, the number of thermally excited carriers will be small compared with the total number; in this case the argument of the inverse hyperbolic sine function in equation (27) is very large, since $\sinh^{-1}x \cong \pm \ln|2x|$ for large values of x; it is clear that under these circumstances equation (29) becomes:

$$E_F = E_{Fi} \pm kT \ln \left|\frac{N_d - N_a}{n_i}\right| \qquad (30)$$

where the plus sign is for n-type material ($N_d > N_a$), and the minus sign is for p-type material ($N_a > N_d$).

At absolute zero the Fermi level lies midway between the donor level and the conduction-band in the case of an n-type semiconductor. As the temperature increases, the Fermi level first increases slightly [35] (remaining, nevertheless, below E_c) and then decreases, moving down through the donor level towards the center of the gap for nondegenerate semiconductors.

Similarly for a p-type semiconductor under these same circumstances, the Fermi level at zero temperature

lies midway between the acceptor levels and the valence-band, and with increasing temperature moves first downward [35] a bit, then upward.

In both n-type and p-type semiconductors, the Fermi level approaches the intrinsic value E_{Fi} for sufficiently high temperatures, since at some high temperature the number n_i of thermally excited carriers will be far in excess of the number $|N_d - N_a|$ contributed by donor and acceptor impurities. Beyond this point the behavior of the material will in every way approximate that of an intrinsic semiconductor. Figure (30) shows the Fermi level as a function of temperature [35] for both n-type and p-type material.

Temperature Dependence of Built-in Voltage

Consider a heterojunction composed of nondegenerate semiconductors. Assume a negligible number of interface states so that position of the Fermi level is independent of interface states at the junction. It is also assumed that the thermal expansion of the two semiconductors is approximately equal so that resulting thermal strain at the junction can be neglected. It has been found due to

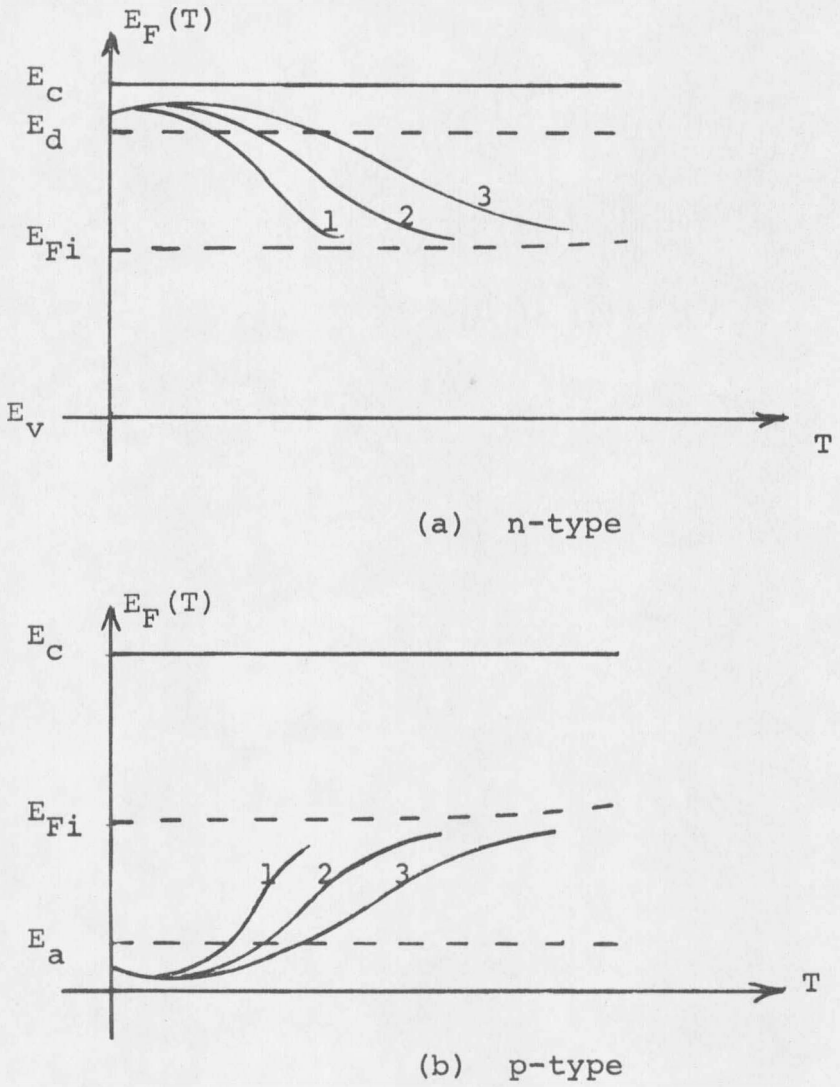


Figure 30. Variation of Fermi level with temperature for (a) n-type and (b) p-type semiconductors, of various impurity densities, those marked "2" to intermediate densities, and those marked "3" to relatively high impurity densities [35].

thermal strain the continuity of crystal structure remains in doubt and dislocations are produced and several times resulting in a crack at the junction [29].

For $\phi_{m_2} > \phi_{m_1}$, the built-in voltage for the heterojunction is given by

$$V_{BHT} = \frac{E_{F_1} - E_{F_2}}{q} ,$$

$$\text{or} \quad V_{BHT} = \frac{\Delta E_v - \Delta E_c}{2q} + \frac{kT}{2q} \ln \left(\frac{p_2 \; n_1}{p_1 \; n_2} \cdot \frac{N_{v_1} \; N_{c_2}}{N_{c_1} \; N_{v_2}} \right)$$

The built-in voltage directly depends on the difference of the Fermi level in the two semiconductors. The Fermi level is a function of temperature and the lower the energy-band gap, the more sensitive is the Fermi level with respect to temperature, because thermal energy kT approaches the smaller energy gap, and can be reached at lower temperatures. Since two different semiconductors are used in a heterojunction, several interesting effects are seen when the temperature dependence of the built-in voltage is considered. If the discontinuities are assumed to remain constant, then the change in built-in voltage is due to change in the factor

$$\frac{kT}{2q} \ln \left(\frac{p_2 \; n_1}{p_1 \; n_2} \cdot \frac{N_{v_1} \; N_{c_2}}{N_{c_1} \; N_{v_2}} \right) .$$

At lower temperature, donors and acceptors in two semiconductors may not be all ionized and there will be a corresponding change in $(\frac{p_2 n_1}{p_1 n_2})$. At higher temperatures there will be a thermal generation of carriers which will be different in the two semiconductors thereby changing the built-in voltage. At still higher temperatures (depending on band gap) the Fermi level in each semiconductor tends to approach the intrinsic level thus occupying the position E_{i_1} and E_{i_2}, respectively; however, in contrast to a homojunction, the built-in voltage may not collapse in the heterojunction. Two different cases will be described showing that the built-in voltage changes sign with increasing temperature, in some cases twice.

Case 1

Figure 31(a) shows two isolated semiconductors with $\Delta E_v > \Delta E_c$ and doped so that the Fermi levels are shown. The built-in voltage is $\frac{E_{F_2} - E_{F_1}}{q}$. At an elevated temperature, E_{F_1} goes to E_{FI_1}, the narrow-gap semiconductor being sensitive to temperature, thus increasing the built-in voltage as shown in Figure 31(b). At still higher temperatures, E_{F_2} tends to come to E_{FI_2}; then built-in voltage starts decreasing; it becomes zero when E_{FI_1} and

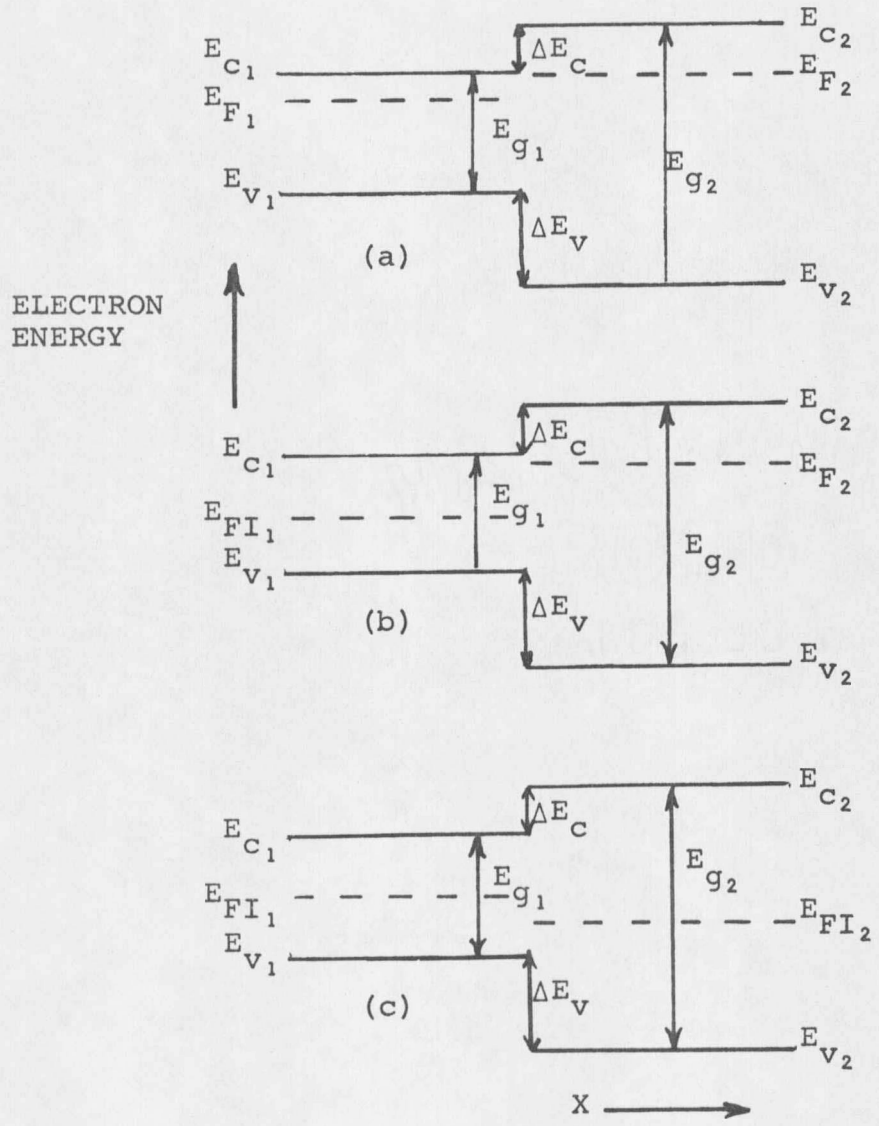


Figure 31. Two isolated semiconductors as discussed in Case 1, space charge neutrality is assumed to exist in every region. (a) At room temperature, (b) at an elevated temperature where narrow-gap semiconductor becomes intrinsic making built-in voltage increase, and (c) at a temperature where broad-gap semiconductor also become intrinsic, show a change in polarity of built-in voltage if compared with Figure (a).

E_{F_2} line up. Upon a further rise of temperature, E_{F_2} takes the position E_{FI_2} as shown in Figure 31(c), thus changing the polarity of the built-in voltage (or the direction of electric field).

The built-in voltage is plotted in Figure 32. Beyond temperature T_1 the narrow-gap semiconductor becomes intrinsic while the broad-gap semiconductor does not. At a still higher temperature T_2, the broad-gap semiconductor also become intrinsic while the narrow-gap semiconductor remains intrinsic. It is possible that these transition temperatures may exceed the melting point of one of the semiconductors. An example is worked out as follows:

Example: Consider an example which describes the change of built-in voltage as discussed in Case I. For convenience consider a Ge-Si heterojunction as shown in Figure 33. For this problem also, the effects of interface states are neglected. The following data for Ge,Si semiconductor can be obtained [36].

$E_{g_1} = 0.66$ eV. $\quad E_{g_2} = 1.11$ eV.

$\chi_{e_1} = 4.13$ eV. $\quad \chi_{e_2} = 4.01$ eV.

The energy discontinuity in the conduction bands, ΔE_c is given by

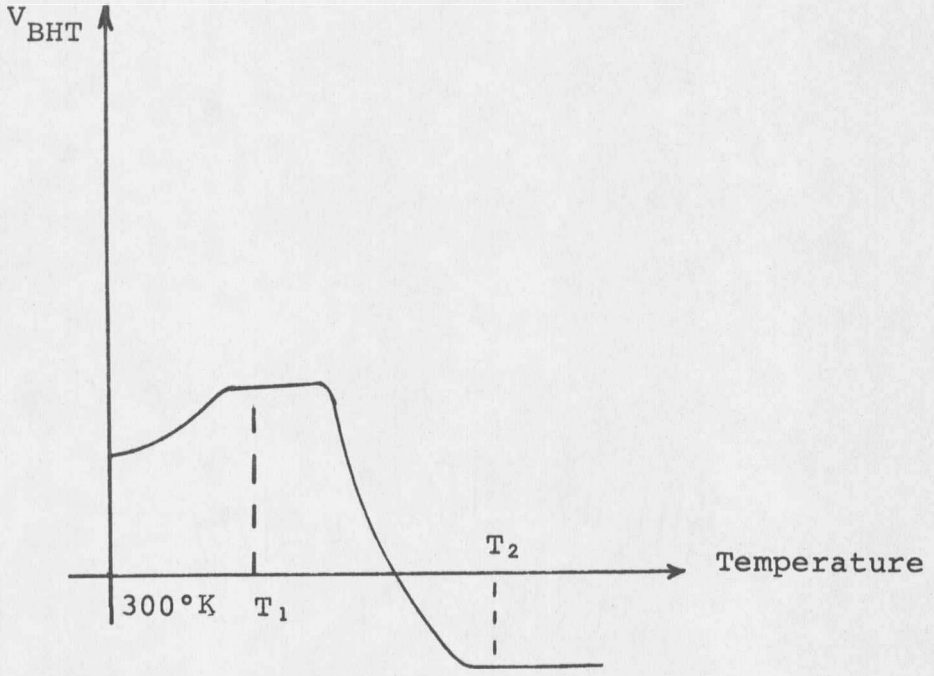


Figure 32. An approximate plot of built-in voltage at the the heterojunction with respect to temperature, in Case 1.

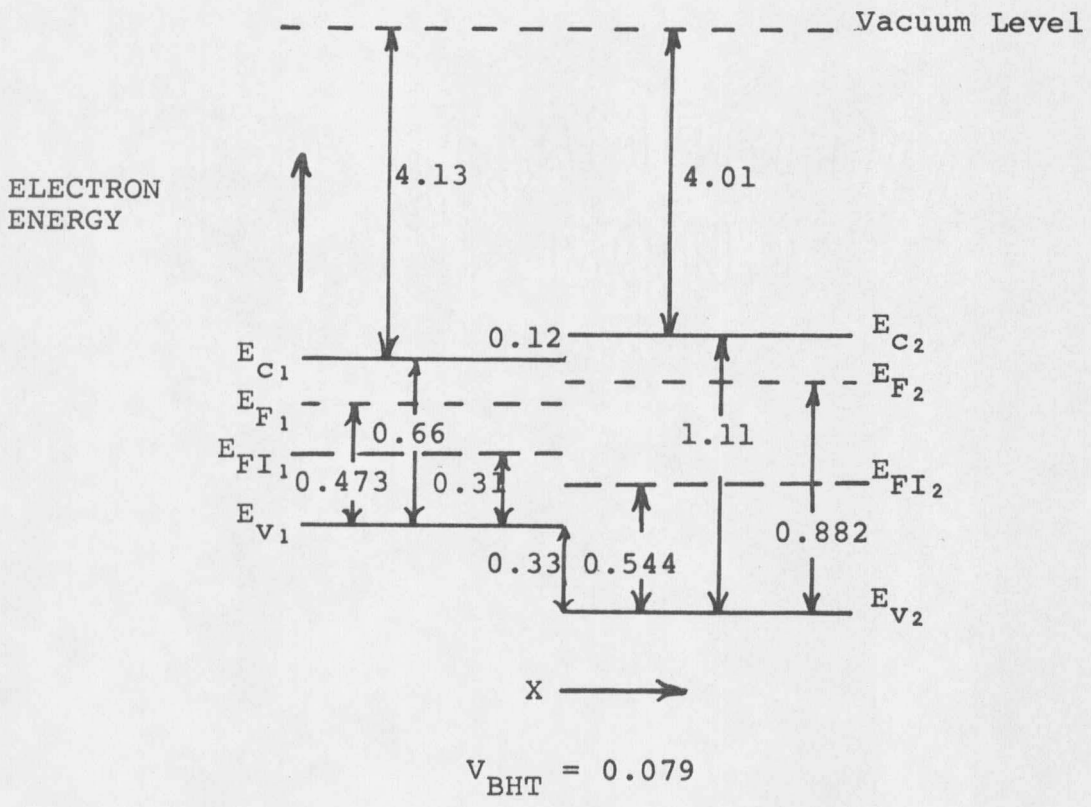


Figure 33. Energy-band diagram of isolated Ge-Si, in which space charge neutrality is assumed to exist in every region at 300°K.

$|\chi_{e_1}-\chi_{e_2}|$ = 0.12 eV. and the energy discontinuity in the valence-band, ΔE_v is given by $E_{g_2} - (E_{g_1}+\Delta E_c)$ = 0.33 eV. Let us consider both n-type semiconductors. The position of the Fermi level is given by equation (30) as follows:

$$E_F = E_{FI} + kT \ln \frac{N_d}{n_i} \text{ ; for Na = 0,} \qquad (31)$$

where E_{FI} is the position of the Fermi level in an intrinsic semiconductor, and is given by [37]:

$$E_{FI} = \frac{E_c+E_v}{2} + \frac{3}{4} kT \ln \left(\frac{m_{dh}}{m_{de}}\right)^{2/3},$$

where m_{dh} is the density-of-state effective mass of the valence-band and m_{de} is the density-of-state effective mass of the conduction-band.

For germanium, the position of the intrinsic Fermi level is given by [37]:

$$E_{FI_1} = \frac{E_c+E_v}{2} + \frac{3}{4} kT \ln \frac{(m_{lh}^{*\,3/2}+m_{hh}^{*\,3/2})^{2/3}}{(m_l^* \cdot m_t^{*2})^{1/3}}$$

$E_c + E_v$ = 0.66 eV.

K = 8.62×10^{-5} eV.°/k

The following data can be obtained [27]:

m_{lh}^* = 0.04 $\quad$ m_l^* = 1.6

m_{hh}^* = 0.3 $\quad$ m_t^* = 0.082

Hence, position of the Fermi level in an intrinsic germanium is given as follows:

$$E_{FI_1} = \left[0.33 - 7.45 \times 10^{-5}\ T\right] \text{ eV.} \qquad (32)$$

$$E_{FI_1}\Big|_{T=300°K} = 0.31 \text{ eV.}$$

Similarly for silicon, the position of the intrinsic Fermi level can be obtained using the following data [27]:

$$E_c + E_v = 1.11 \text{ eV.}$$

$$m^*_{lh} = 0.16 \qquad m^*_l = 0.97$$

$$m^*_{hh} = 0.5 \qquad m^*_t = 0.19$$

$$E_{FI_2} = [0.555 - 3.7 \times 10^{-5}\ T] \text{ eV.} \qquad (33)$$

$$E_{FI_2}\Big|_{T=300°K} = 0.544 \text{ eV.}$$

Let the doping level of donor atoms in germanium be 1.5×10^{16} atoms/c.c. and that in Si be 10^{16} atoms/c.c. Therefore, the position of the Fermi level can be obtained using equation (31). n_i for Ge at 300°K is 2.4×10^{13} atoms/c.c. [38]

$$E_{F_1} = E_{FI_1} + 6.4\ kT \qquad (34)$$

$$= 0.473 \text{ eV. at } 300°K$$

Similarly for silicon the position of the Fermi level using equation (33) and the intrinsic carrier concentration 1.45×10^{10} atom/c.c. at 300°K [38], E_{F_2} is given by

$$E_{F_2} = 0.882 \text{ eV.}$$

Therefore, the built-in voltage is $(\phi_{m_1} - \phi_{m_2})$ or the difference in Fermi level on a common base is given by 0.079 eV. at 300°K. Figure 33 describes the energy band diagram at 300°K.

At about 450°K the intrinsic concentration of carrier in germanium becomes equal to $1.5 \times 10^{16}/cm^3$ [38] and germanium becomes intrinsic.

Therefore, $E_{F_1} = E_{FI_1}$

$= 0.30$ eV. using equation (32)

Similarly for silicon the position of the Fermi level using equation (31), (33) and intrinsic carrier concentration 4×10^{13} atoms/c.c. at 450°K [38], E_{F_2} is given by

$$E_{F_2} = 0.754 \text{ eV.}$$

Therefore, the built-in voltage is given by 0.124 eV.: showing an increase of 0.045 eV. compared to the built-in voltage at 300°K. Figure 34 describes the energy band diagram at 450°K.

At 600°K the intrinsic carrier concentration in silicon becomes 10^{16}/c.c. [38]; hence, silicon becomes

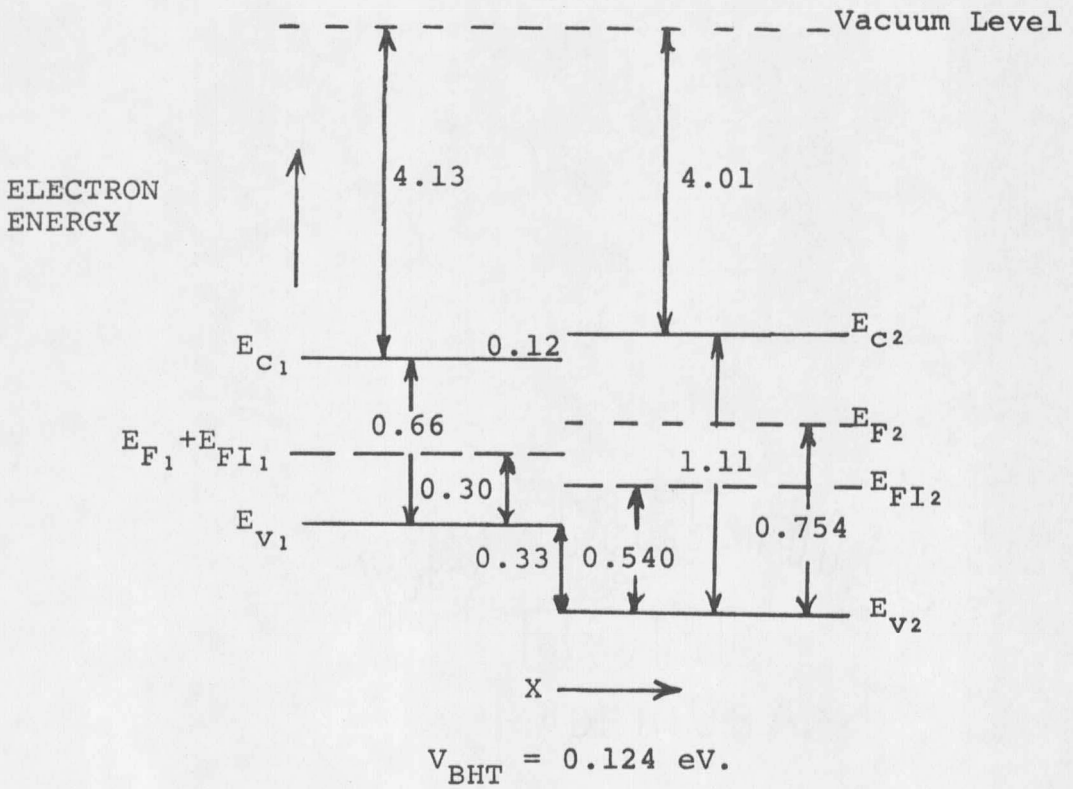


Figure 34. Energy-band diagram of isolated Ge-Si, in which space charge neutrality is assumed to exist in every region at 450°K.

intrinsic at this temperature. The position of the Fermi level in germanium and silicon is obtained using equations (32) and (33).

$$E_{F_1} = E_{FI_1} = 0.29 \text{ eV.}$$

$$E_{F_2} = E_{FI_2} = 0.533 \text{ eV.}$$

Now $\phi_{m_1} < \phi_{m_2}$, since the built-in voltage has changed sign and is given by -0.087 eV. at 600°K. The energy band diagram is described in Figure 35 at 600°K.

The built-in voltage is calculated at various temperature and tabulated as follows:

T°K	V_{BHT} in eV.
300	0.079
375	0.084
450	0.124
475	0.079
500	0.0488
550	-0.092
600	-0.087

V_{BHT} is plotted as a function of temperature in Figure 36. It should be noted that this plot will vary as the doping level in the semiconductor changes and that changes the sign of built-in voltage can be achieved at lower temperatures if the semiconductors are lightly doped.

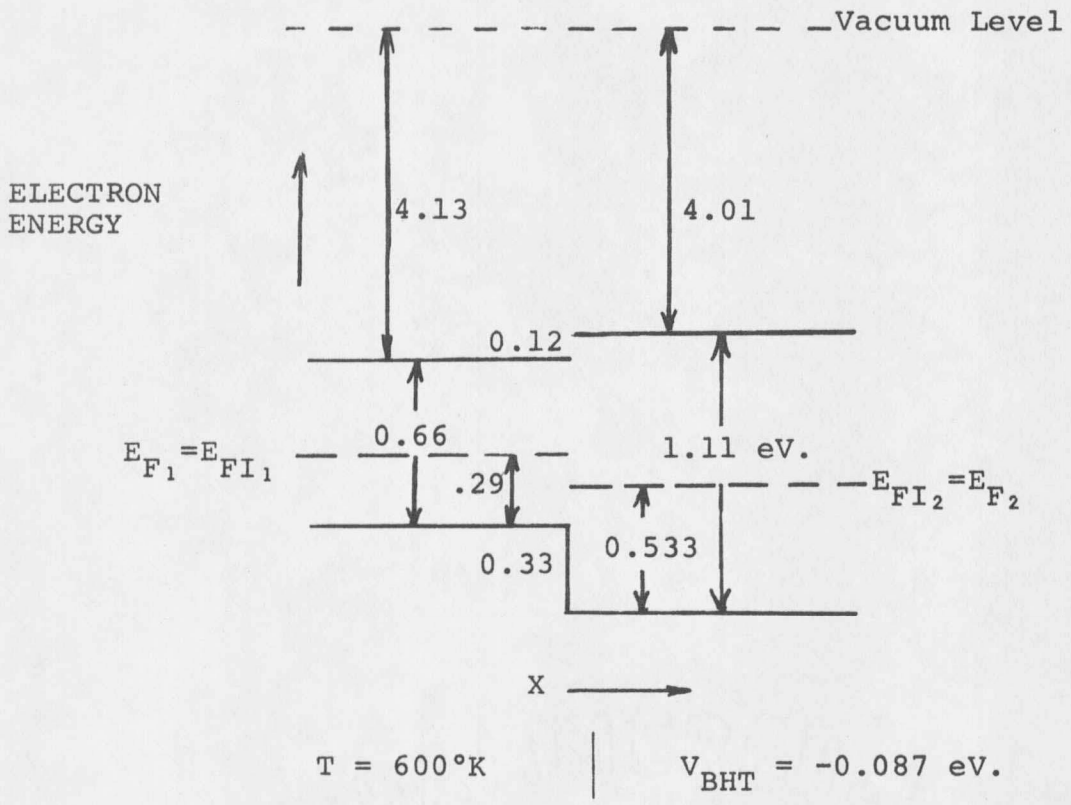


Figure 35. Energy-band diagram of isolated Ge-Si, in which space charge neutrality is assumed to exist in every region at 600°K.

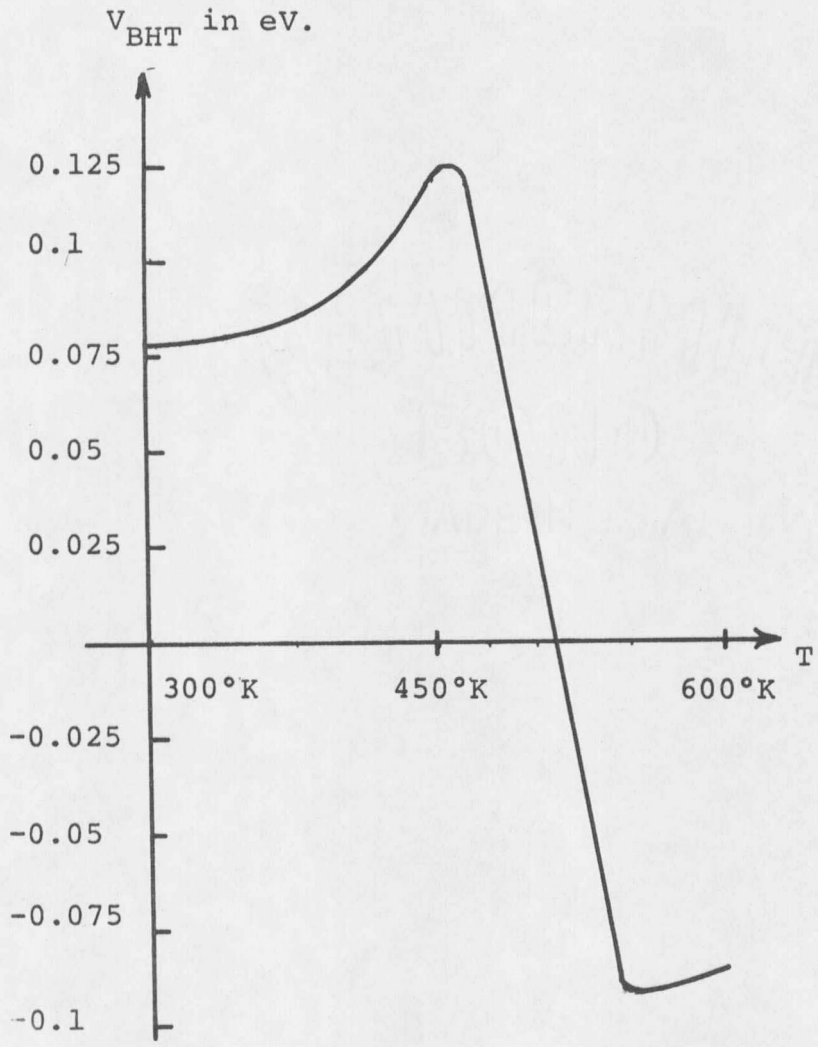


Figure 36. Built-in voltage at the Ge-Si heterojunction as considered in the example of Case 1.

Case 2

Consider two isolated semiconductors doped in such a way that the positions of the Fermi levels are as shown in Figure 37(a). If a junction is formed, a built-in voltage of value $\frac{E_{F_1}-E_{F_2}}{q}$ can be obtained.

As the temperature of the diode is increased E_{F_1} will move down and at a sufficient temperature acquire a position E_{FI_1}, thus changing the sign of the built-in voltage as shown in Figure 37(b). E_{F_2} will be affected only slightly as semiconductor 2 has a broad gap compared to semiconductor 1. At a still higher temperature, E_{FI_1} will remain almost fixed while E_{F_2} will move down acquiring a position of E_{FI_2}, thus changing the direction of the built-in voltage once again, as shown in Figure 37(c). The built-in voltage is plotted in Figure 38. Similar effects with a p-p heterojunction ($\Delta E_c > \Delta E_v$) can be obtained by changing junction temperature. For example, consider the working space (Chapter 2) described by $\chi_{2h} > \chi_{1h} \chi_{1e} > \chi_{2e}$ and the case $\phi_{m_1} = \phi_{m_2}$. There is no built-in voltage present; however, at a higher temperature ϕ_{m_1} and ϕ_{m_2} may move in such a way that it gives rise to built-in voltage at the junction. Such effects are not possible with homojunctions.

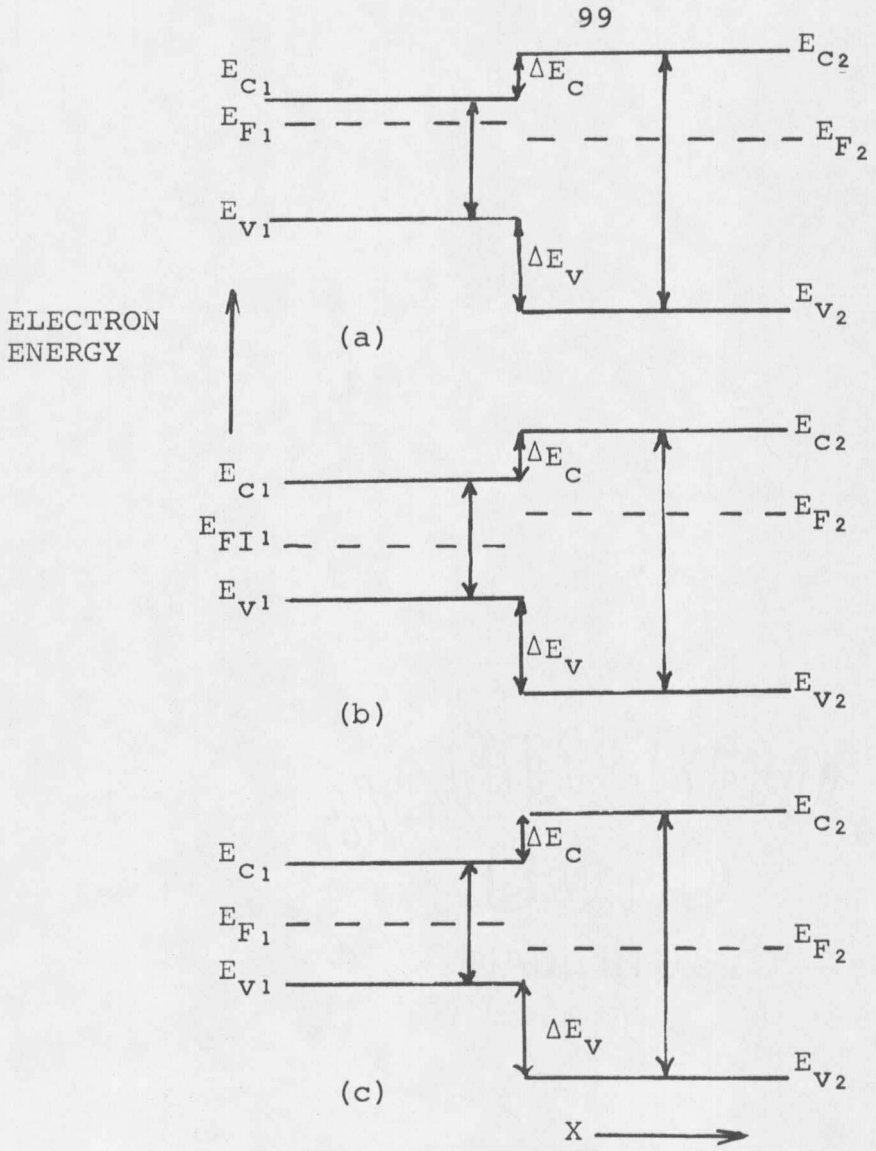


Figure 37. Two isolated semiconductors as discussed in Case II, space charge neutrality is assumed to exist in every region with $\Delta E_V > \Delta E_C$. (a) At room temperature, (b) at an elevated temperature where narrow-gap semiconductor becomes intrinsic making built-in-voltage to change sign, and (c) at a temperature where broad-gap semiconductor also becomes intrinsic, changing the sign of built-in voltage once over again.

Temperature Dependence of Discontinuities

The total discontinuities in the conduction and valence-band appear due to the difference in energy-band gaps of the two different semiconductors. Assume that the junction is characterized by an abrupt change in the band structure and that interface states can be neglected. Also assume that the magnitude of the conduction-band discontinuity, ΔE_c, is determined by bulk band energies and is equal to the difference of their electron affinities.

The general relation between energy-band gap and temperature is repeated as follows: (Equation 22)

$$E_g = E_g(0) - \frac{\alpha T^2}{(T+\beta)}$$

where $E_g(0)$ is the energy gap at 0°K, β is the approximate 0°K Debye temperature, and α is an empirical constant. In the case of a semiconductor heterojunction, the total discontinuity can be expressed as a function of temperature:

$$\Delta E_c + \Delta E_v = E_{g_1}(T) - E_{g_2}(T)$$

$$\Delta E_c + \Delta E_v = E_{g_1}(0) - E_{g_2}(0) + \frac{T^2[\alpha_2(T+\beta_1) - \alpha_1(T+\beta_2)]}{(T+\beta_1)(T+\beta_2)},$$

where $E_{g_1}(0)$ and $E_{g_2}(0)$ are the energy-band gaps at 0°K, β_1 and β_2 are the Debye temperatures at 0°K and α_1, α_2 are

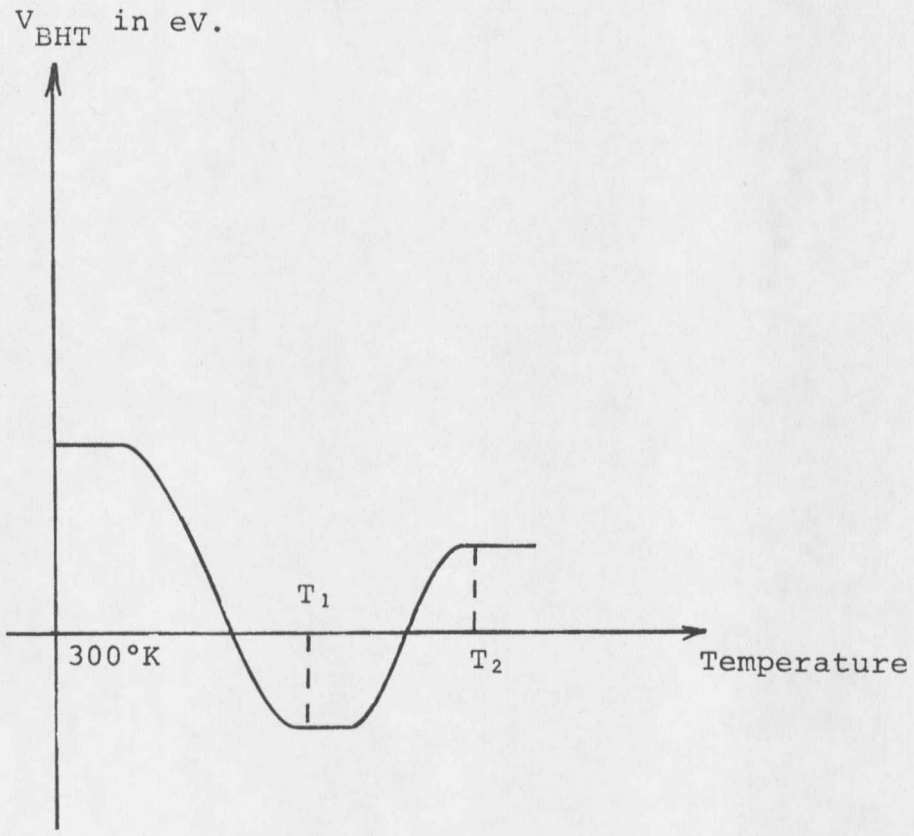


Figure 38. Built-in voltage at the n-n heterojunction with respect to temperature in Case II.

empirical constants of the two semiconductors comprising the heterojunction.

If $\frac{\alpha_2}{\alpha_1} \cong \frac{T+\beta_2}{T+\beta_1}$, then the change in discontinuity will be negligible. If $\alpha_2(T+\beta_1) > \alpha_1(T+\beta_2)$ for $E_{g_1}(0) > E_{g_2}(0)$ at a given temperature T, the total discontinuities will increase with increasing temperature. The change of total discontinuities have been computed for Ge-GaAs[33], GaP-Si [33] and Si-Ge [33] as shown in Figure 39 and tabulated in Appendix B. In the case of Ge-GaAs and GaP-Si junctions, the total discontinuities decrease with increasing temperature, while in the case of Si-Ge it increases with increasing temperature. Relative changes of the two discontinuities are one of the important considerations in a heterojunction. If the conduction and valence-bands (of E-k plot) in the two semiconductors are symmetric, then the change of the two discontinuities should be proportional to their magnitudes. If, however, the valence-bands of the two semiconductors (for example, Ge-GaAs) are symmetric, the total change of discontinuity can be approximated by the change of ΔE_c [34]; a similar argument holds for ΔE_v.

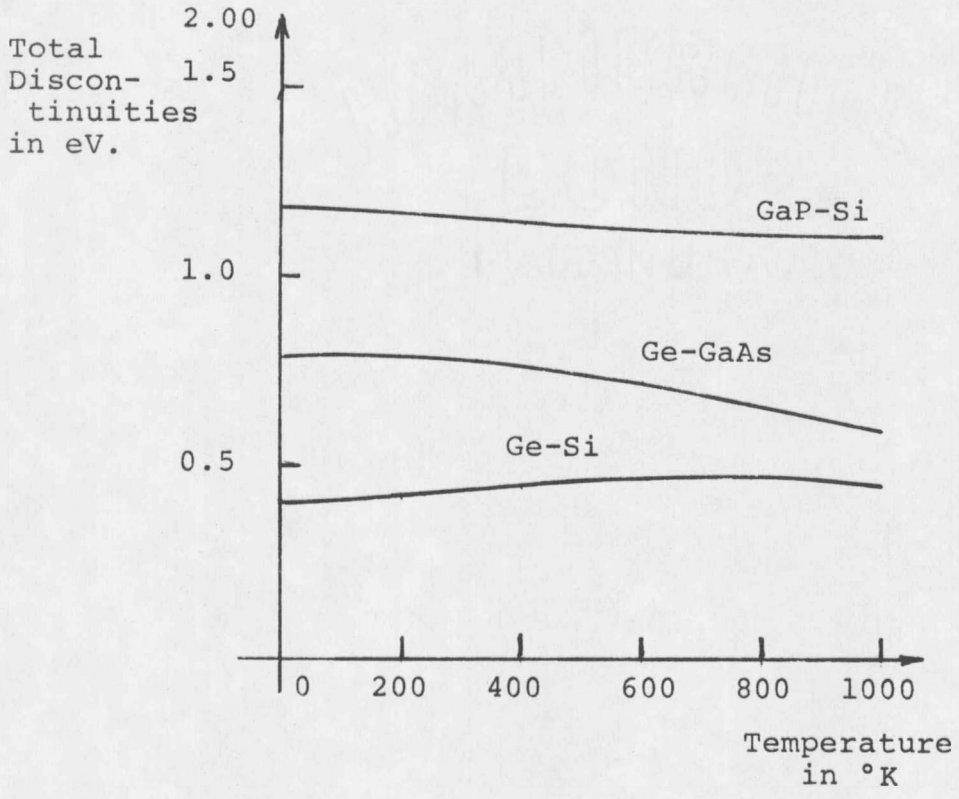


Figure 39. Change in total discontinuities with changing temperature are plotted for GaP-Si, Ge-GaAs and Ge-Si heterojunctions [see Appendix B].

Variation of the total discontinuities depends upon the properties of the two semiconductors, and for a given semiconductor it will depend upon the orientation of the crystal [39]. Relative change of discontinuities depends on the shape of the conduction and valence-bands of the semiconductors. It is believed that the change of the band position with temperature is accompanied by a negligible change in the shapes of the bands [40] and so the change of effective masses can be assumed to be negligible.

The changes of discontinuities have been found to be very small and hence can be ignored for many applications.

Chapter 5

INTRINSIC SEMICONDUCTOR HETEROJUNCTIONS

A homojunction diode is doped on either side of the junction to create electron and hole gradients across the junction and hence to obtain a useful built-in voltage. When a potential is applied to such a diode, it appears at the junction, since the junction offers much higher resistivity compared to the n or p region of the diode. The reason for high resistivity at the junction is that the transition region is depleted of electrons and holes. In such a diode the voltage drop in n and p regions is small and, in general, heating loss (I^2R) should be small.

In the case of a heterojunction, it is possible to get a built-in voltage at the junction without doping the two semiconductor crystals. Introduction of impurities into a uniform crystal not only increases the cost of the device processing, but also distorts the uniform arrangement of crystal atoms. If an intrinsic semiconductor heterojunction is considered, two questions can arise: (1) At what temperature can thermal equilibrium be obtained [42] so that the Fermi level lines up to give the required built-in voltage at the junction, and (2) Will the

voltage drop in the two regions across the junction be so high that it produces heat, which is not desirable.

Both questions suggest use of moderate conductivity semiconductors at the temperature at which the device is to be used. If the device is to be used at room temperature, one should use semiconductors with a small energy-gap. The smaller the energy-gap, the higher the intrinsic carrier concentration and thus the higher the conductivity. Therefore, an attempt is made to study intrinsic semiconductor heterojunctions on the basis of conductivity. Variation of built-in voltage with temperature is also considered in this chapter.

Intrinsic Conductivity

An intrinsic semiconductor is generally an insulator at low temperatures and a conductor at high ones, its conductivity tending to increase with temperature. This occurs because in the intrinsic semiconductor the increase in the number of free carriers with temperature far outweighs the reduction of mobility. The critical dimension in the problem of the generation of free carriers in the insulator or semiconductor is the size of the energy gap E_g compared to thermal energy kT.

The conductivity of a semiconductor is given by:

$$\sigma = q(n\mu_n + p\mu_p) \tag{35}$$

where n is the population of conduction electrons and p is the population of conduction holes. μ_n and μ_p are the mobilities of electrons and holes, respectively. The condition of minimum conductivity can be obtained by differentiating equation (35) with respect to n:

$$\frac{\partial\sigma}{\partial n} = q(\mu_n + \mu_p \frac{\partial p}{\partial n}) = 0$$

$$= q[\mu_n + \mu_p n_i^2 \frac{\partial}{\partial n} (\frac{1}{n})] = 0$$

or $n\mu_n = p\mu_p$ is the condition for minimum conductivity since $\frac{\partial^2\sigma}{\partial n^2}$ is positive.

Therefore, minimum conductivity is:

$$\sigma_{min} = 2qn\mu_n = 2qp\mu_p$$

However, intrinsic conductivity in general is greater than the minimum conductivity:

$$\sigma_i = qn_{i_1} (\mu_n + \mu_p)$$

Silicon has a band gap of 1.1 eV. and when extremely pure has a resistivity as high as 2×10^5 ohm - cm. Germanium,

with a band gap of 0.7 eV. in very pure form, has the moderately high resistivity of 47 ohm - cm at room temperature. The above discussion of intrinsic semiconductor heterojunction devices restricts itself to only those semiconductors with an energy band gap of less than 0.7 eV. and thus with moderate conductivity.

Theory of Intrinsic Semiconductor Devices

The built-in voltage in intrinsic semiconductor devices can be obtained by putting $n_1 = p_1$; $n_2 = p_2$ in the V_{BHT} expression. Therefore,

$$V_{BHT\ int} = \frac{\Delta E_v - \Delta E_c}{2q} + \frac{3}{4}\frac{kT}{q} \ln \left(\frac{m^*_{1h}}{m^*_{2h}} \frac{m^*_{2e}}{m^*_{1e}}\right). \qquad (36)$$

This is valid for $\phi_{m_2} > \phi_{m_1}$. For $\phi_{m_2} < \phi_{m_1}$, the expression changes sign. Equation (36) is independent of electron and hole concentration since equal electron and hole gradients exist from narrow-gap to broad-gap semiconductors. Carrier concentration is plotted in Figure 40.

The built-in voltage of intrinsic semiconductor heterojunctions is a function of energy discontinuities (ΔE_c, ΔE_v) and effective masses. Referring to the previous arguments it can be stated that energy discontinuities in

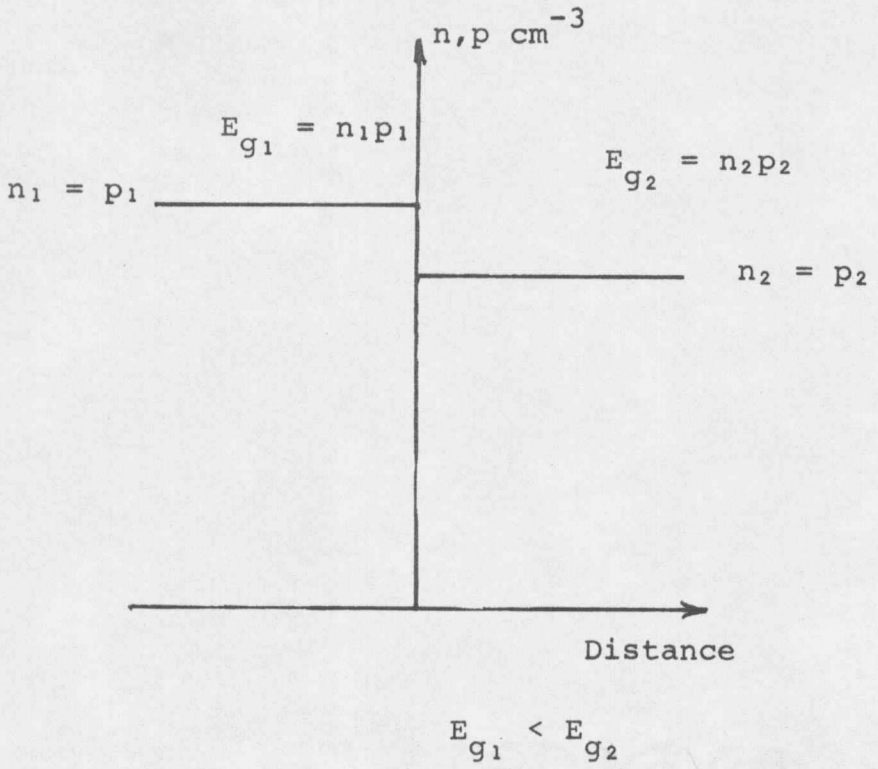


Figure 40. Carrier concentration has been plotted for an abrupt intrinsic semiconductor heterojunction, $n_1 = p_1 \neq n_2 = p_2$.

the conduction and valence-bands as well as effective masses do not change significantly with temperature. Hence, V_{BHT} (intrinsic) remains constant over a wide range of temperatures. An example follows.

Example: Consider an intrinsic semiconductor heterojunction composed of GaSb and InAs semiconductors.
InAs has a band gap of 0.36 eV. (E_{g_1}), electron affinity $\chi_{e_1} = 4.9$ eV.
It has lattice constant of 6.058 A°.
GaSb has a band gap of $E_{g_2} = 0.68$ eV., electron affinity $\chi_{e_2} = 4.06$ eV.
It has a lattice constant of 6.095 A°.
Figure 41 represents energy band diagrams of InAs - GaSb isolated semiconductors. It is assumed that effective masses of electrons and holes in each semiconductor are equal, so that Fermi level lies in the middle of the energy gap.

The built-in voltage obtained is 0.67 volts and it should be constant considering the above assumptions.

It should be noted that if the choice of effective masses is possible, while choosing two intrinsic

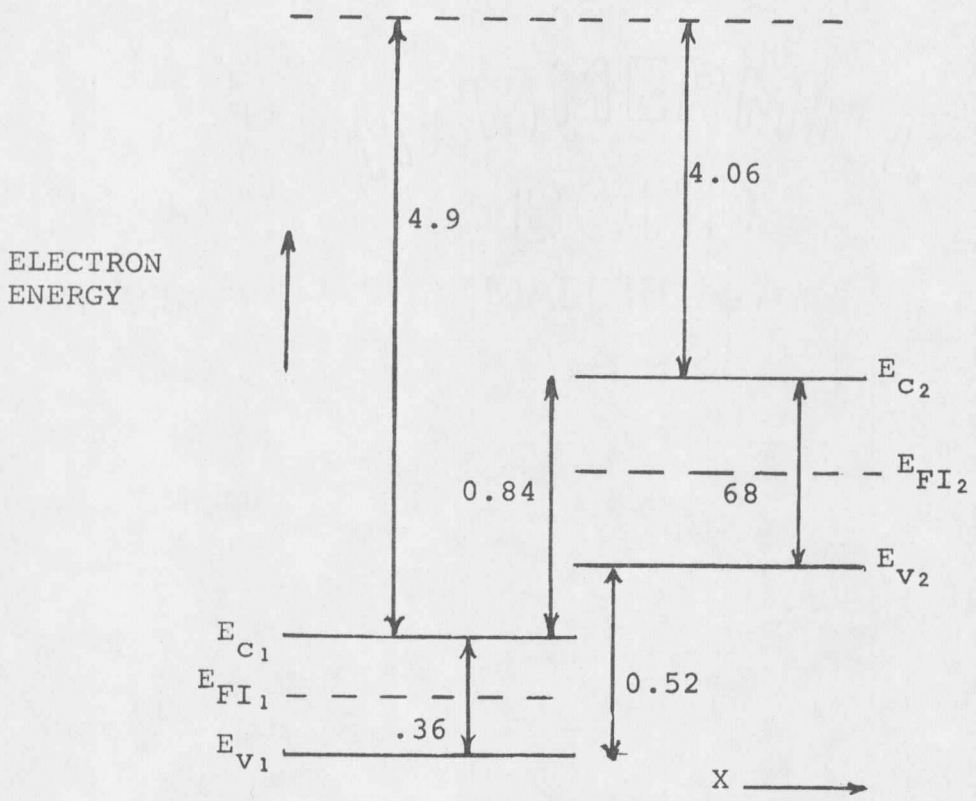


Figure 41. Energy-band diagram of InAs - GaSb, in which space charge neutrality is assumed to exist in every region at 300°K.

semiconductors, one may choose,

$$\frac{m^*_{1h}}{m^*_{2h}} \cdot \frac{m^*_{2e}}{m^*_{1e}} \cong 1.$$

This reduces equation (36) as follows:

$$V_{BHT\ int} = \frac{\Delta E_v - \Delta E_c}{2q} \qquad (37)$$

Equation (37) is valid for $\phi_{m_2} > \phi_{m_1}$. For $\phi_{m_2} < \phi_{m_1}$, the expression changes sign. As discussed in Chapter 4, it is not possible to find the exact variation of ΔE_c and ΔE_v with temperature change, though it is small. It can be thus concluded that V_{BHT}, with the above choice of effective masses, is independent of temperature and can vary slightly as a result of variation in energy discontinuities ΔE_c and ΔE_v.

Devices Using An Intrinsic and An Extrinsic Semiconductor

In the section describing intrinsic conductivity, it was concluded that only semiconductors with a band gap of less than 0.7 eV. will be useful for intrinsic semiconductor devices. That is a very small class of semiconductors. Semiconductors that have been developed are Ge, GaSb InAs, InSb and PbTe. Considering that matching the lattice

constant is also required, it can be suggested that a narrow-gap semiconductor with a band gap less than 0.7 eV. be used as the intrinsic semiconductor, and a broad-gap semiconductor with a band gap more than 0.7 eV. be used as the extrinsic semiconductor.

If, however, the intrinsic semiconductor hetero-junction is to be used at a high temperature, then both semiconductors can have a band gap greater than 0.7 eV. so that the conductivity is sufficiently high, at that temperature, due to the thermal generation of the carriers.

Advantages of Intrinsic Semiconductor Devices

1. In the case of intrinsic semiconductor hetero-junction devices, the uniformity of crystal lattice is not disturbed, as it is when impurity atoms are introduced into the crystal.

2. Since no doping is required, the cost of device processing is reduced.

3. The built-in voltage varies only slightly with the temperature; with the proper choice of effective masses it remains essentially constant. It suggests its use in producing temperature insensitive device.

Chapter 6

CONCLUSIONS AND SUGGESTIONS

A new classification for semiconductor heterojunctions has been formulated by considering the different mutual positions of conduction-band and valence-band edges. To the nine different classes of semiconductor heterojunction thus obtained, effects of different work functions, different effective masses of carriers and types of semiconductors are incorporated in the classification. General expressions for the built-in voltages in thermal equilibrium have been obtained considering only nondegenerate semiconductors. Built-in voltage at the heterojunction is analyzed. The approximate distribution of carriers near the boundary plane of an abrupt n-p heterojunction in equilibrium is plotted. In the case of a p-n heterojunction, considering diffusion of impurities from one semiconductor to the other, a practical model is proposed and analyzed. The effect of temperature on built-in voltage leads to the conclusion that built-in voltage in a heterojunction can change its sign, in some cases twice, with the choice of an appropriate doping level. The total change of energy discontinuities ($\Delta E_c + \Delta E_v$) with increasing temperature has

been studied, and it is found that this change depends on an empirical constant and the 0°K Debye temperature of the two semiconductors. The total change of energy discontinuity can increase or decrease with the temperature. Intrinsic semiconductor-heterojunction devices are studied; band gaps of value less than 0.7 eV. are suggested if such devices are to be used at room temperature. Built-in voltage in the case of intrinsic semiconductor heterojunction devices varies slightly with the temperature. With proper choice of effective masses, the built-in voltage remains essentially constant with the temperature. The advantages of intrinsic semiconductor devices are discussed. A three-dimensional energy-distance-momentum diagram is described; it suggests a change in the wave vector of a carrier, in transit from one semiconductor to the other. Thus, the probability of transition of a carrier across the heterojunction is reduced.

Since device potentials are reduced with the presence of interface states, semiconductor-heterojunction device research should be restricted to semiconductor-heterojunction pairs with a negligible number of interface states present at the junction. It is also suggested that

practical work should be carried out to verify the changes in built-in voltages at higher temperatures and to study intrinsic semiconductor heterojunction devices. Finally, it is suggested to investigate the possibility of drawing E - X - K diagrams, wherever feasible, since they describe the actual process of transport of the carriers.

APPENDIX

Appendix A

3-D ENERGY BAND DIAGRAM

This section considers a 3-D energy-band diagram. The 3-D diagram described here is a combination of Energy-Momentum and Energy-Distance diagrams. It describes the actual process of transition of the carriers at the heterojunction.

Quantum-mechanically, one should, in general, describe electron states by quantum numbers, whereas classically, one should use momentum and position components. In the case of an energy-band diagram, the situation is actually intermediate. The validity of a semiclassical description of the dynamic behaviour of conduction-band electrons and valence-band holes can be discussed, based on the use of effective mass.

Energy-versus-distance and energy-versus-momentum diagrams are possible. Heisenberg's Uncertainty Principle relates quantitatively the lack of precision with which the position and momentum coordinates may be specified together as,

$$\Delta x \quad \Delta p_x \geq h$$

$$\Delta y \quad \Delta p_y \geq h$$

$$\Delta z \quad \Delta p_z \geq h$$

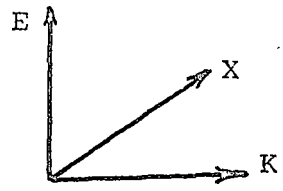
Therefore, it is impossible to consider together the precise position and momentum of any single particle.

The energy-versus-momentum diagram can describe the momentum of particles with respect to energies. The basic properties of the semiconductors are classified according to this diagram. This diagram distinguishes direct and indirect semiconductors. According to Heisenberg's Uncertainity Principle, it is not possible to know the position of particle by means of this diagram.

The energy-versus-distance diagram is the most common diagram used to describe the behaviour of homojunctions and semiconductor heterojunctions. Changes across a homojunction are well described by this diagram, since the same semiconductor exists on both sides of the junction. In the case of heterojunctions, however, the energy-versus-distance diagram lacks certain information that can only be described by a 3-D diagram.

E - X - K

In the energy-distance-momentum diagram, the three vectors are assumed to be mutually perpendicular as follows:



Thus, the energy-versus-distance and the energy-versus-momentum diagrams are superimposed. Though both E-K and E-X are independent, both momentum and position can be known approximately simultaneously.

E - X - K show that as the electron goes from one semiconductor to the other, there must exist a change of the K vector together with a change in energy. Usually there exists a change in mass ($m^* = \frac{\hbar^2}{\partial^2 E / \partial K^2}$) due to a change in the energy-momentum structure of the two semiconductors. It can be said that when an electron changes its energy, while transporting to the other semiconductor, it also changes its momentum but exactly where the change occurs cannot be said, according to the Heisenberg Uncertainty Principle.

Figure B represents a 3-D energy band diagram of two direct-gap semiconductors.

Figure B shows that in order to conserve the K vector, the electron in the transition needs some

scattering agent such as a phonon or impurities. Thus, the probability of transition is reduced and the process is an indirect one. The E - X - K diagram describes the actual process of transition and helps understand hetero-junction better.

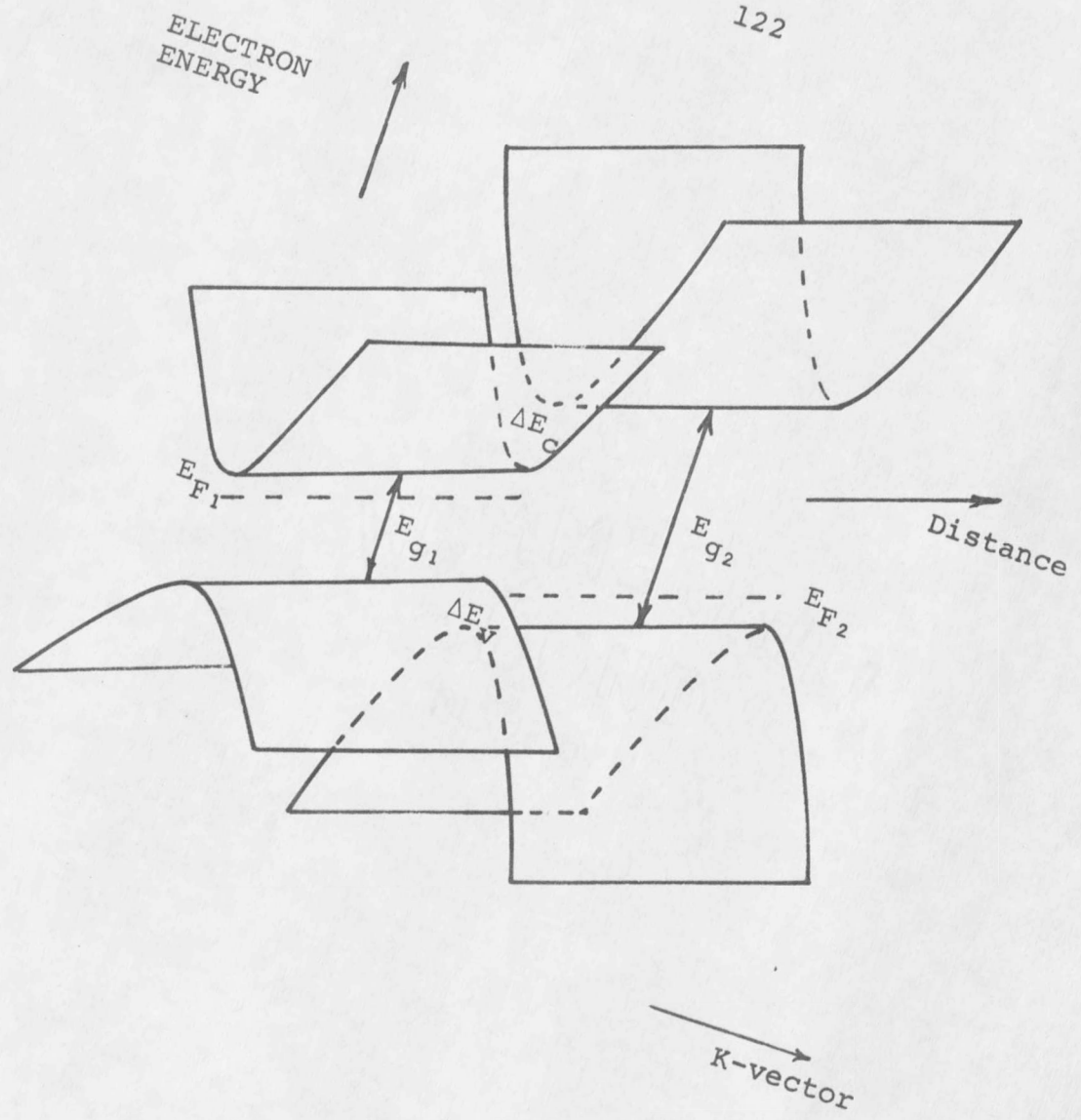


Figure B. E - X - K plot of two isolated direct gap semiconductors.

Appendix B

CHANGE OF TOTAL ENERGY DISCONTINUITIES ($\Delta E_c + \Delta E_v$)

The usual practice for expressing the temperature dependence of E_g has been by a linear variation given as

$$E_g = E_g(0) - bT. \qquad \text{(B-1)}$$

where $E_g(0)$ is an energy gap extrapolated to 0°K, b is an empirical constant evaluated near 300°K and T is the absolute temperature.

The general form of the energy-gap temperature dependence is given by Varshni [32]

$$E_g = E_g(0) - \frac{\alpha T^2}{(T+\beta)} \qquad \text{(B-2)}$$

where $E_g(0)$ is the energy gap at 0°K, β is approximately the 0°K Debye temperature θ, and α is an empirical constant. This was proposed by Varshni on the basis of theoretical considerations by Vasileff [43] and Adams [44]. Vasileff considered the shift of the band edge by electron-phonon interactions, and this calculation led Varshni to suggest that E_g should vary linearly with temperature for $T >> \theta$, and quadratically with temperature for $T << \theta$. Adams points out that Vasileff's theory fails for the

usual semiconductors but agrees with Vasileff's conclusion on the temperature dependence of band edge. Equation (B-2) supports the concept that variation of the energy gap is largely due to electron-phonon interactions rather than thermal expansion. Equation (23) describing temperature variation of total energy discontinuity based on equation (B-2) can be used to predict the total change of energy discontinuities $[\Delta E_c + \Delta E_v]$,

1. Ge-GaAs heterojunction is studied, following data is given [32,33].

Table 1. Change in Discontinuities With Changing Temperature for Ge-GaAs heterojunction.

E_{g_1} = 1.5216 (GaAs)
E_{g_2} = 0.7412 (Ge)
α_1 = 8.870×10^{-4}
α_2 = 4.561×10^{-4}
β_1 = 572.00
β_2 = 210.0

Temp (°K)	Discontinuity in eV. $(\Delta E_c + \Delta E_v)$	
0	0.7804	
100	0.7819	
200	0.7789	
300	0.7693	
400	0.7540	
500	0.7341	decreasing
600	0.7106	
700	0.6843	
800	0.6556	
900	0.6251	
1000	0.5930	

2. Si-GaP heterojunction is studied, following data is given [32,33].

Table 2. Change in Discontinuities With Changing Temperature for GaP-Si heterojunction.

E_{g_2} = 2.338 (GaP)
E_{g_2} = 1.1557 (Si)
α_1 = 6.2×10^{-4}
α_2 = 7.02×10^{-4}
β_1 = 460.0
β_2 = 1108.0

Temp (°K)	Discontinuity in eV. $(\Delta E_c + \Delta E_v)$	
0	1.182	
100	1.177	
200	1.166	
300	1.154	
400	1.141	
500	1.13	decreasing
600	1.12	
700	1.111	
800	1.103	
900	1.096	
1000	1.091	

3. Ge-Si heterojunction is studied, following data is given [32,33].

Table 3. Change in Discontinuities With Changing Temperature for Si-Ge heterojunction.

E_{g_2} = 1.1557 (Si)
E_{g_1} = 0.741200 (Ge)
α_1 = 7.021×10^{-4}
α_2 = 4.561×10^{-4}
β_1 = 1102.
β_2 = 210.

Temp (°K)	Discontinuity in eV. $(\Delta E_c + \Delta E_v)$
0	0.414
100	0.423
200	0.437
300	0.4499
400	0.459
500	0.4655
600	0.468
700	0.469
800	0.467
900	0.463
1000	0.457

BIBLIOGRAPHY

BIBLIOGRAPHY

1. Hayashi, I., Panish, M. B., and Reinhart, F. K. (1971). GaAs-$Al_xGa_{1-x}As$ double heterostructure injection lasers. J. Appl. Phys. 42,1929.

2. Kruse, P. W., Pribble, F. C., and Schulze, R. G. (1967). Solid-State infrared-wavelength converter employing high-quantum efficiency Ge-GaAs heterojunctions, J. Appl. Phys. 38,1718.

3. Anderson, R. L. (1962). Experiments on Ge-GaAs heterojunctions. Solid-State Electron, 5,341.

4. Sahai, R., and Milnes, A. G. (1970). Heterojunction solar cell calculations. Solid-State Electron, 13,1289.

5. Milnes, A. G., and Feucht, D. L., Heterojunctions and metal-semiconductor junctions. Academic Press, New York, 1972,115.

6. Sonnenberg, H. (1970). InAs-Cs_2O, a high efficiency infrared-photocathode. Appl. Phys. Lett. 16,245.

7. Kressel, H., Kohn, E. S., Nelson, H., Tietjen, J. J. (1970). An optoelectronic cold cathode using an $Al_xGa_{1-x}As$ structure. Appl. Phys. Lett. 16,359.

8. Milnes, A. G., and Feucht, D. L., Heterojunctions and metal-semiconductor junctions. Academic Press, New York, page 218.

9. Preston, J. S. (1950). The constitution and mechanism of the Se rectifier photocell. Proc. Roy. Soc. Ser. A202, A449.

10. Gubanov, A. I. (1950). Theory of the contact between two semiconductors with different types of conduction. Zh. Tekh. Fiz. 20,1287.

11. Shockley, W. (1951). Circuit element Using Semiconductor Material. U.S. Patent 2,569,347.

12. Kroemer, H. (1957). Theory of a wide gap emitter for transistors. Proc. IRE 45,1535.

13. Perlman, S. S., and Feucht, D. L. (1965). Abrupt heterojunction emitters for transistors. J. Electron. Contr. 18,159.

14. _____, and _____. (1964). p-n heterojunctions. Solid-State Electron. 7,911.

15. Oldham, W. G., and Milnes, A. G. (1963). n-n semiconductor heterojunctions. Solid-State Electron. 6,121.

16. Van Ruyven, L. J., Papenhuijzen, J. M. P., and Verhoeven, A. C. J. (1965). Optical phenomena in Ge-GaP heterojunctions. Solid-State Electron. 8,631.

17. Hogarth, C. A. (1970). Wither heterojunction? Proc. Int. Conf. Phys. Chem. Semicond. Heterojunctions Layer Structures, Budapest, 1970. 384. Hung. Acad. Sciences, Budapest, Hungary.

18. Kressel, H., Lockwood, H. F., and Ettenberg, M. Progressive Laser diode. I.E.E.E. Spectrum, May 1973, page 59.

19. Anderson, R. L. (1970). The present state of the theory of heterojunctions. Proc. Int. Conf. Phys. Chem. Semicond. Heterojunctions Layer Structures, Budapest, 1970. 2,55. Hung. Acad. Sciences, Budapest, Hungary.

20. Milnes, A. G., and Feucht, D. L. (1972). Heterojunctions and metal-semiconductor junction, Academic Press, New York, page 45.

21. Moore, R. M., and Busanovich, C. J. (1970). Vacuum-deposited thin-film p-Se n-CdSe heterojunction diodes. I.E.E.E. Trans. Electron. Devices ED-17, 305.

22. Lang, J., Kispeter, J., and Gombay, L. (1970). Dependence of electric properties of Se-CdSe heterojunction on doping. Abstr. Int. Conf. Phys. Chem. Semicond. Heterojunctions Layer Structures, Budapest 1970, page 63. Hung. Acad. Sciences, Budapest, Hungary.

23. Sonnenberg, H. (1969). Effect of acceptor density on photoemission from p GaAs-Cs and -Cs_2O. J. Appl. Phys. 40,3414.

24. Dobrynin, S. N. (1969). Analysis of the band diagrams of Degenerate Heterojunctions. Soviet Physics--Semiconductors, Vol. 3, No. 1.

25. Milnes, A. G., and Feucht, D. L., Heterojunctions and metal-semiconductor junctions. Academic Press, New York, 1972, page 12.

26. Gray, P. E., DeWitt, D., Boothroyd, R. A., and Gibbons, J. F. (1964). Physical Electronics and Circuit Models of Transistors. John Wiley and Sons, page 11.

27. Sze, S. M. (1969). Physics of Semiconductor Devices. John Wiley and Sons, New York, page 20.

28. _____. (1969). Physics of Semiconductor Devices. John Wiley and Sons, New York, page 57.

29. Milnes, A. G., and Feucht, D. L. (1972). Heterojunctions and metal-semiconductor junction. Academic Press, New York, Chapter 9.

30. Anderson, R. L. (1960). Germanium-gallium assenide contacts, Ph.D. Thesis.

31. McKelvey, John P. (1966). Solid-State and semiconductor Physics. Harper & Row, New York, page 404.

32. Varshni, V. P. (1967). Temperature Dependence of the energy gap in semiconductors. Physics 34,149-154.

33. Panish, M. B., and Casey, Jr., M. C. (1969). Temperature Dependence of the energy gap in GaAs and GaP. Journal of Applied Physics, Vol. 40, No. 1, page 163.

34. Howard, W. E., Fowler, A. B., and McLeod, D. (1968). Pressure Dependence of Barrier Heights in Ge-GaAs n-n heterojunctions. J. Appl. Phys., Vol. 39, No. 3, page 1533.

35. McKelvey, J. P. (1966). Solid-State and semiconductor Physics. Harper & Row, New York, page 277.

36. Milnes, A. G., and Feucht, D. L. Heterojunctions and metal-semiconductor junctions. Academic Press, New York, 1972, page 8.

37. Sze, S. M. (1969). Physics of semiconductor devices. John Wiley and Sons, New York, page 23-27.

38. _____. (1969). Physics of semiconductor devices. John Wiley and Sons, New York, Figure 11.

39. Fang, F. F., and Howard, W. E. (1964). Effect of crystal orientation on Ge-GaAs heterojunctions. J. Appl. Phys., 35,612.

40. Fan, H. Y. (1951). Temperature dependence of the Energy Gap in Semiconductor. Physical Review, Vol. 82, No. 6, page 900-905.

41. Moore, R. M., and Busanovich, C. J. (1969a). An evaporated heterojunction diode strain sensor. Proc. I.E.E.E., 57,735.

42. Spenke, E. (1958). Electronic Semiconductors. McGraw-Hill Book Co., Inc., 53.

43. Vasileff, H. D. (1957). Phys. Rev. 105,441.

44. Adams, E. N. (1957). Phys. Rev. 107,671.

MONTANA STATE UNIVERSITY LIBRARIES
3 1762 10011549 0

[redacted]
D378
T155 Tandan, Naresh
cop.2 Junction analysis and temperature effects in semi-conductor heterojunctions.

NAME AND ADDRESS

[redacted]

D378
T155
Cop. 2